

Electronic Supplementary Information

*Subtle substitution controls the rainbow chromatic behaviour of
multi-stimuli responsive core-expanded pyrenes*

David T. Hogan, Benjamin S. Gelfand, Denis M. Spasyuk and Todd C. Sutherland*

Email at: todd.sutherland@ucalgary.ca

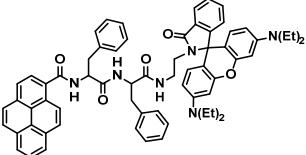
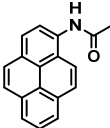
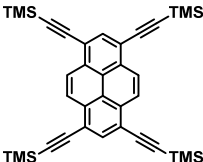
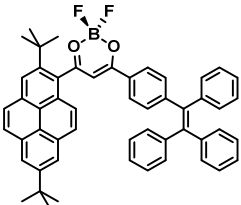
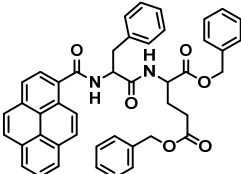
Contents

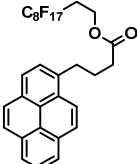
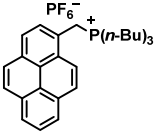
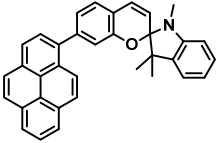
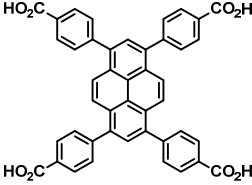
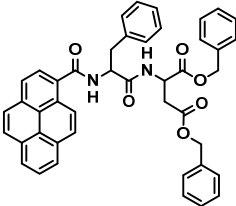
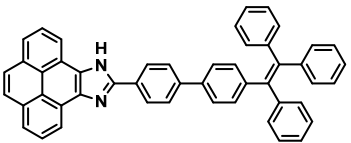
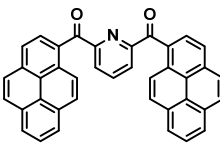
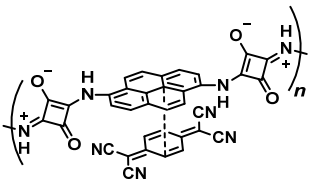
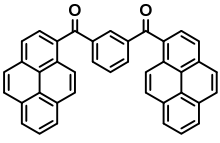
Section 1	Mechanochromic Pyrenes Literature Survey
Section 2	General Considerations
Section 3	Synthesis
Section 4a	^1H NMR and $^{13}\text{C}\{^1\text{H}\}$ NMR of Synthesized Compounds
Section 4b	^1H NMR and $^{13}\text{C}\{^1\text{H}\}$ NMR with TFA, post-HCl and post-grinding
Section 5a	Results of Single Molecule Calculations
Section 5b	Calculated and Experimental ^1H NMR Comparisons
Section 5c	Results of Crystal Packing Calculations
Section 6	Single-crystal X-ray Diffraction
Section 7	Powder X-ray Diffraction
Section 8	Solution-State UV-visible Absorption and Fluorescence Spectroscopy
Section 9	Solid-State UV-visible Absorption and Fluorescence Spectroscopy
Section 10	References

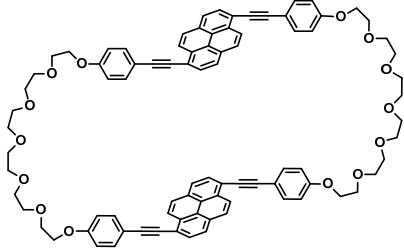
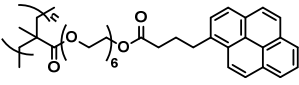
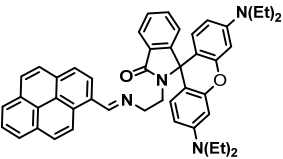
Section 1 Mechanochromic Pyrenes Literature Survey

The following was created from a Web of Science search for journal articles using the terms “mechanochromic” AND “pyrene” in the topic. The column marked “Before & After X-ray...” is to indicate if single crystal polymorphs were analyzed of the pre- and post-grinding material, to pinpoint changes in molecular packing induced by mechanical force.

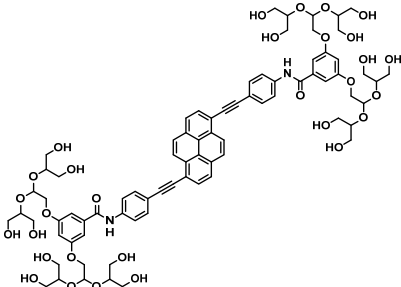
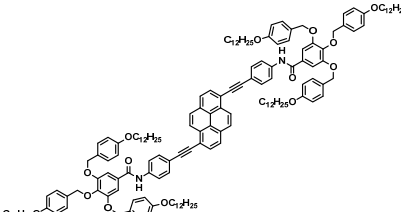
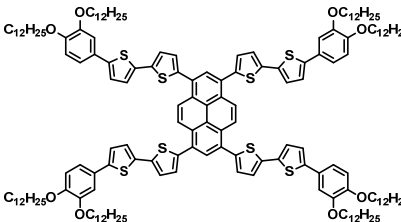
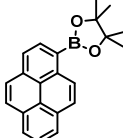
- *PART A*. Transformation from crystalline/ordered states into amorphous states.
- *PART B*. Transition from crystalline/ordered states into semi-ordered but ill-defined states.
- *PART C*. Those that exhibit a true crystal-to-crystal polymorph transition.

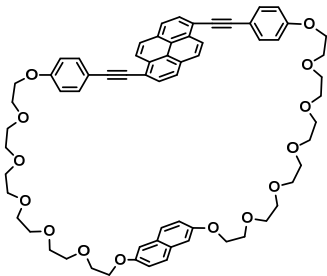
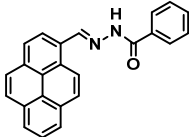
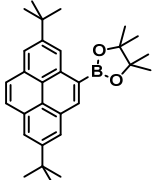
##	Reference	Structure	Nature of Transition	Before & After X-ray Crystal Structures?
PART A				
1	Z. Ma, Z. Wang, Z. Xu, X. Jia and Y. Wei, <i>J. Mater. Chem. C</i> , 2015, 3 , 3399–3405.		Ordered xerogel→ amorphous	NO
2	E. Nagata, S. Takeuchi, T. Nakanishi, Y. Hasegawa, Y. Mawatari and H. Nakano, <i>ChemPhysChem</i> , 2015, 16 , 3038–3043.		Crystalline→ amorphous	NO
3	F. Xu, T. Nishida, K. Shinohara, L. Peng, M. Takezaki, T. Kamada, H. Akashi, H. Nakamura, K. Sugiyama, K. Ohta, A. Orita and J. Otera, <i>Organometallics</i> , 2017, 36 , 556–563.		Crystalline→ amorphous	NO
4	T. Sun, F. Zhao, G. Xi, J. Gong, M. Sun, C. Dong and J. Qiu, <i>RSC Adv.</i> , 2019, 9 , 19641–19647.		Crystalline→ amorphous	NO
5	L. Huang, C. Wu, L. Zhang, Z. Ma and X. Jia, <i>ACS Appl. Mater. Interfaces</i> , 2018, 10 , 34475–34484.		Ordered xerogel→ amorphous	NO

6	Z. Qian, W. Deng, X. Zhang, H. Miao and G. Zhang, <i>RSC Adv</i> , 2017, 7 , 46721–46725.		Crystalline→ amorphous	NO
7	G. Li, Y. Xu, W. Zhuang and Y. Wang, <i>RSC Adv.</i> , 2016, 6 , 84787–84793.		Crystalline→ amorphous	NO
8	X. Meng, G. Qi, X. Li, Z. Wang, K. Wang, B. Zou and Y. Ma, <i>J. Mater. Chem. C</i> , 2016, 4 , 7584–7588.		Crystalline→ amorphous	NO
9	S. Yamaguchi, I. Yoshikawa, T. Mutai and K. Araki, <i>J. Mater. Chem.</i> , 2012, 22 , 20065.		Amorphous→ amorphous	NO
10	M.-J. Teng, X.-R. Jia, S. Yang, X.-F. Chen and Y. Wei, <i>Adv. Mater.</i> , 2012, 24 , 1255–1261.		Crystalline→ amorphous	NO
11	T. Jadhav, B. Dhokale, S. M. Mobin and R. Misra, <i>J. Mater. Chem. C</i> , 2015, 3 , 9981–9988.		Crystalline→ amorphous	NO
12	W. Li, P.-P. Yang, L. Wang and H. Wang, <i>J. Mater. Chem. C</i> , 2015, 3 , 3783–3789.		Crystalline→ amorphous	NO
13	A. Nagai and Y. Okabe, <i>Chem Commun</i> , 2014, 50 , 10052–10054.		Crystalline polymer→ amorphous	NO
14	W. Li, L. Wang, J.-P. Zhang and H. Wang, <i>J. Mater. Chem. C</i> , 2014, 2 , 1887.		Crystalline→ amorphous	NO
15	Y. Li, Z. Ma, A. Li, W. Xu, Y. Wang, H. Jiang, K. Wang, Y. Zhao and X. Jia, <i>ACS Appl. Mater. Interfaces</i> , 2017, 9 , 8910–8918.		Crystalline→ amorphous	NO

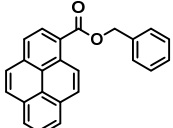
16	Y. Sagara and N. Tamaoki, <i>RSC Adv</i> , 2017, 7 , 47056–47062.		Semi-ordered solid→amorphous	NO
17	F. Cellini, L. Block, J. Li, S. Khapli, S. D. Peterson and M. Porfiri, <i>Sens. Actuators B Chem.</i> , 2016, 234 , 510–520.		Ordered polymer→amorphous	NO
18	Z. Ma, M. Teng, Z. Wang and X. Jia, <i>Tetrahedron Lett.</i> , 2013, 54 , 6504–6506.		Undetermined	NO

PART B

19	Y. Sagara, T. Komatsu, T. Ueno, K. Hanaoka, T. Kato and T. Nagano, <i>Adv. Funct. Mater.</i> , 2013, 23 , 5277–5284.		Micelles→disordered micelles	NO
20	Y. Sagara and T. Kato, <i>Angew. Chem. Int. Ed.</i> , 2008, 47 , 5175–5178.		Cubic liquid crystal→columnar liquid crystal	NO
21	K. P. Gan, M. Yoshio and T. Kato, <i>J. Mater. Chem. C</i> , 2016, 4 , 5073–5080.		Columnar liquid crystal→disordered columnar liquid crystal	NO
22	T. Wang, N. Zhang, K. Zhang, J. Dai, W. Bai and R. Bai, <i>Chem. Commun.</i> , 2016, 52 , 9679–9682.		Crystalline→Semi-crystalline	NO

23	Y. Sagara, C. Weder and N. Tamaoki, <i>Chem. Mater.</i> , 2017, 29 , 6145–6152.		Nematic liquid crystal → disordered nematic liquid crystal	NO
24	Y. Li, W. Huang, J. Yong, S. Huang, Y. Li, Y. Liu and D. Wu, <i>New J. Chem.</i> , 2018, 42 , 12644–12648.		Crystalline → semi-crystalline	NO
25	Y.-B. Gong, P. Zhang, Y. Gu, J.-Q. Wang, M.-M. Han, C. Chen, X.-J. Zhan, Z.-L. Xie, B. Zou, Q. Peng, Z.-G. Chi and Z. Li, <i>Adv. Opt. Mater.</i> , 2018, 6 , 1800198.		Crystalline → semi-crystalline	NO

PART C

26	Q. Kong, W. Zhuang, G. Li, Y. Xu, Q. Jiang and Y. Wang, <i>New J. Chem.</i> , 2017, 41 , 13784–13791.		Crystal → crystal polymorphism	NO
----	--	---	--------------------------------	----

Section 2 General Considerations

Pyrene (98%), RuCl₃ hydrate (95+%), TBABr (99%), NaOH (>97%), SO₄(CH₃)₂ (97%), Br₂ (reagent grade), Cs₂CO₃ (Cabot high-purity), BBr₃/CH₂Cl₂ (1M), phenylenediamine (99.5%), TFA (99%) and 4-bromo-*N,N*-dimethylaniline (97%) were all purchased from Millipore-Sigma and used without purification. PhB(OH)₂ (97%) from Millipore-Sigma was recrystallized from boiling water to decompose the boroxine. NaIO₄ (98%), *N*-methylimidazole (99%) and citric acid hydrate (97%) were purchased from Alfa-Aesar and used as received. Na₂S₂O₄ (>85%) was purchased from BDH, NMe₂PhBPIn (99%) was purchased from Oakwood Chemical and NEt₃ (>99.5%) was purchased from Merck KGaA. Solvents, including those used for spectroscopy, are listed as follows. CH₂Cl₂ (40 ppm amylene, >99.5%), THF (250 ppm BHT, >99%), EtOAc (>99.5%), hexanes (HPLC, >98.5%), acetone (99%), acetic acid (>99.7%), toluene (>99.5%), MTBE (98%), piperidine (99%) and 1,4-dioxane (>99%) were purchased from Millipore-Sigma and used without purification. DMSO (99.9%) was purchased from Fisher Chemicals and cyclohexane (>99%) was purchased from Merck KGaA and each was used as received.

Column chromatography was performed using Silicycle SiliaFlash P60 40-63 μm diameter silica gel. Thin-layer chromatography (tlc) was performed on Merck KGaA TLC Silica gel 60 F₂₅₄ analytical plates supported on aluminium.

UV-visible absorption spectroscopy was performed using a Varian Cary 5000 UV-visible-NIR spectrophotometer in dual beam mode. Solutions were measured at 298 K, continuously referenced against blank solvent in quartz 10 mm path length cuvettes. Solid-state measurements were acquired in transmission mode on the same instrument, continuously referenced against a blank Corning 75 mm long \times 25 mm wide \times 1 mm thick glass microscope slide. Samples were prepared by allowing single drops of CH_2Cl_2 solutions to evaporate and spotting multiple layers in a 1-inch \times 1-inch square on the glass slide.

Samples for polarized optical microscopy (POM) were prepared by manually picking crystals and placing them onto Corning glass slides, applying minimal oil to immobilize them and sandwiching another glass slide on the top. Images were acquired on an Olympus BX41 light microscope and captured with an Olympus U-TV1X-2 colour camera. The same samples were observed using a Carl Zeiss Axiovert 200M fluorescence microscope fitted with a black/white/fluorescence AxioCam MRm camera with the following filter sets. Blue: excitation from 365 nm, observing 395 to 495 nm. Green: excitation from 430 to 510 nm, observing 475 to 575 nm. Orange: excitation from 520 to 570 nm, observing 545 to 675 nm. Red: excitation from 520 to 600 nm, observing 555 to 705 nm.

Thermo-gravimetric analysis (TGA) and differential scanning calorimetry (DSC) were both performed on a Netzsch STA 409 PC supplied with a Netzsch Pu 1.851.08 power unit. Samples were loaded into tared 25 μL aluminium crucibles before measurement, and the thermograms were background-subtracted using backgrounds obtained with the same time and temperature parameters as the actual samples. The instrument was not equipped with a fan and thus all cooling runs were performed by allowing the oven to naturally cool down. Heating runs were ramped at 10 $^\circ\text{C}/\text{minute}$ under nitrogen, because there were no events visible ramping at 1 $^\circ\text{C}/\text{minute}$.

Crystals of **H₂quin** were grown by dissolving c. 0.5 mg in minimal CH_2Cl_2 in a 2 mL screwcap vial and layering on methanol to fill the volume. The vial was tightly capped and yellow lances grew over 1 week. Crystals of **H₂pyr** were serendipitously grown by heating a solid sample inside a sealed glass capillary to 330 $^\circ\text{C}$ during melting point determination, and red plates sublimated on the walls of the capillary above the bulk solid. Crystals of **NMe₂quin** were grown by dissolving c. 0.5 mg in CH_2Cl_2 in a 2 mL screwcap vial

and layering on cyclohexane to fill the volume. The vial was tightly capped and allowed to sit for 1 week, then opened to evaporate, and crystals were collected after solvent evaporation. Both polymorphs were discovered in the same vial; **NMe₂quin-grou** as orange rods and **NMe₂quin-pris** as yellow plates. Suitable crystals were selected and mounted on a glass loop using Paratone. Diffraction experiments were performed on a Nonius Kappa diffractometer equipped with a Siemens Fine Focus Ceramic Tube (graphite monochromated Mo K α , $\lambda = 0.71069 \text{ \AA}$) and an APEX II CCD detector. The crystal was kept at 173 K during data collection. Diffractions spots were integrated and scaled with SAINT¹ and the space group was determined with XPREP². Using Olex2,³ the structure was solved with the ShelXT⁴ structure solution program using Intrinsic Phasing and refined with the ShelXL⁵ refinement package using Least Squares minimisation.

Powder x-ray diffraction (PXRD) patterns were collected using a Bruker D8 Advance ECO instrument equipped with Cu K α source ($\lambda = 1.54178 \text{ \AA}$, kV = 40, mA = 25) and a LYNXEYE XE detector. Samples were dry loaded onto a Si low background wafer. High temperature measurements, and their ambient control measurement, were collected on samples dry-loaded onto a PtRh alloy strip using a Bruker MTC-HIGHTEMP, equipped with Kapton windows. Qualitative Rietveld refinements were done using GSAS-2⁶ and preferred orientations of PXRD patterns with respect to those predicted from single-crystal structures were approximated with Mercury 3.0.^{7,8}

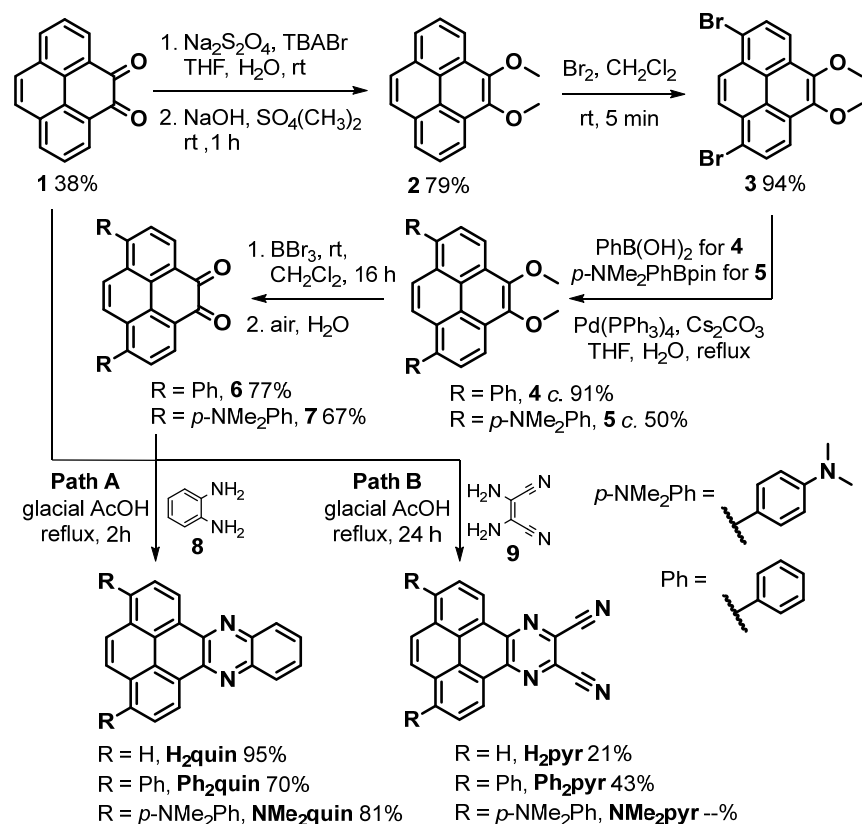
Crystals of **Ph₂pyr** were prepared by dissolving *c.* 0.5 mg in boiling toluene in a 2 mL screwcap vial. After dissolution, the vial was left open and crystals were recovered once all the solvent had evaporated. Crystals of **Ph₂quin** were prepared by the same procedure using benzene instead of toluene. Single crystal X-ray diffraction data for compounds **Ph₂pyr** and **Ph₂quin** was collected using the Canadian Macromolecular Crystallography Facility CMCF-BM beamline at the Canadian Light Source (CLS).⁹ The CMCF-BM is a bending magnet beamline equipped with a Si (111) double crystal monochromator, Rayonix MX300HE CCD detector and MD2 microdiffractometer equipped with Mini Kappa Goniometer Head. Data for compound **Ph₂pyr** and **Ph₂quin** was collected at 18.000 keV (0.6888 \AA) and 16.000 keV respectively. Data for all crystals was collected at 100 K using a single crystal. Cell refinement and data reduction were performed using XDS.¹⁰ An empirical absorption correction, based on the multiple measurements of equivalent reflections, and merging of data was performed using SADABS.¹¹ Data conversion from XDS file format to SADABS file format was performed using XDS2SAD¹². The space group was confirmed by XPREP¹³ routine. The structures were solved by direct-methods and refined by full-matrix least squares and difference Fourier techniques with SHELXL-2014.⁵ All non-hydrogen atoms were refined with anisotropic

displacement parameters. Hydrogen atoms were set in calculated positions and refined as riding atoms with a common thermal parameter. All publication materials were prepared using LinX^{TL}¹⁴ and Mercury^{7,8} programs. CheckCIF routine and structure factor analyses were performed by Platon.¹⁵

Bulk samples of **NMe₂quin** were ground in an agate mortar and pestle supplied by VWR. To collect the UV-visible absorption and fluorescence of the ground sample, a generous sample of **NMe₂quin** on a microscope slide, prepared as above, was pressed and rubbed manually with another microscope slide. To regenerate the ground samples with CH₂Cl₂ vapours, the slide was put next to 5 mL of CH₂Cl₂ in a small flask and covered together with an inverted beaker. To expose **NMe₂quin**, **H₂quin**, and **Ph₂quin** to HCl vapours, slides of the solids were placed next to a cotton ball soaked in concentrated HCl and covered together with an inverted beaker. Variable temperature UV-visible absorption and fluorescence collections on solid samples were done by preparing the samples on glass microscope slides as described above and heating them to the specified temperature on a Linkam Scientific Instruments T95-HS heating stage.

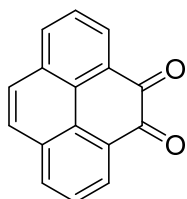
Fluorescence spectroscopy was performed using a Jasco FP-6600 on low sensitivity mode collecting a single scan. The excitation bandwidth was 10 nm, emission bandwidth of 6 nm, integration time of 0.2 seconds, data pitch of 1 nm, scanning speed of 200 nm/minute. Excitation spectra were corrected for the lamp profile. For spectra of solid samples, glass slides were prepared as above and put at a 45° angle to the excitation and emission slits using a solid sample holder. The parameters were identical, but the instrument was set to medium sensitivity.

All ¹H NMR spectra were collected at 400 MHz and ¹³C{¹H} NMR spectra at 100 MHz on a Bruker DRY400 spectrometer at 298 K. ¹H NMR and ¹³C{¹H} NMR spectra were referenced against the residual solvent signals from CHCl₃ in CDCl₃ (¹H δ = 7.26, ¹³C δ = 77.2).¹⁶ High-resolution mass spectra (HR MS) were collected using either EI on a Waters GCT Premier mass spectrometer or ESI on an Agilent Q-TOF mass spectrometer. All chemical formula confirmations were made with less than 5 ppm difference between calculated and observed masses. Infra-red (IR) spectroscopy was performed using an Agilent Cary FT-IR with a diamond attenuated total reflectance (ATR) module. Melting points were collected on an Electrothermal melting point apparatus and are uncorrected.



Scheme S1. Synthetic routes towards core-expanded pyrenes.

Pyren-4,5-dione 1



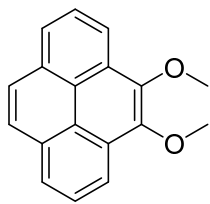
This experimental was adapted from a literature procedure.¹⁷ Into a 500 mL RBF were added a large magnetic stir bar and pyrene (5.00 g, 24.7 mmol, 1.0 eq.). CH₂Cl₂ (100 mL) and THF (100 mL) were added in one portion and the mixture was stirred to dissolution at room temperature. RuCl₃ hydrate (0.5134 g, 2.475 mmol, 0.10 eq.) was added which turned the mixture dark brown-black, followed by *N*-methylimidazole (0.1 mL, 1.25 mmol, 0.10 eq.) and deionized H₂O (125 mL). The stirring was turned as vigorous as permissible, and powdered NaIO₄ (23.77 g, 111.1 mmol, 4.5 eq.) was added over the next 20-

25 minutes, in spatula tip-sized portions. During addition, the temperature of the reaction was monitored by placing a hand on the outside of the flask and small chunks of crushed ice were added as required to maintain ambient temperature.

After 2.5 hours the reaction was quenched by filling the flask with deionized H₂O, stopping stirring and instead manually swirling to dissolved salts. The aqueous layer was decanted directly into a 2L separatory funnel. This process was repeated twice more, and the organics were then partially removed under reduced pressures, leaving a chunky and thick mud-like residue in the flask. Enough CH₂Cl₂ was added to reconstitute the solids and the mixture was transferred to the separatory funnel. The layers were swirled and separated, and the aqueous layer was extracted with CH₂Cl₂ (3 × 100 mL) using a rod to disperse the black film between the aqueous and organic layers, which held extra CH₂Cl₂. The organics were broken into two portions and each was washed vigorously to remove black-green colouration: a total of six times for each portion with H₂O (200 mL), re-using the bulk of the H₂O between washes and only disposing of black film-containing solution. After six washes the organic layer became clear orange-red, which was concentrated under reduced pressures into a brown-orange solid.

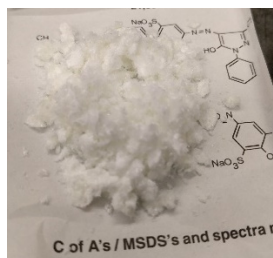
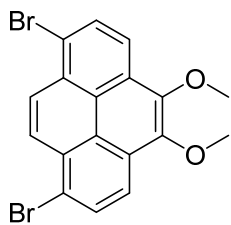
The resulting solid was suspended in a 500 mL RBF, using just enough CH₂Cl₂ to create a thick, paint-like consistency (c. 75 mL) then twice as much methanol was added. The flask was capped and allowed to sit undisturbed in the fridge for 2 days. The mixture was then suction filtered, the residue was washed with minimal ice-cold methanol and dried *in-vacuo*. (*Note: the above precipitation step can be skipped, but the column will have to be packed taller because precipitation removes some co-eluting impurities*). The resulting rusty orange-brown solid was adsorbed to silica and loaded onto a 7 cm tall × 6 cm wide silica column packed in CH₂Cl₂. The column was eluted with CH₂Cl₂ (c. 1.7 L), first removing pyrene as a cyan fluorescent band, second a deep blue-purple fluorescent band and finally the product as a deep orange-red band. The elution of product was stopped before another deep blue-purple fluorescence band eluted. All visibly yellow eluate was collected and concentrated under reduced pressures to yield pyren-4,5-dione **1** (2.1561 g, 38%) as bright orange micro-needles: ¹H NMR (400 MHz, Chloroform-d) δ = 8.50 (dd, J = 7.4, 1.2 Hz, 1H), 8.18 (dd, J = 8.0, 1.2 Hz, 1H), 7.86 (s, 1H), 7.76 (t, J = 7.7 Hz, 1H); DEPT-Q ¹³C{¹H} NMR (100 MHz, Chloroform-d) δ = 180.6, 135.9, 132.2, 130.3, 130.3, 128.6, 128.1, 127.4; HRMS (EI, positive) calculated for [C₁₆H₈O₂]⁺ *m/z* = 232.0524, found *m/z* = 232.0527, 1.3 ppm difference; R_f (40% EtOAc/hexanes) = 0.50.

4,5-Dimethoxyppyrene



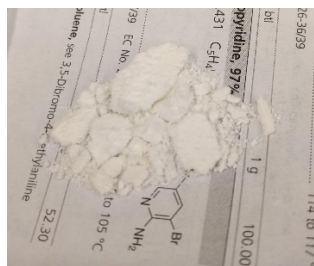
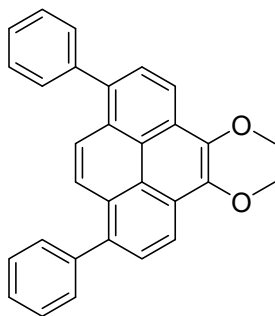
This experimental was adapted from a literature procedure.¹⁸ Into a 100 mL RBF were added a magnetic stir bar, pyren-4,5-dione **1** (1.0039 g, 4.3231 mmol, 1.0 eq.) and TBABr (0.4203 g, 1.304 mmol, 0.30 eq.). THF (20 mL) and deionized H₂O (20 mL) were added to suspend the solids, and then Na₂S₂O₄ (2.4905 g, 12.964 mmol, 3.0 eq.) was added. The resulting light-yellow solution was stirred, capped, at room temperature for 5 minutes. Separately, a solution of NaOH (2.07 g, 51.8 mmol, 12.0 eq.) in deionized H₂O (20 mL) was prepared and added in one portion, turning the pyren-4,5-dione solution deep orange-red. SO₄(CH₃)₂ (2.05 mL, 21.5 mmol, 5.0 eq.) was added by syringe in one portion, and the mixture was vigorously stirred (*Note: if the solution is left idle, black colouration appears at the air-solution interface and stirring alleviates this problem*). The mixture was allowed to stir for 1 hour at room temperature, after which time it became light-yellow and translucent. The mixture was diluted with 10 mL EtOAc and the layers were shaken and separated in a separatory funnel. The aqueous layer was extracted with EtOAc (3 × 10 mL), the combined organics were brine-washed, dried over anhydrous Na₂SO₄ and concentrated under reduced pressures to yield a light-orange oil, which solidified into a yellow-orange solid upon standing. The solid was taken and recrystallized from minimal boiling methanol (*Note: avoid excess heating, as this melts the solid and it does not easily re-dissolve*). The crystallized solid was suction filtered, washed with minimal ice-cold methanol and dried *in-vacuo* to yield 4,5-dimethoxyppyrene (0.8981 g, 79%) as pale, straw-yellow needles: ¹H NMR (400 MHz, Chloroform-*d*) δ = 8.49 (dd, *J* = 7.8, 1.1 Hz, 1H), 8.15 (dd, *J* = 7.6, 1.2 Hz, 1H), 8.07 (s, 1H), 8.04 (t, *J* = 7.7 Hz, 1H), 4.22 (s, 3H); DEPT-Q ¹³C{¹H} NMR (100 MHz, Chloroform-*d*) δ = 145.0, 131.2, 128.5, 127.5, 126.2, 124.6, 123.0, 119.4, 61.3; HRMS (EI, positive) calculated for [C₁₈H₁₄O₂]⁺ *m/z* = 262.0994, found *m/z* = 262.0989, -1.9 ppm difference; R_f (20% EtOAc/hexanes) = 0.70.

1,8-Dibromo-4,5-dimethoxyppyrene



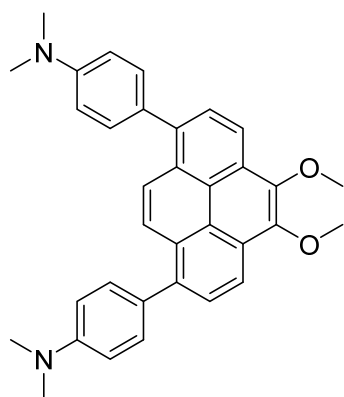
This experimental was adapted from a literature procedure.¹⁸ Into a 100 mL RBF were added a magnetic stir bar, 4,5-dimethoxyppyrene (0.7504 g, 2.861 mmol, 1.0 eq.) and dried CH₂Cl₂ (70 mL) (*Note: if undried solvent is used, demethylation is observable by tlc analysis, likely from in-situ generated HBr*). The mixture was stirred to dissolution at room temperature. Separately, a solution of Br₂ (0.32 mL, 6.2 mmol, 2.2 eq.) in dried CH₂Cl₂ (5 mL) was prepared, which was added dropwise to the 4,5-dimethoxyppyrene solution. The vibrant red solution was stirred for a further 5 minutes after full addition, and then the mixture was diluted with CH₂Cl₂ (5 mL) and poured into a separatory funnel with saturated aqueous Na₂S₂O₃ (20 mL). The mixture was shaken to decolorize the organic layer, the layers were separated and the aqueous layer was extracted with CH₂Cl₂ (3 × 10 mL). The combined organics were brine-washed, dried over anhydrous Na₂SO₄ and concentrated under reduced pressures into a light-yellow solid. This was adsorbed to silica and loaded onto a 3 cm tall × 6.5 cm wide silica plug in a sintered glass funnel. This was eluted with 50% CH₂Cl₂/hexanes (*c.* 800 mL). All eluate was collected and concentrated under reduced pressures to yield 1,8-dibromo-4,5-dimethoxyppyrene (1.1323 g, 94%) as a fluffy, fibrous white solid: ¹H NMR (400 MHz, Chloroform-*d*) δ = 8.53 (s, 1H), 8.36 (d, *J* = 8.4 Hz, 1H), 8.28 (d, *J* = 8.4 Hz, 1H), 4.19 (s, 3H); DEPT-Q ¹³C{¹H} NMR (100 MHz, Chloroform-*d*) δ = 144.6, 130.9, 129.6, 128.3, 127.6, 123.6, 120.84; HRMS (EI, positive) calculated for [C₁₈H₁₂O₂⁷⁹Br₂]⁺ *m/z* = 417.9204, found *m/z* = 417.9205, 0.2 ppm difference; R_f (10% EtOAc/hexanes) = 0.55.

1,8-Diphenyl-4,5-dimethoxyppyrene



This experimental was adapted from a literature procedure on a related system.¹⁹ Into a 50 mL RBF were added a magnetic stir bar, THF (20 mL) and deionized H₂O (10 mL). The flask was capped with a rubber septum, the headspace was purged with N₂ and the solvent was taken through 3 × freeze-pump-thaw cycles. The solvent was frozen again and under N₂, 1,8-dibromo-4,5-dimethoxyppyrene (0.5011 g, 1.193 mmol, 1.0 eq.), Pd(PPh₃)₄ (0.1382 g, 0.1196 mmol, 0.10 eq.), Cs₂CO₃ (2.7219 g, 8.3537 mmol, 7.0 eq.) and PhB(OH)₂ (0.5819 g, 4.772 mmol, 4.0 eq.) were deposited into the flask. A pre N₂-flushed water condenser was equipped to the neck of the flask and the apparatus was warmed to room temperature. The flask was then put into a 75-80 °C oil bath and refluxed with stirring, under N₂ for 24 hours. After this time, the dark brown-black mixture was cooled to room temperature, diluted with EtOAc (10 mL) and poured into a separatory funnel with brine (20 mL). The layers were shaken and then separated. The aqueous layer was extracted with EtOAc (3 × 5 mL), the combined organics were dried over anhydrous Na₂SO₄ and then concentrated under reduced pressures to yield a dark black-brown residue. This was adsorbed to silica and loaded onto a 6 cm tall × 4 cm wide silica column packed in 10% CH₂Cl₂/hexanes. The column was eluted with a gradient of this solvent (c. 800 mL), then 20% CH₂Cl₂ (c. 600 mL) then 40% CH₂Cl₂ (c. 400 mL), which eluted the product as a cyan fluorescent band. This eluate was collected and concentrated to yield 1,8-diphenyl-4,5-dimethoxyppyrene (0.4517 g, c. 91%) as a pale-yellow oil, which was dissolved in boiling pentane, and then the solvent was removed to leave a white granular solid. (Note: by ¹H NMR analysis this product was a mixture of desired product and two other substances, likely singly and doubly proto de-brominated starting materials, which were inseparable and thus full purification was not performed): ¹H NMR (400 MHz, Chloroform-*d*) δ = 8.56 (d, *J* = 8.1 Hz, 1H), 8.11 (s, 1H), 8.03 (d, *J* = 8.0 Hz, 1H), 7.61 (d, *J* = 7.2 Hz, 2H), 7.53 (t, *J* = 7.5 Hz, 2H), 7.46 (t, *J* = 7.2 Hz, 1H), 4.26 (s, 3H); ¹³C {¹H} NMR due to lack of purity, no carbon NMR was performed; HRMS (ESI, positive) calculated for [C₃₀H₂₂O₂+H]⁺ *m/z* = 415.1693, found *m/z* = 415.1686, 1.5 ppm difference; R_f (10% EtOAc/hexanes) = 0.51.

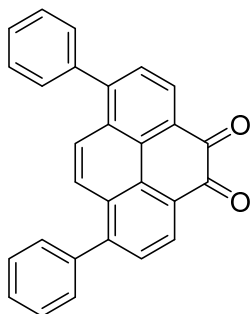
1,8-Bis(4-*N,N*-dimethylaminophenyl)-4,5-dimethoxyppyrene



This experimental was adapted from a literature procedure on a related system.¹⁹ Into a 50 mL RBF were added a magnetic stir bar, THF (10 mL) and deionized H₂O (5 mL). The flask was capped with a rubber septum, the headspace was purged with N₂ and the solvent was taken through 3 × freeze-pump-thaw cycles. The solvent was frozen again and under N₂, 1,8-dibromo-4,5-dimethoxyppyrene (0.2512 g, 0.5980 mmol, 1.0 eq.), Pd(PPh₃)₄ (0.0694 g, 0.06006 mmol, 0.10 eq.), Cs₂CO₃ (1.3649 g, 4.1890 mmol, 7.0 eq.) and NMe₂PhBpin (0.3693 g, 1.494 mmol, 2.5 eq.) were deposited into the flask. A pre N₂-flushed water condenser was equipped to the neck of the flask and the apparatus was warmed to room temperature. The flask was then put into a 75-80 °C oil bath and refluxed with stirring, under N₂ for 72 hours. After this time, the mixture had gathered tan-brown precipitates. The mixture was cooled to room temperature and diluted with enough CH₂Cl₂ to dissolve all solids (c. 20 mL). The solution was poured into a separatory funnel with brine (20 mL) and the layers were shaken, then separated. The aqueous layer was extracted with CH₂Cl₂ (3 × 5 mL), the combined organics were dried over anhydrous Na₂SO₄ and concentrated under reduced pressures to yield a deep brown-black residue. (*Note: the reaction has only been carried out on this relatively small scale due to difficulty in follow-up column chromatography, that being extreme insolubility of the product in the eluent system. This causes baseline-to-stopcock streaking, significant loss of product and renders full chromatographic purification nearly impossible*). The residue was adsorbed to silica and loaded onto a 10 cm tall × 4 cm wide silica column packed in 5% acetone/hexanes. This eluent was used (c. 700 mL) to elute excess boronic ester and an intensely yellow fluorescent band. The system was switched to 10% acetone/hexanes (c. one column-volume) then to 20% acetone/hexanes (c. 800 mL) which eluted the product. All such visibly yellow and cyan-blue fluorescent eluate was collected and concentrated under reduced pressures to yield 1,8-bis(4-*N,N*-dimethylaminophenyl)-4,5-dimethoxyppyrene as mustard-yellow solid (0.1513 g, c. 50%): ¹H NMR (400 MHz, Chloroform-*d*) δ = 8.50 (d, *J* = 8.1 Hz, 1H), 8.20 (s, 1H), 8.00 (d, *J* = 8.1 Hz, 1H), 7.53 (d, *J* = 8.8 Hz, 2H), 6.91 (d, *J* = 8.8 Hz, 2H), 4.24 (s, 3H), 3.06 (s, 6H); ¹³C{¹H} NMR due

to lack of purity, no carbon NMR was performed; HRMS (EI, positive) calculated for $[C_{34}H_{32}N_2O_2]^+$ $m/z = 500.2464$, found $m/z = 500.2460$, -0.8 ppm difference; R_f (10% EtOAc/hexanes) = 0.32.

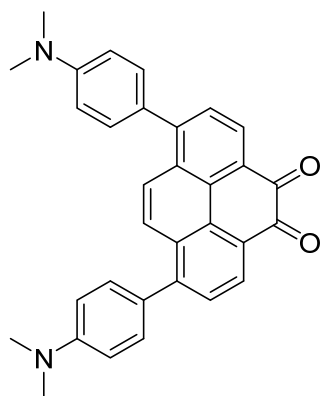
1,8-Diphenylpyren-4,5-dione **2**



This experimental was adapted from a literature procedure on a related system.²⁰ Into a 250 mL RBF that had been flame-dried under vacuum for 2 minutes and cooled under a stream of N_2 were added a magnetic stir bar and 1,8-diphenyl-4,5-dimethoxy pyrene (0.1002 g, 0.2417 mmol, 1.0 eq.). The flask was capped with a rubber septum, dried CH_2Cl_2 (100 mL) was added by syringe and the mixture was stirred to dissolution at room temperature. (*Note: if anhydrous precautions are not taken, the reaction will not go to completion even if a great excess of BBr_3 is added*). 1 M BBr_3 in CH_2Cl_2 was added dropwise by syringe, and the peachy-orange mixture was stirred under N_2 at room temperature for 16 hours. After this time, the orange-brown translucent mixture was quenched with a solution of citric acid monohydrate (1.4940 g, 0.711 mmol, 10 eq. vs boron) in deionized H_2O (40 mL). (*Note: if citric acid is not added to the workup to coordinate boron, the isolated yield will be c. 10% lesser*). An inlet was dipped into the solution, air was bubbled through the mixture and it was vigorously stirred for 1 hour, becoming pineapple-yellow in colour. This was poured into a separatory funnel with deionized H_2O (10 mL) and CH_2Cl_2 (10 mL), the layers were shaken and separated, and the aqueous layer was extracted with CH_2Cl_2 (1×10 mL). The combined organics were brine washed, dried over anhydrous Na_2SO_4 and concentrated under reduced pressures to yield a burgundy residue. This was adsorbed to silica and loaded into a 10 cm tall \times 3 cm wide silica column packed in 50% CH_2Cl_2 /hexanes. The column was eluted with a gradient of this solvent (c. 400 mL) then CH_2Cl_2 (c. 450 mL), which eluted the product as visibly yellow eluate. All such solvent was collected and concentrated under reduced pressures to yield 1,8-diphenylpyren-4,5-dione **2** (0.0714 g, 77%) as a red-orange solid: 1H NMR (400 MHz, Chloroform- d) $\delta = 8.59$ (d, $J = 7.6$ Hz, 1H), 7.86 (s, 1H), 7.73 (d, $J = 7.8$ Hz, 1H), 7.53 (m, 5H); uDEFT $^{13}C\{^1H\}$ NMR (100 MHz, Chloroform- d) $\delta = 180.7, 148.8, 139.4, 130.2, 130.1, 129.8, 129.6, 129.5$,

128.8, 128.6, 125.5; HRMS (EI, positive) calculated for $[C_{28}H_{16}O_2]^+$ $m/z = 384.1150$, found $m/z = 384.1153$, 0.8 ppm difference; R_f (20% EtOAc/hexanes) = 0.47.

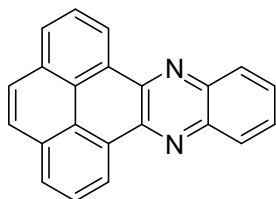
1,8-Bis(4-*N,N*-dimethylaminophenyl)pyren-4,5-dione **3**



This experimental was adapted from a literature procedure on a related system.²⁰ Into a 250 mL RBF that had been flame-dried under vacuum for 2 minutes and cooled under a stream of N_2 were added a magnetic stir bar and 1,8-bis(4-*N,N*-dimethylaminophenyl)-4,5-dimethoxy pyrene (0.1205 g, 0.2407 mmol, 1.0 eq.). The flask was capped with a rubber septum, dried CH_2Cl_2 (100 mL) was added by syringe and the mixture was stirred to dissolution at room temperature. (*Note: if anhydrous precautions are not taken, the reaction will not go to completion even if a great excess of BBr_3 is added*). 1 M BBr_3 in CH_2Cl_2 was added dropwise by syringe, and the orange-brown mixture was stirred under N_2 at room temperature for 16 hours. After this time the milky beige mixture was quenched with a solution of citric acid monohydrate (1.4592 g, 0.6944 mmol, 10 eq. vs boron) in deionized H_2O (40 mL) that was adjusted to pH 7-8 with 5 M NaOH solution. (*Note: if citric acid alone is used in this step, the aniline nitrogen becomes protonated and oxidation does not occur on any timescale. If the solution is more basic than pH 11 then the oxidation will also not occur, due to unavailability of protons for the O_2 to H_2O reduction process*). An inlet was dipped into the solution, air was bubbled through the mixture and it was vigorously stirred for 3 hours, becoming deep wine red-purple. (*Note: times less than 3 hours lead to incomplete oxidation, and the vicinal diol intermediate complicates follow-up chromatographic purification*). The mixture was poured into a separatory funnel with CH_2Cl_2 (10 mL) and deionized H_2O (10 mL) and the layers were shaken then separated. The aqueous layer was extracted with CH_2Cl_2 (3×10 mL) (*Note: caution, emulsions!*) and all organics were dried over anhydrous Na_2SO_4 and concentrated under reduced pressures to yield a deep purple residue. This was adsorbed to

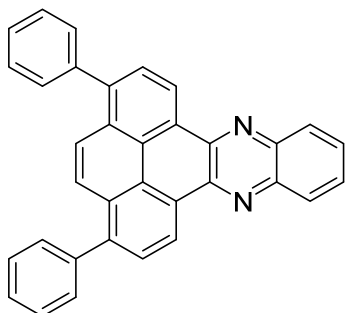
silica and loaded onto a 7.5 cm tall × 3 cm wide silica column packed in 1% EtOAc/CH₂Cl₂. A gradient elution was used of this solvent (c. 300 mL), which eluted a brown-yellow band, followed by 2% EtOAc/CH₂Cl₂ (c. 600 mL) to elute the deep purple-black band. This visibly pink-purple eluate was collected and concentrated to yield 1,8-bis(4-*N,N*-dimethylaminophenyl)pyren-4,5-dione **3** (0.0766 g, 67%) as a dark purple-black solid: ¹H NMR (400 MHz, Chloroform-*d*) δ = 8.55 (d, *J* = 7.7 Hz, 1H), 8.02 (s, 1H), 7.69 (d, *J* = 7.7 Hz, 1H), 7.45 (d, *J* = 8.8 Hz, 2H), 6.87 (d, *J* = 8.8 Hz, 2H), 3.07 (s, 6H); uDEFT ¹³C{¹H} NMR (100 MHz, Chloroform-*d*) δ = 180.9, 150.7, 149.3, 131.1, 130.3, 130.1, 129.6, 129.1, 128.7, 127.1, 125.5, 112.2, 40.6; HRMS (EI, positive) calculated for [C₃₂H₂₆N₂O₂]⁺ *m/z* = 470.1994, found *m/z* = 470.1996, 0.4 ppm difference; R_f (20% EtOAc/hexanes) = 0.13.

Phenanthro[4,5-*abc*]phenazine H₂quin



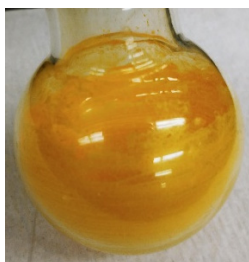
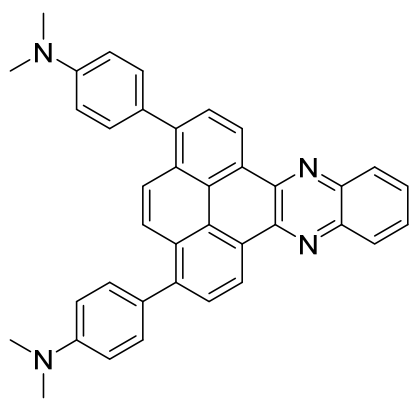
This experimental was adapted from a literature procedure.²¹ Into a 25 mL RBF were added a magnetic stir bar, pyren-4,5-dione **1** (0.1509 g, 0.6498 mmol, 1.0 eq.) and *o*-phenylene diamine (0.0781 g, 0.722 mmol, 1.1 eq.). Glacial acetic acid (15 mL) was added, the flask was equipped with a water condenser and refluxed on a 125 °C oil bath for 1 hour. Over this time, the mixture became pale-orange then precipitated fluffy yellow solids. The mixture was cooled to room temperature and poured into ice-H₂O (80 mL). The mixture was stirred and then suction filtered, washing the filter cake with excess ice-cold H₂O to remove acetic acid and drying *in-vacuo*. This yielded phenanthro[4,5-*abc*]phenazine **H₂quin** (0.1872 g, 95%) as a fluffy canary yellow solid: ¹H NMR (400 MHz, Chloroform-*d*) δ = 9.61 (dd, *J* = 7.7, 1.2 Hz, 1H), 8.41 – 8.37 (m, 1H), 8.30 (dd, *J* = 7.7, 1.2 Hz, 1H), 8.10 (t, *J* = 7.7 Hz, 1H), 8.05 (s, 1H), 7.90 (m, 1H); uDEFT ¹³C{¹H} NMR (100 MHz, Chloroform-*d*) δ = 143.5, 142.6, 131.6, 130.0, 129.8, 129.7, 129.4, 127.4, 127.0, 126.3, 124.1; HRMS (EI, positive) calculated for [C₂₂H₁₂N₂]⁺ *m/z* = 304.1000, found *m/z* = 304.1003, 1.0 ppm difference; R_f (20% acetone/hexanes) = 0.60; IR (cm⁻¹) = 3045 (weak, broad), 1623 (weak, broad), 1480 (mid, sharp), 1359 (mid, sharp) (Lit.²¹ 3040, 1484, 1362); mp (uncorr. acetic acid) = 275-277 °C (Lit.²¹ 277.6-278.4 from PhCl); UV-vis (ε, DMSO) = 437 (5 000), 346 (6 000), 327 (10 000).

1,8-Diphenylphenanthro[4,5-*abc*]phenazine Ph₂quin



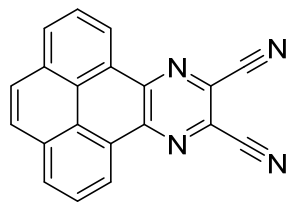
This experimental was adapted from a literature procedure on a related system.²¹ Into a 10 mL RBF were added a magnetic stir bar, 1,8-diphenylpyren-4,5-dione **2** (0.0306 g, 0.0796 mmol, 1.0 eq.) and *o*-phenylene diamine (0.0136 g, 0.123 mmol, 1.5 eq.). Glacial acetic acid (4.5 mL) was added, the mixture was gently sonicated to break up chunks then the flask was equipped with a water condenser and refluxed in a 125 °C oil bath for 2 hours. Over this time the mixture turned from intense red-orange to pale-orange, and after 2 hours the mixture was cooled to room temperature. It was poured into ice-H₂O (30 mL) and stirred then suction filtered and washed with excess ice-cold H₂O to remove acetic acid. Drying *in-vacuo* yielded a pale orange powdered solid (*Note: caution, static!*) which was adsorbed to silica and loaded onto a 7.5 cm tall × 3 cm wide silica column packed in 50% CH₂Cl₂/hexanes. This solvent (*c.* 700 mL) was used to elute a deep orange band, and when this colour had drained from the column elution was stopped. This solvent was collected and concentrated under reduced pressures. The solid was taken up in CH₂Cl₂ and allowed to evaporate under ambient pressure, yielding 1,8-diphenylphenanthro[4,5-*abc*]phenazine **Ph₂quin** (0.0255 g, 70%) as a golden yellow solid: ¹H NMR (400 MHz, Chloroform-*d*) δ = 9.71 (d, *J* = 7.9 Hz, 2H), 8.42 (m, 2H), 8.14 – 8.07 (m, 4H), 7.91 (m, 2H), 7.65 (d, *J* = 6.9 Hz, 3H), 7.57 (t, *J* = 7.3 Hz, 4H), 7.51 – 7.47 (m, 2H); uDEFT ¹³C{¹H} NMR (100 MHz, Chloroform-*d*) (10/15 carbons identified) δ = 130.5, 130.1, 129.7, 129.2, 129.1, 128.7, 128.6, 127.8, 125.3, 123.9; HRMS (EI, positive) calculated for [C₃₄H₂₀N₄]⁺ *m/z* = 456.1626, found *m/z* = 456.1628, 0.4 ppm difference; R_f (20% EtOAc/hexanes) = 0.77; IR (cm⁻¹) = 3058 (weak, broad), 2922 (weak, broad), 1476 (mid, sharp), 1353 (mid, sharp); mp (uncorr. 50% CH₂Cl₂/hexanes) = >360 °C; Anal. Calcd.: C, 89.45; H, 4.42; N, 6.14. Found: C, 87.43 (inefficient comb.); H, 4.45; N, 5.86; UV-vis (ε, DMSO) = 451 (9 000), 339 (14 000), 294 (21 000).

1,8-Bis(4-*N,N*-dimethylaminophenyl)phenanthro[4,5-*abc*]phenazine NMe₂quin



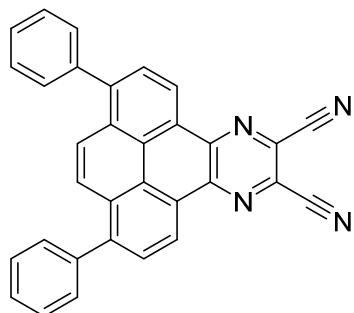
This experimental was adapted from a literature procedure on a related system.²¹ Into a 10 mL RBF were added a small magnetic stir bar, 1,8-bis(4-*N,N*-dimethylaminophenyl)pyren-4,5-dione **3** (0.0535 g, 0.114 mmol, 1.0 eq.) and *o*-phenylene diamine. Glacial acetic acid (6 mL) was added, the mixture was gently sonicated to break up chunks and then it was equipped with a water condenser and refluxed in a 125 °C oil bath for 2 hours. Over this time, it went from deep purple-black to muddy red-brown. After 2 hours the mixture was cooled to room temperature and poured into H₂O (30 mL). It was brought to pH 8-9 with solid NaOH pellets and then poured into a separatory funnel with CH₂Cl₂ (20 mL). The layers were shaken and separated, and the aqueous layer was extracted with CH₂Cl₂ (5 × 5 mL). The combined organics were dried over anhydrous Na₂SO₄ and concentrated under reduced pressures to yield a mustard yellow solid. This was adsorbed to silica and loaded onto a 7.5 cm tall × 3 cm wide silica column packed in 50% CH₂Cl₂/hexanes. Gradient elution using this solvent (*c.* 50 mL) eluted a green fluorescent band, switching to CH₂Cl₂ (*c.* 100 mL) and then 2% EtOAc/CH₂Cl₂ (*c.* 150 mL) eluted an orange-red band which was orange fluorescent. All eluate of such colour was collected and concentrated. The solid was taken up in CH₂Cl₂ and allowed to evaporate at ambient pressure, yielding 1,8-bis(4-*N,N*-dimethylaminophenyl)phenanthro[4,5-*abc*]phenazine **NMe₂quin** (0.0501 g, 81%) as a saffron-yellow solid: ¹H NMR (400 MHz, Chloroform-*d*) δ = 9.65 (d, *J* = 8.0 Hz, 1H), 8.39 (m, 1H), 8.20 (s, 1H), 8.06 (d, *J* = 8.0 Hz, 1H), 7.87 (m, 1H), 7.57 (d, *J* = 8.7 Hz, 2H), 6.93 (d, *J* = 8.8 Hz, 2H), 3.08 (s, 6H); uDEFT ¹³C{¹H} NMR (100 MHz, Chloroform-*d*) (6/16 carbons identified) δ = 131.7, 131.4, 129.6, 122.3, 112.5, 29.9; HRMS (EI, positive) calculated for [C₃₈H₃₀N₄]⁺ *m/z* = 542.2470, found *m/z* = 542.2488, 3.3 ppm difference; R_f (50% CH₂Cl₂/hexanes) = 0.20; IR(cm⁻¹) = 2882 (weak, broad), 2805 (weak, broad), 1607 (strong, sharp), 1353 (strong, sharp); mp (uncorr. 2% EtOAc/CH₂Cl₂) = 310-320 °C (decomp.); Anal. Calcd.: C, 84.10; H, 5.57; N, 10.32. Found: C, 83.53 (inefficient comb.); H, 5.12; N, 10.15; UV-vis (ε, CH₂Cl₂) = 469 (14 000), 369 (29 000), 294 (33 000).

Phenanthro[4,5-*fg*h]quinoxaline-10,11-dicarbonitrile H₂pyr



This experimental was adapted from a literature procedure.²² Into a 25 mL RBF were added a magnetic stir bar, pyren-4,5-dione **1** (0.1515 g, 0.6523 mmol, 1.0 eq.) and diaminomaleonitrile (0.1061 g, 0.9815 mmol, 1.5 eq.). Glacial acetic acid (15 mL) was added, a water condenser was equipped to the flask and the mixture was refluxed on a 125 °C oil bath for 24 hours. The brown mixture was cooled to room temperature, poured into ice-H₂O (80 mL) and stirred. The mixture was suction filtered, slowly because of fine particulate, the filter cake was washed with excess ice-cold H₂O to remove acetic acid and dried *in vacuo* overnight into a muddy-brown solid. The solid was adsorbed to silica and loaded onto a 10 cm tall × 3 cm wide silica column packed in 20% CH₂Cl₂/hexanes. Gradient elution using this solvent (100 mL), then 40% CH₂Cl₂/hexanes (400 mL) eluted a cyan-blue fluorescent band first, followed by green fluorescent product. The system was switched to 60 % CH₂Cl₂/hexanes (600mL) to speed up elution of the product. Just before a visibly orange band reached the bottom of the column, elution was stopped and all green fluorescent eluate was collected and concentrated. The solid was taken up in CH₂Cl₂ and allowed to evaporate at ambient pressure, yielding phenanthro[4,5-*fg*h]quinoxaline-10,11-dicarbonitrile **H₂pyr** (0.0417 g, 21%) as a saffron yellow solid: ¹H NMR (400 MHz, Chloroform-*d*) δ = 9.41 (dd, *J* = 7.8, 1.2 Hz, 1H), 8.46 (dd, *J* = 7.8, 1.2 Hz, 1H), 8.19 (t, *J* = 7.8 Hz, 1H), 8.13 (s, 1H); uDEFT ¹³C{¹H} NMR (100 MHz, Chloroform-*d*) (8/9 carbons identified) δ = 150.1, 131.7, 131.6, 130.6, 127.8, 126.7, 125.4, 114.0; HRMS (EI, positive) calculated for [C₂₀H₈N₄]⁺ *m/z* = 304.0749, found *m/z* = 304.0745, -1.3 ppm difference; R_f (40% CH₂Cl₂/hexanes) = 0.40; IR (cm⁻¹) = 3056 (weak, broad), 2238 (weak, sharp), 1623 (mid, sharp), 1495 (mid, sharp), 1362 (strong, sharp) (Lit.²³ 3060, 2240, 1625, 1500); mp (uncorr. 60% CH₂Cl₂/hexanes) = 340-350 °C (decomp.) (Lit.²³ >330 °C from acetic acid); Anal. Calcd. for C₂₀H₈N₄: C, 78.94; H, 2.65; N, 18.41. Found: C, 77.79 (inefficient comb.); H, 2.72; N, 18.30; UV-vis (ε, DMSO) = 440 (6 000), 355 (15 000), 313 (13 000) (Lit.²³ 283, 312, 355 in DMF).

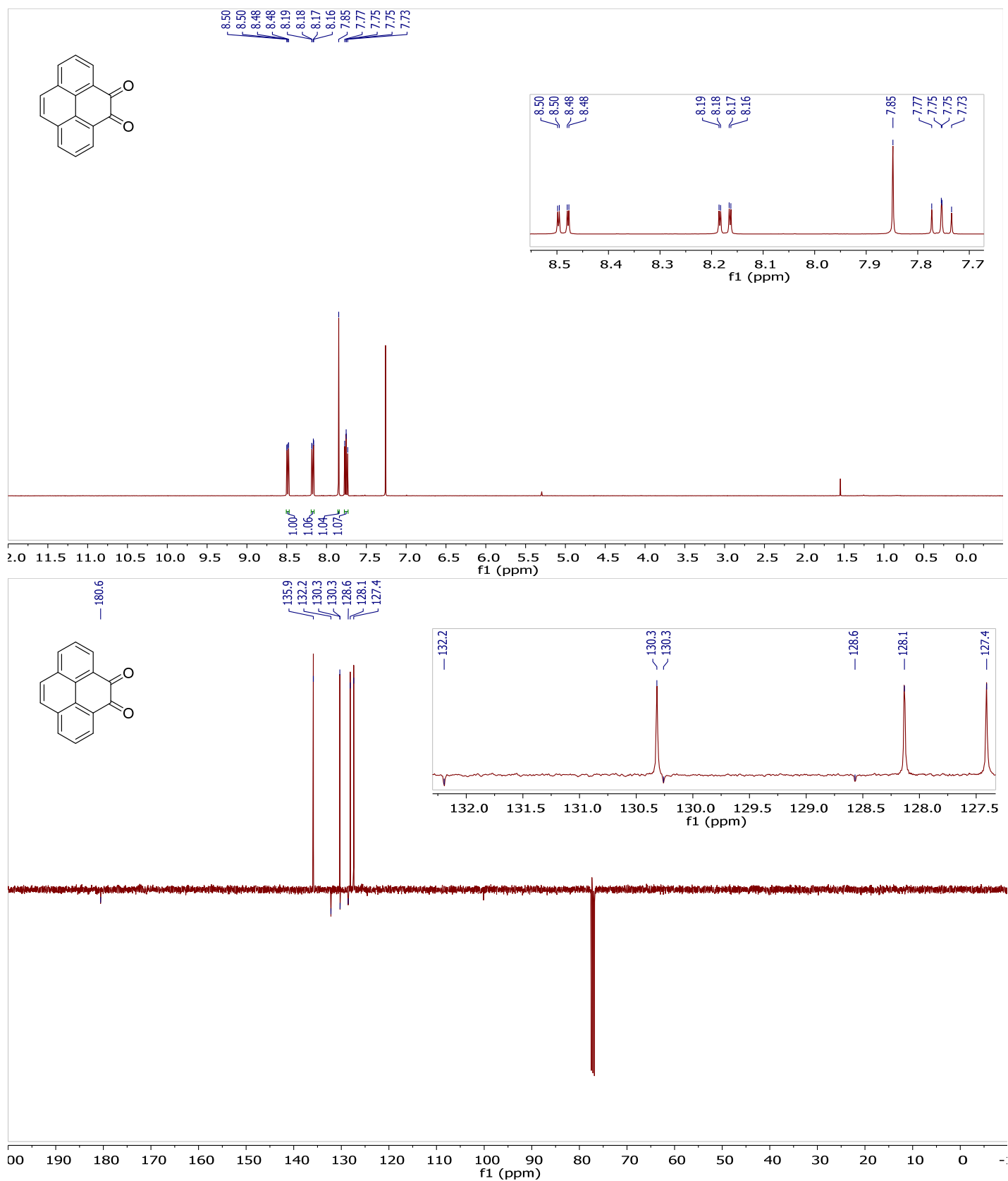
1,8-Diphenylphenanthro[4,5-*fg*h]quinoxaline-10,11-dicarbonitrile Ph₂pyr



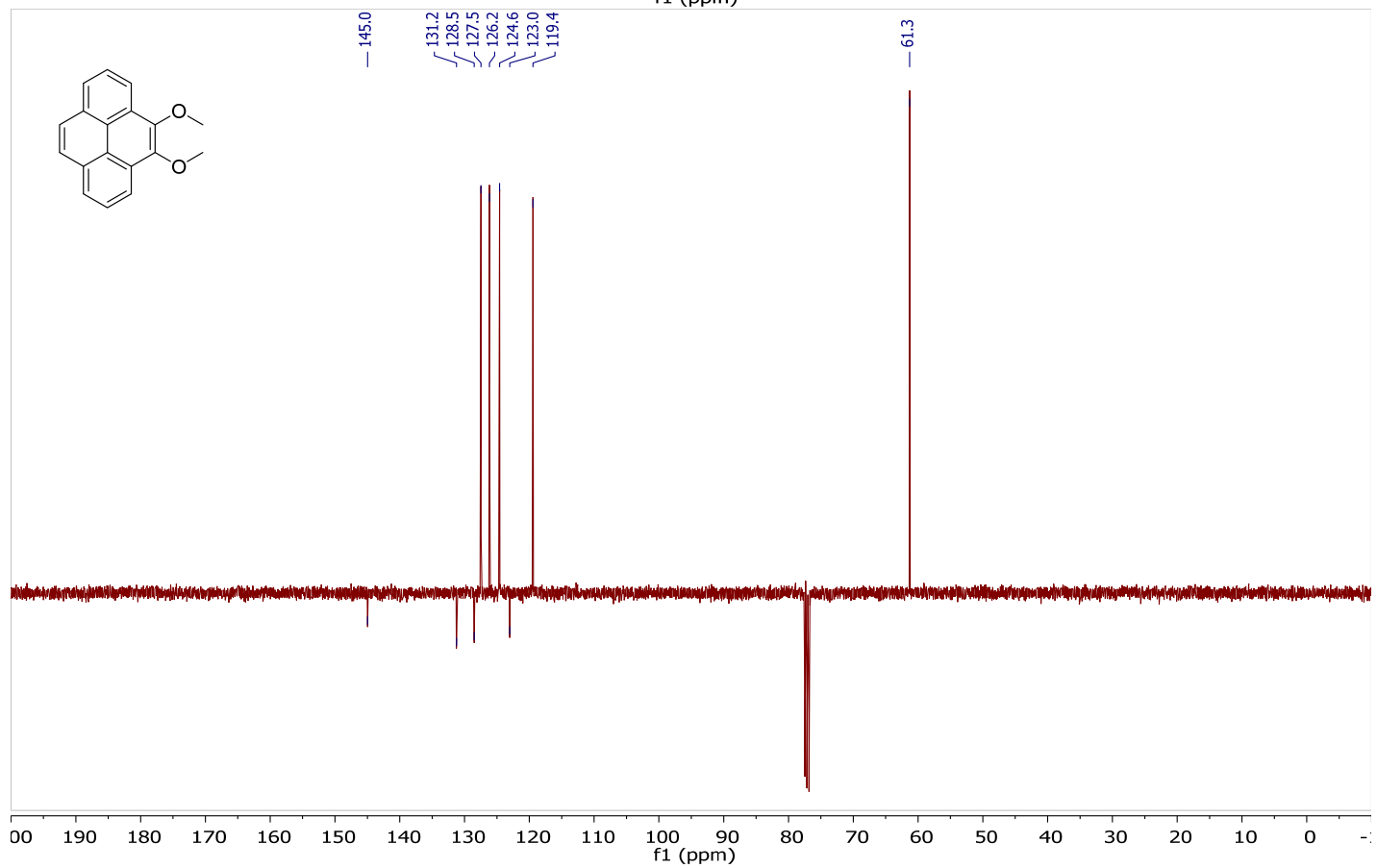
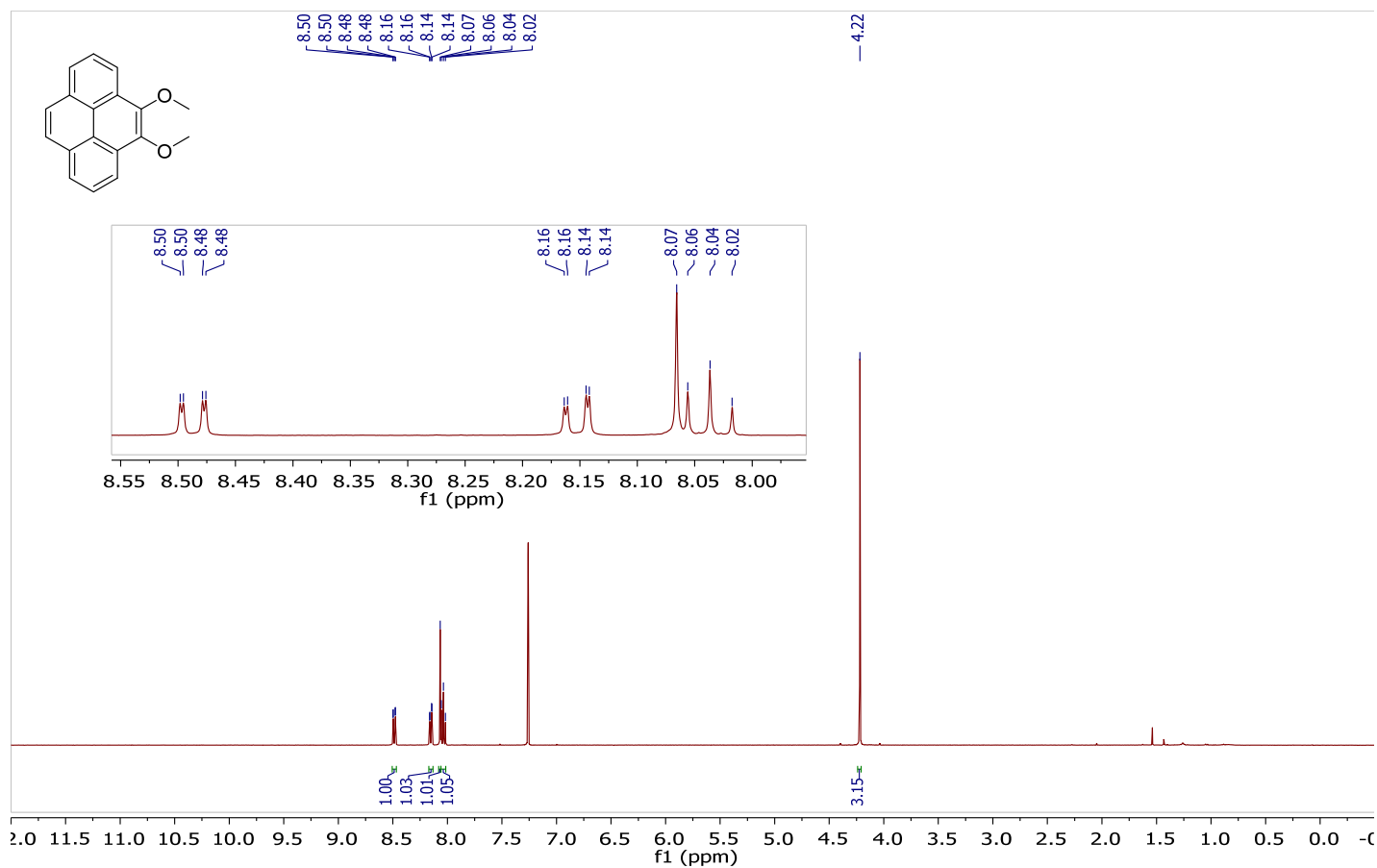
This experimental was adapted from a literature procedure on a related system.²² Into a 10 mL RBF were added a small magnetic stir bar, 1,8-diphenylpyren-4,5-dione **2** (0.0326 g, 0.0848 mmol, 1.0 eq.) and diaminomaleonitrile (0.0186 g, 0.172 mmol, 2.0 eq.). Glacial acetic acid (4.5 mL) was added, the mixture was gently sonicated to break up chunks and the flask was equipped with a water condenser and refluxed in a 125 °C oil bath for 24 hours. Over this time the mixture became intensely red then deep brown-black. After 24 hours the mixture was cooled to room temperature and poured into H₂O (20 mL), then brought up to pH 8-9 with solid NaOH pellets. The mixture was poured into a separatory funnel with CH₂Cl₂ (10 mL) and H₂O (10 mL), and the layers were gently shaken and separated (*Note: caution, emulsion!*). The aqueous layer was extracted with CH₂Cl₂ (5 × 5 mL), the aqueous layer was removed, all emulsion was taken with the organics, and all combined organics were put back into the separatory funnel. The emulsion was broken manually with a stirring rod and the organic layer was drained, dried over anhydrous Na₂SO₄ and concentrated under reduced pressures to yield a brown residue. This was adsorbed to silica and loaded onto a 10 cm tall × 2.5 cm wide silica column packed in 20% CH₂Cl₂/hexanes. Gradient elution using this solvent (*c.* 150 mL) eluted a cyan fluorescent band and then 30% CH₂Cl₂/hexanes eluted the product as an orange band. All such eluate was collected and concentrated under reduced pressures. The solid was taken up in CH₂Cl₂ and allowed to evaporate at ambient pressure, yielding 1,8-diphenylphenanthro[4,5-*fg*h]quinoxaline-10,11-dicarbonitrile **Ph₂pyr** (0.0168 g, 43%) as a red-orange solid: ¹H NMR (400 MHz, Chloroform-*d*) δ = 9.50 (d, *J* = 8.0 Hz, 1H), 8.17 (d, *J* = 8.0 Hz, 1H), 8.13 (s, 1H), 7.64 – 7.54 (m, 5H); uDEFT ¹³C{¹H} NMR (100 MHz, Chloroform-*d*) δ = 144.4, 143.8, 139.9, 130.6, 130.3, 128.8, 129.4, 129.1, 128.8, 127.5, 126.0, 125.7, 125.0, 114.1; HRMS (EI, positive) calculated for [C₃₂H₁₆N₄]⁺ *m/z* = 456.1375, found *m/z* = 456.1391, 3.5 ppm difference; R_f (50% CH₂Cl₂/hexanes) = 0.51; IR (cm⁻¹) = 3055 (weak, broad), 2924 (weak, broad), 2239 (weak, sharp), 1616 (mid, sharp), 1489 (mid, sharp), 1351 (strong, sharp) ; mp (uncorr. 40% CH₂Cl₂/hexanes) = 310-320 °C (decomp.); UV-vis (ε, DMSO) = 454 (8 000), 366 (21 000), 291 (40 000).

Section 4a ^1H NMR and $^{13}\text{C}\{^1\text{H}\}$ NMR of Synthesized Compounds

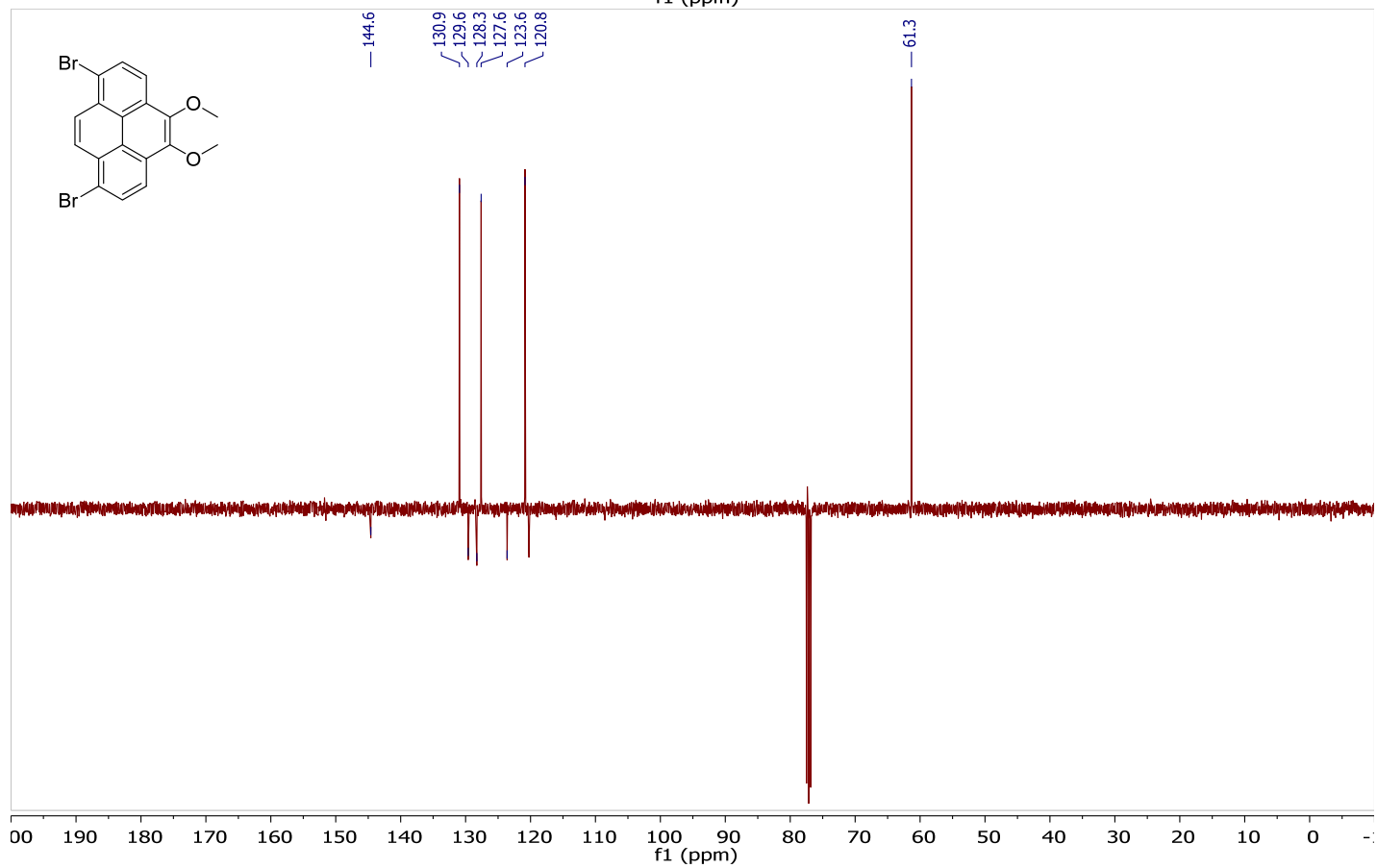
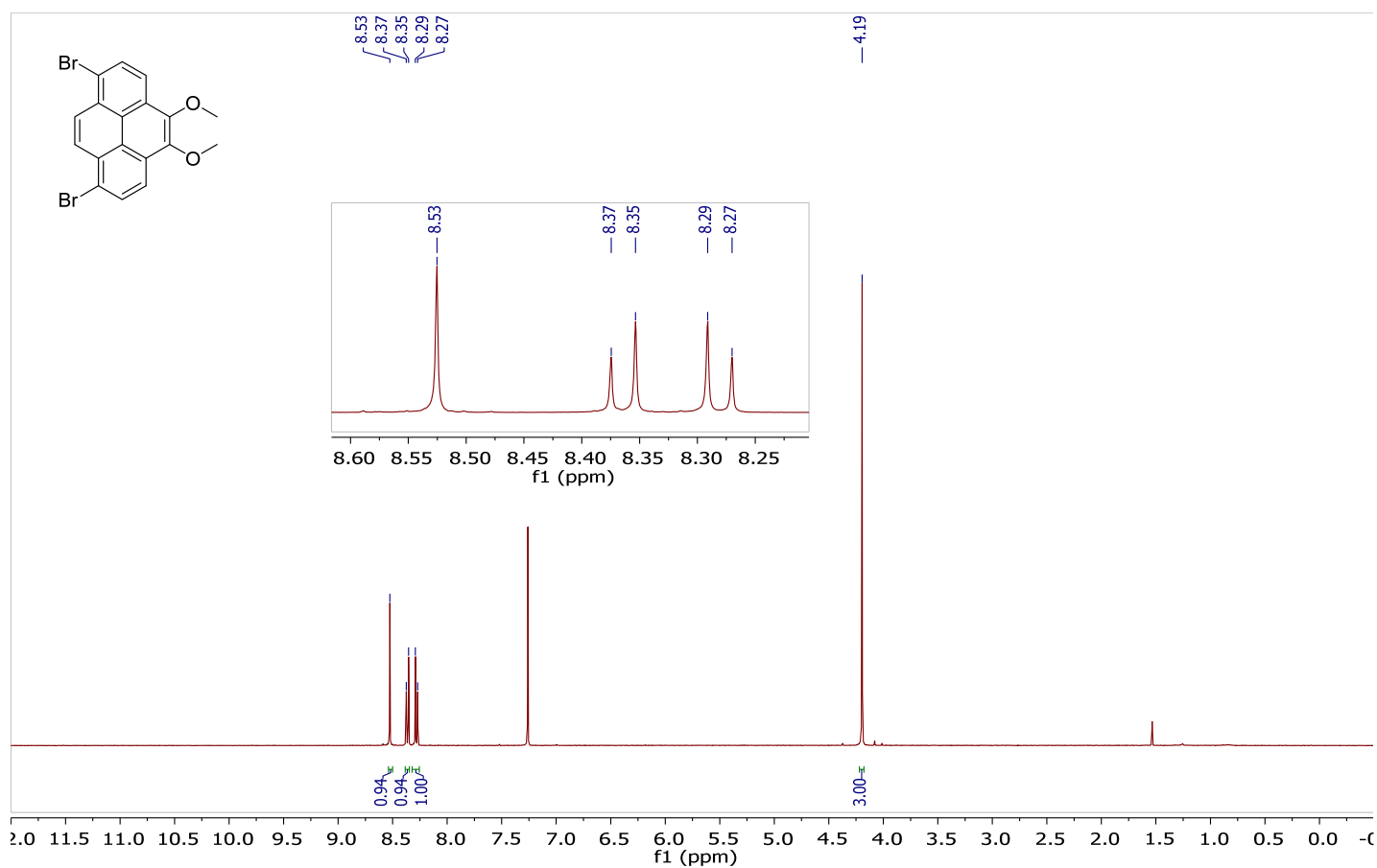
^1H NMR (400 MHz, CDCl_3 , top) and DEPT-Q $^{13}\text{C}\{^1\text{H}\}$ NMR (100 MHz, CDCl_3 , bottom) for pyren-4,5-dione **1**



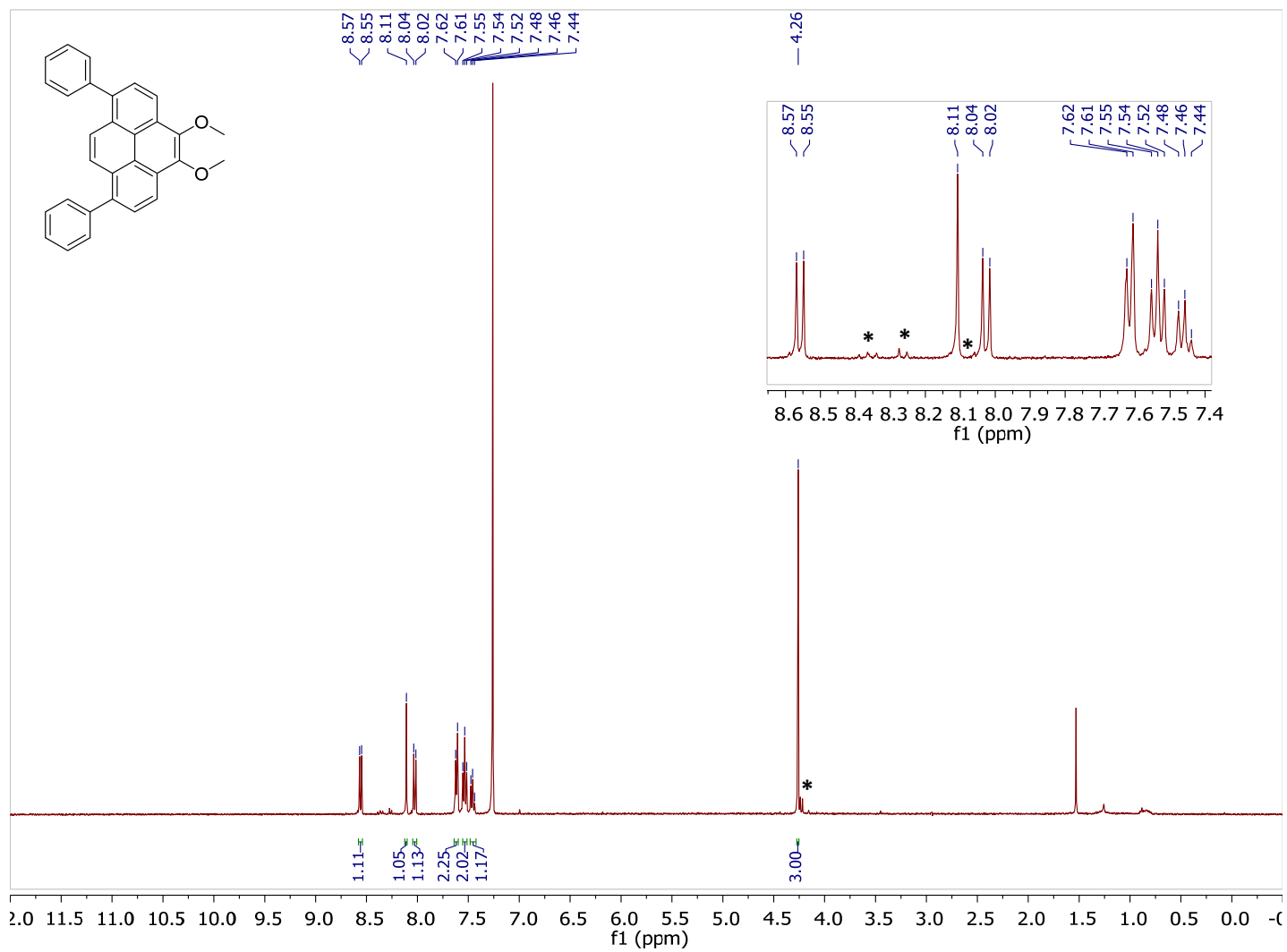
^1H NMR (400 MHz, CDCl_3 , top) and DEPT-Q $^{13}\text{C}\{^1\text{H}\}$ NMR (100 MHz, CDCl_3 , bottom) for 4,5-dimethoxyphenanthrene



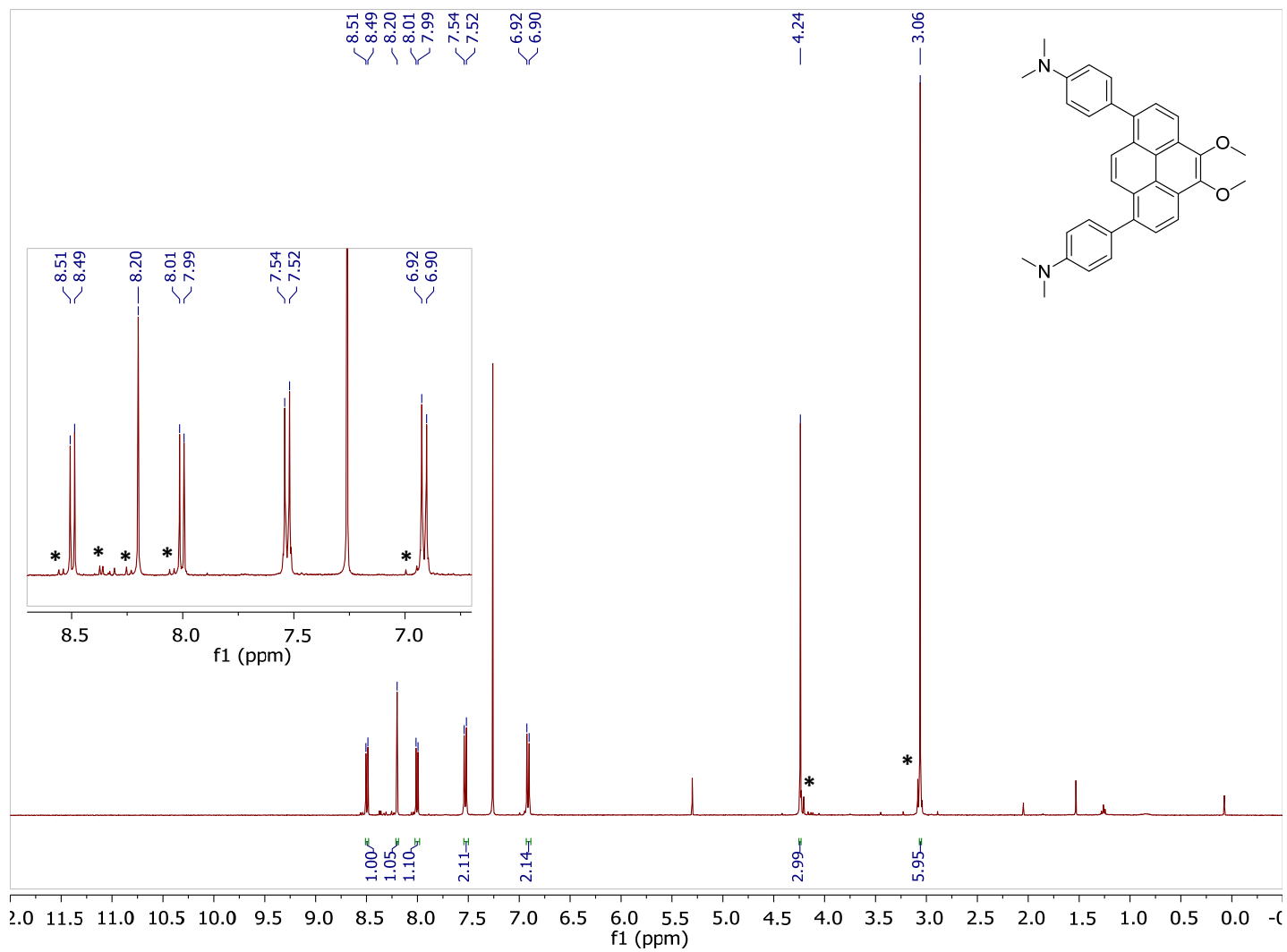
^1H NMR (400 MHz, CDCl_3 , top) and DEPT-Q $^{13}\text{C}\{^1\text{H}\}$ NMR (100 MHz, CDCl_3 , bottom) for 1,8-dibromo-4,5-dimethoxyppyrene



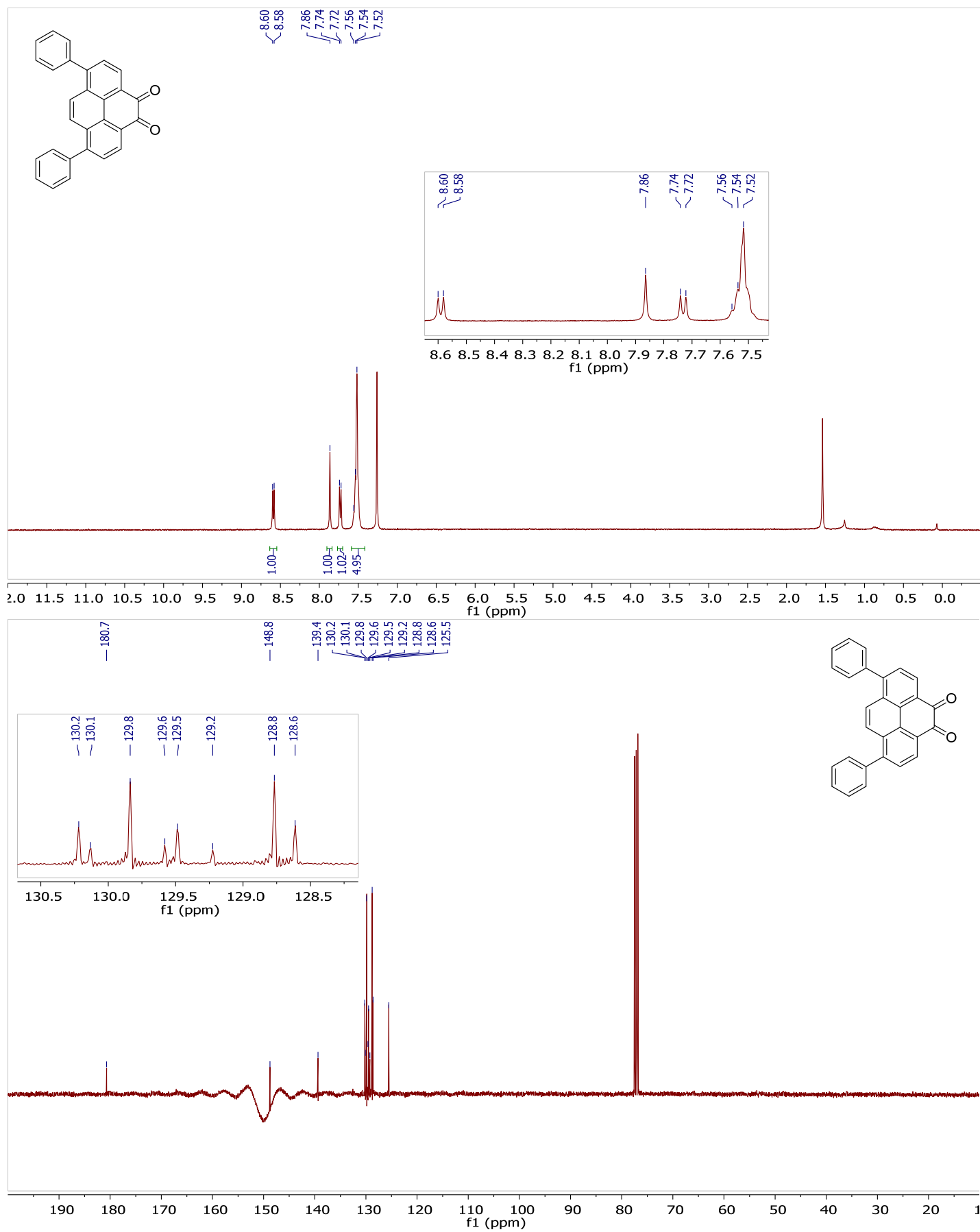
^1H NMR (400 MHz, CDCl_3) for 1,8-diphenyl-4,5-dimethoxyppyrene. The black asterisks mark the positions of extraneous signals, likely from 1-phenyl-4,5-dimethoxyppyrene. Since the sample was impure, no carbon NMR was acquired.



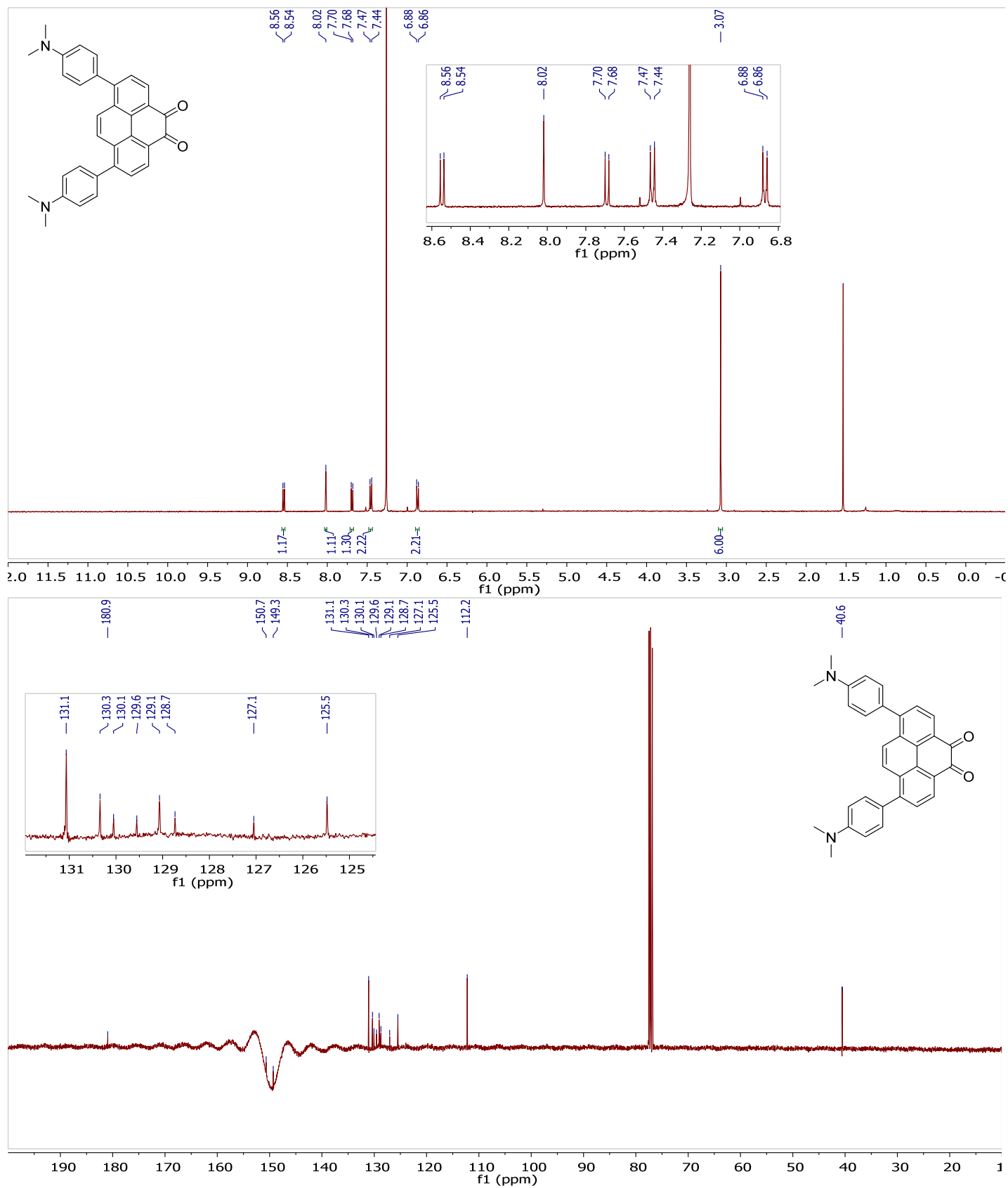
^1H NMR (400 MHz, CDCl_3) for 1,8-bis(4-*N,N*-dimethylaminophenyl)-4,5-dimethoxyppyrene. The black asterisks mark the positions of extraneous signals, likely from 1-dimethylaminophenyl-4,5-dimethoxyppyrene. Since the sample was impure, no carbon NMR was acquired.



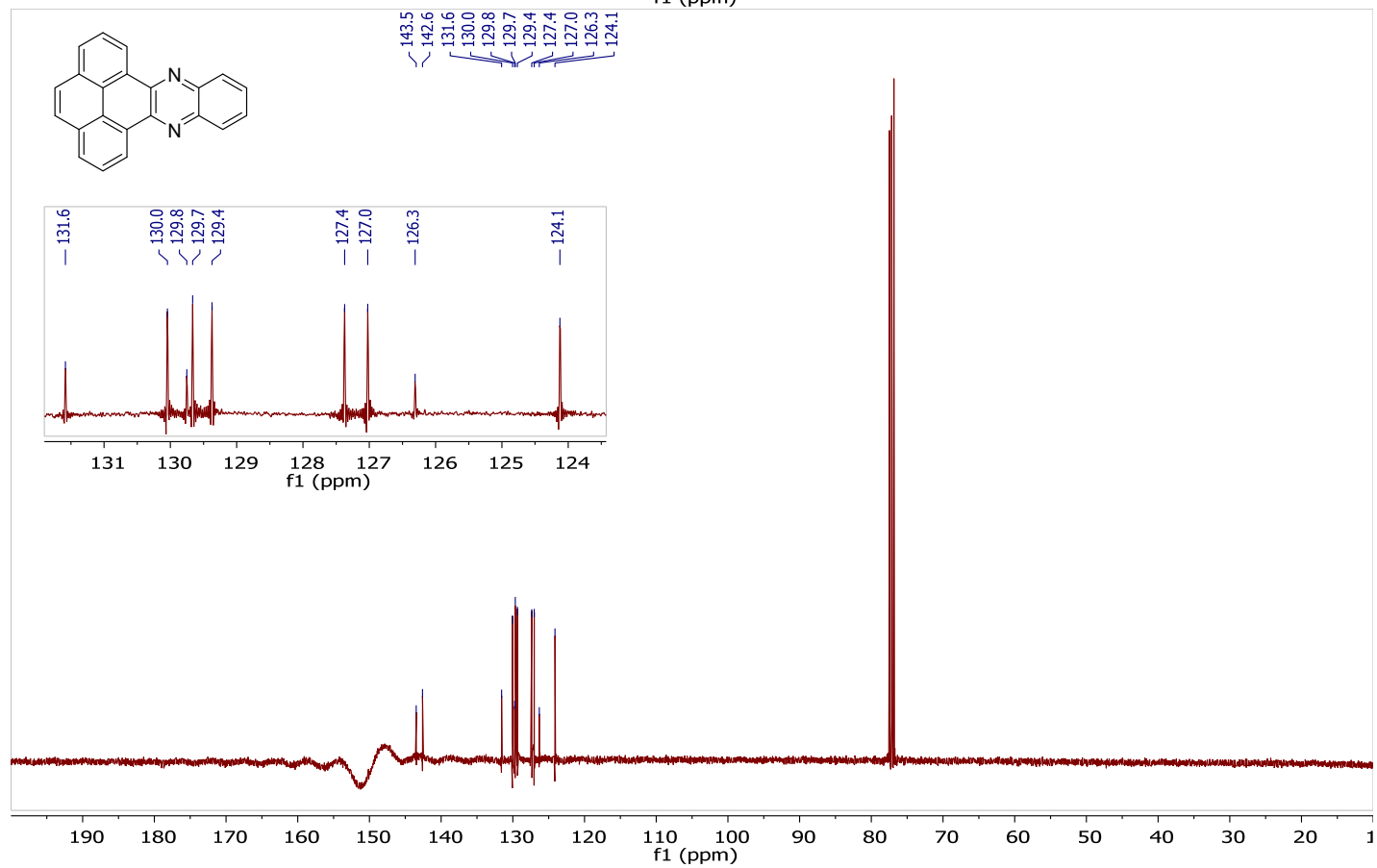
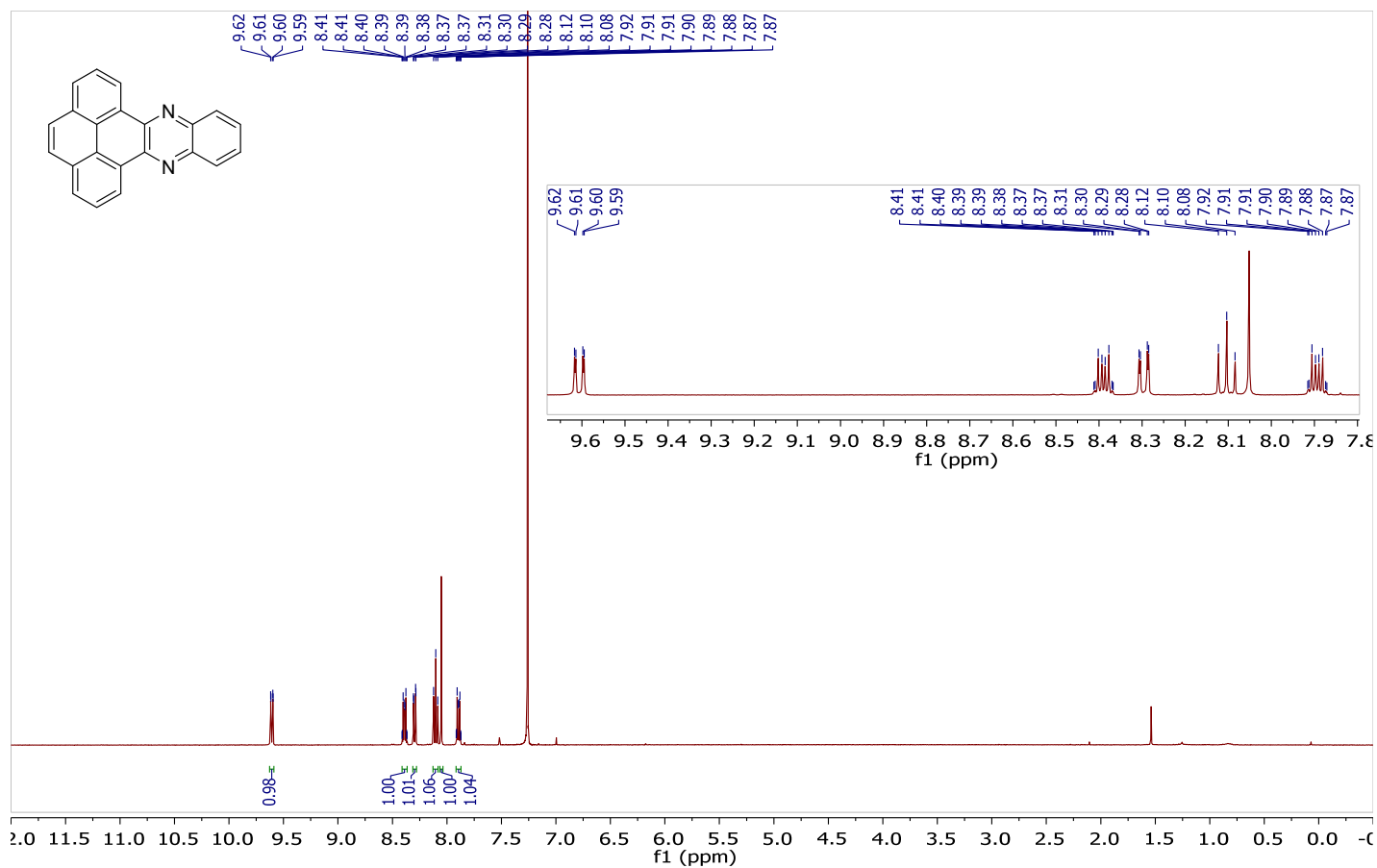
^1H NMR (400 MHz, CDCl_3 , top) and uDEFT $^{13}\text{C}\{^1\text{H}\}$ NMR (100 MHz, CDCl_3 , bottom) for 1,8-diphenylpyren-4,5-dione **2**



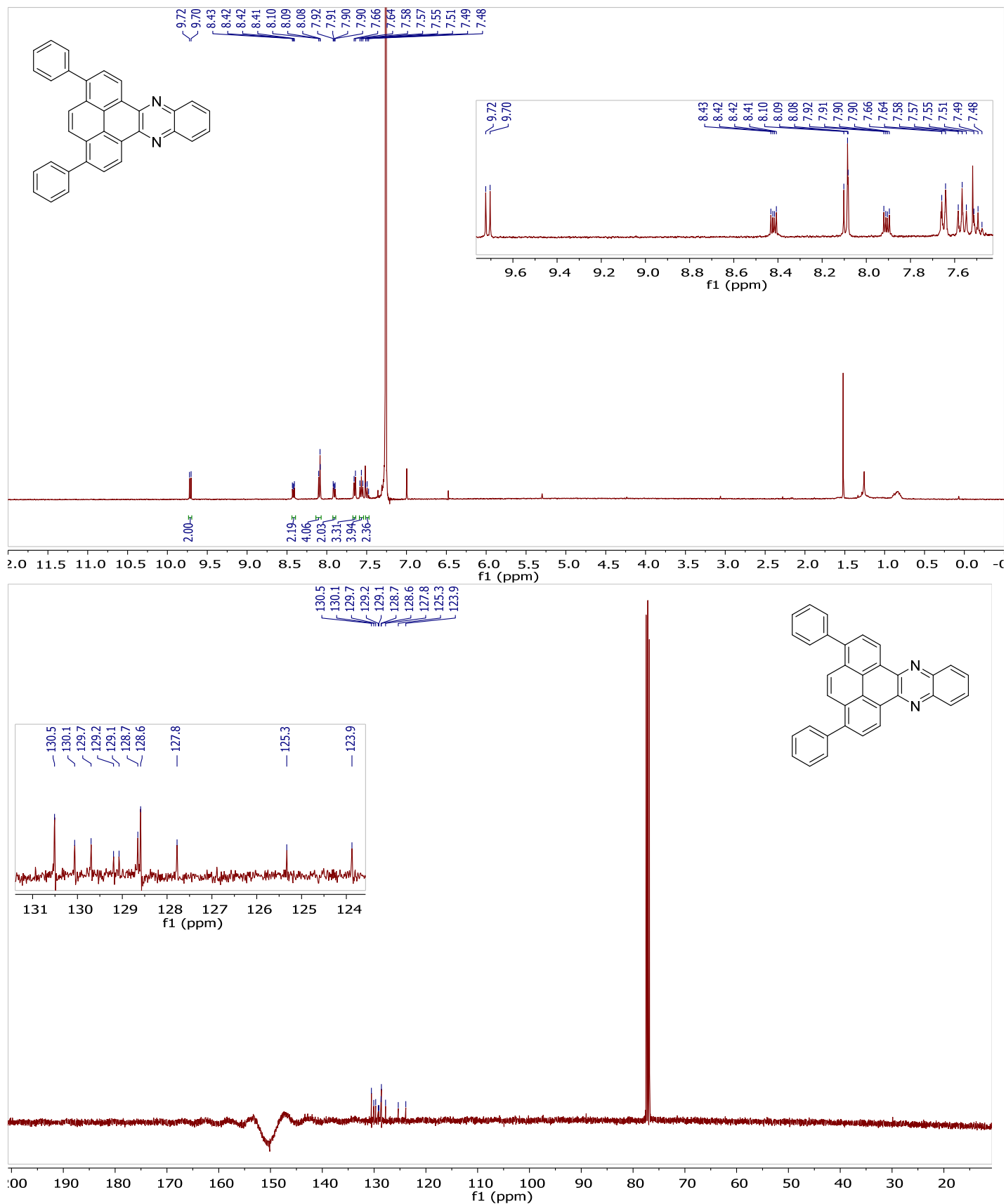
^1H NMR (400 MHz, CDCl_3 , top) and uDEFT $^{13}\text{C}\{^1\text{H}\}$ NMR (100 MHz, CDCl_3 , bottom) for 1,8-bis(4-*N,N*-dimethylaminophenyl)pyren-4,5-dione **3**



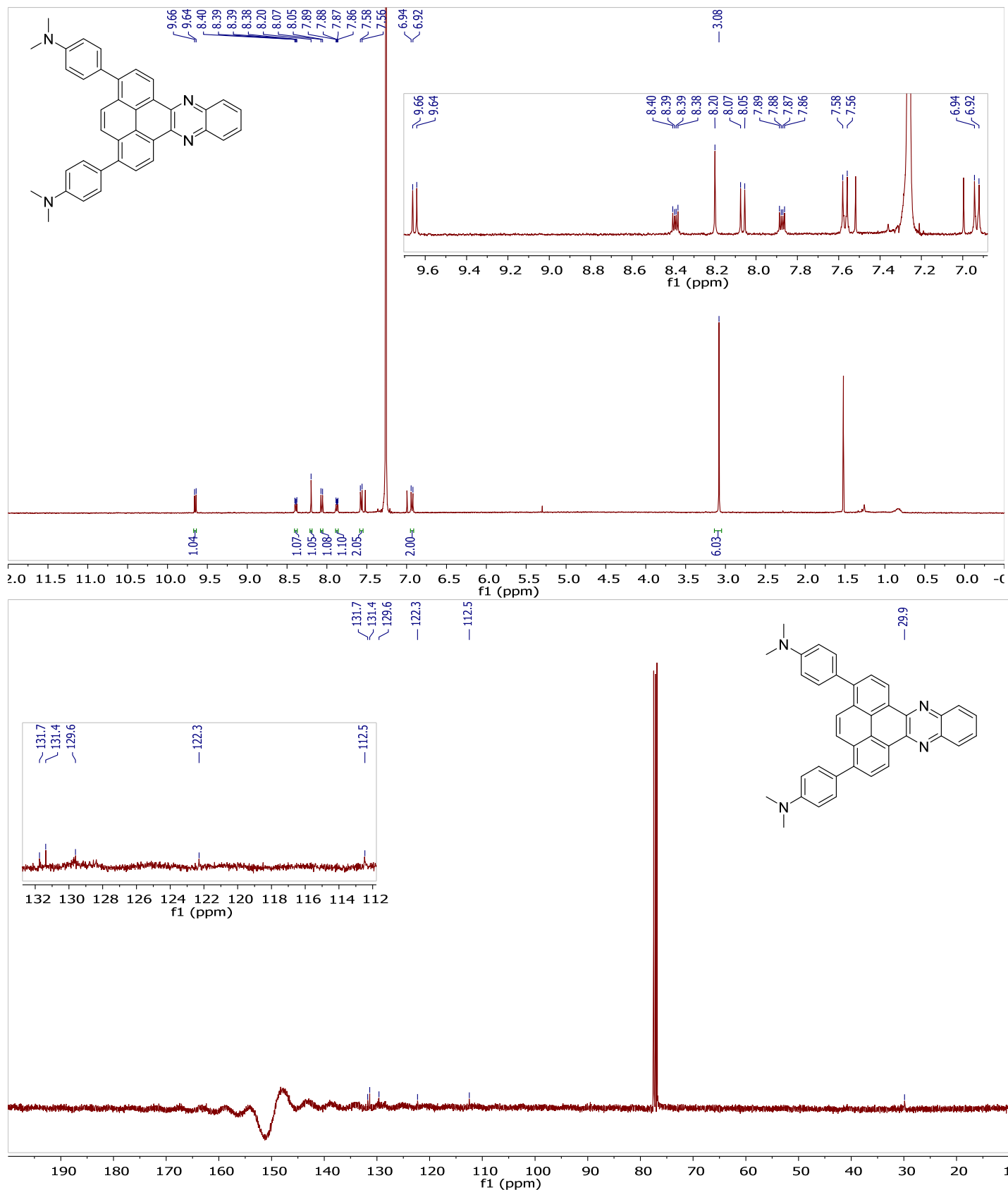
^1H NMR (400 MHz, CDCl_3 , top) and uDEFT $^{13}\text{C}\{^1\text{H}\}$ NMR (100 MHz, CDCl_3 , bottom) for phenanthro[4,5-*abc*]phenazine **H₂quin**



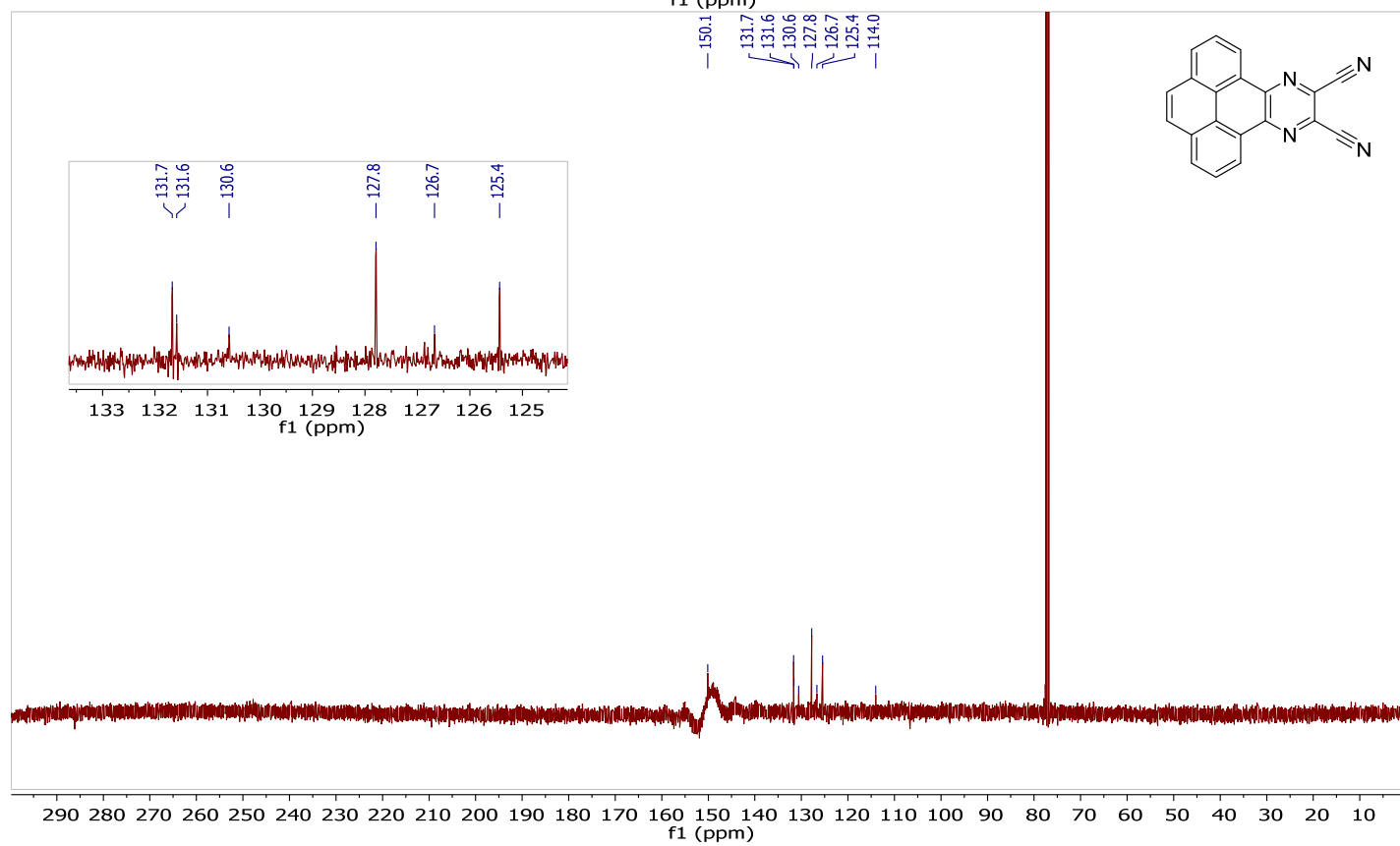
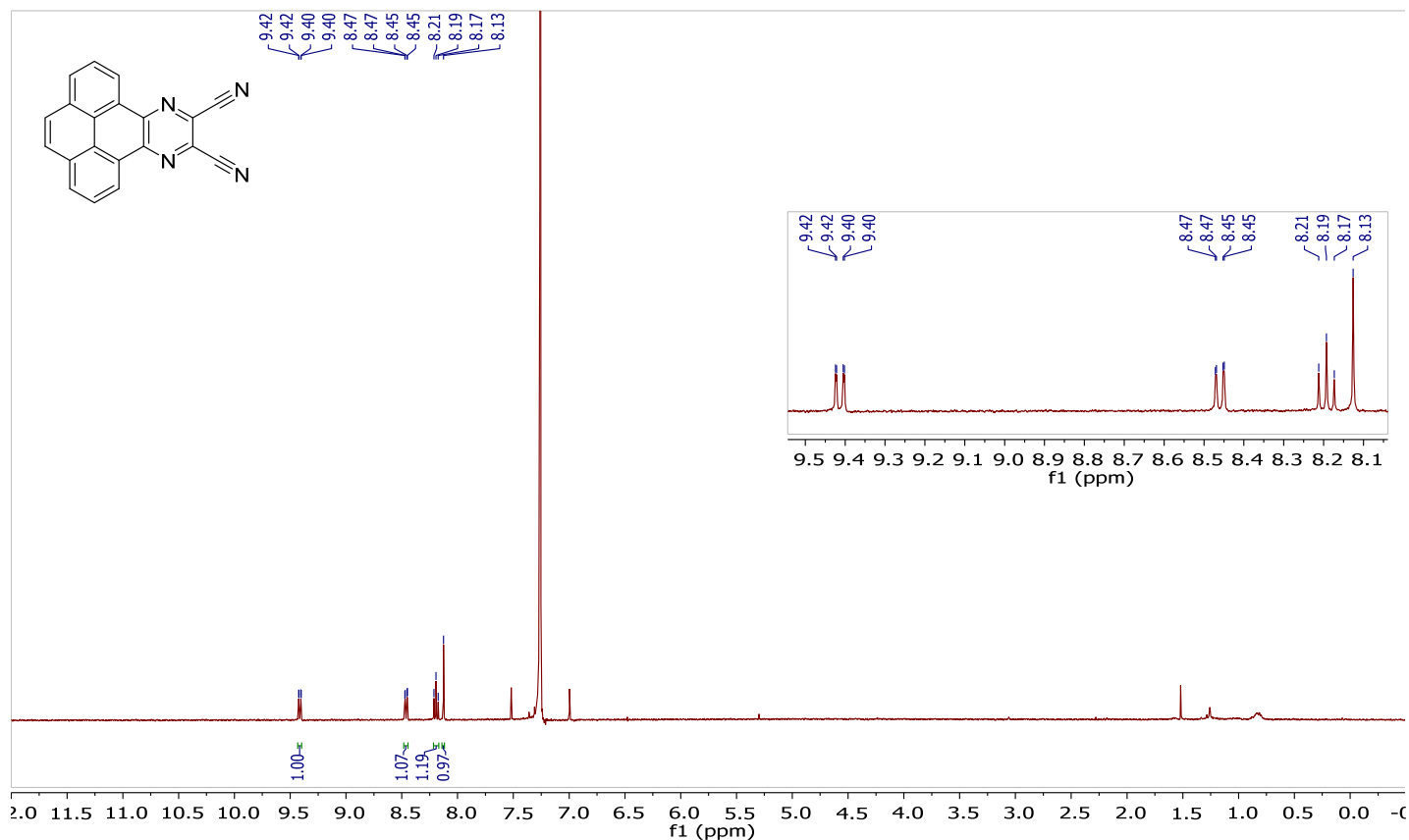
^1H NMR (400 MHz, CDCl_3 , top) and uDEFT $^{13}\text{C}\{^1\text{H}\}$ NMR (100 MHz, CDCl_3 , bottom) for 1,8-diphenylphenanthro[4,5-*abc*]phenazine **Ph₂quin**. Only 10/15 carbons are visible despite running 10 000 scans for 12 hours on a saturated CDCl_3 solution.



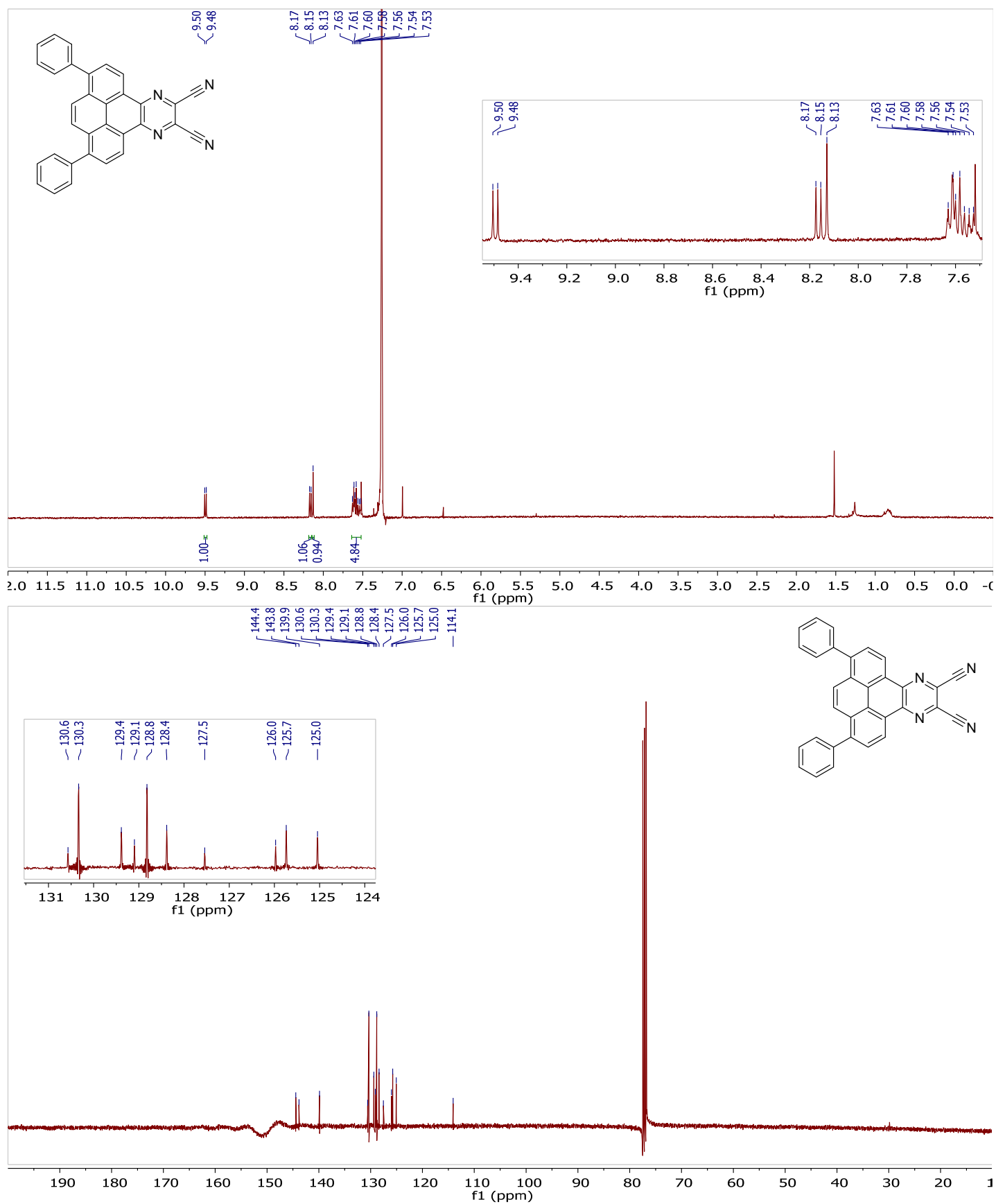
^1H NMR (400 MHz, CDCl_3 , top) and uDEFT $^{13}\text{C}\{^1\text{H}\}$ NMR (100 MHz, CDCl_3 , bottom) for 1,8-bis(4-*N,N*-dimethylaminophenyl)phenanthro[4,5-*abc*]phenazine **NMe₂quin**. Only 6/15 carbons are visible despite running 10 000 scans for 12 hours on a saturated CDCl_3 solution.



^1H NMR (400 MHz, CDCl_3 , top) and uDEFT $^{13}\text{C}\{^1\text{H}\}$ NMR (100 MHz, CDCl_3 , bottom) for phenanthro[4,5-*gh*]quinoxaline-10,11-dicarbonitrile **H₂pyr**. Only 8/9 carbons are visible despite running 10 000 scans for 12 hours on a saturated CDCl_3 solution.



^1H NMR (400 MHz, CDCl_3 , top) and uDEFT $^{13}\text{C}\{^1\text{H}\}$ NMR (100 MHz, CDCl_3 , bottom) for 1,8-diphenylphenanthro[4,5-*fg*h]quinoxaline-10,11-dicarbonitrile **Ph₂p_{yr}**



Section 4b ^1H NMR and $^{13}\text{C}\{^1\text{H}\}$ NMR with TFA, post-HCl and post-grinding

^1H NMR (400 MHz, CDCl_3) of commercial 4-bromo-*N,N*-dimethylaniline a) with and b) without TFA.

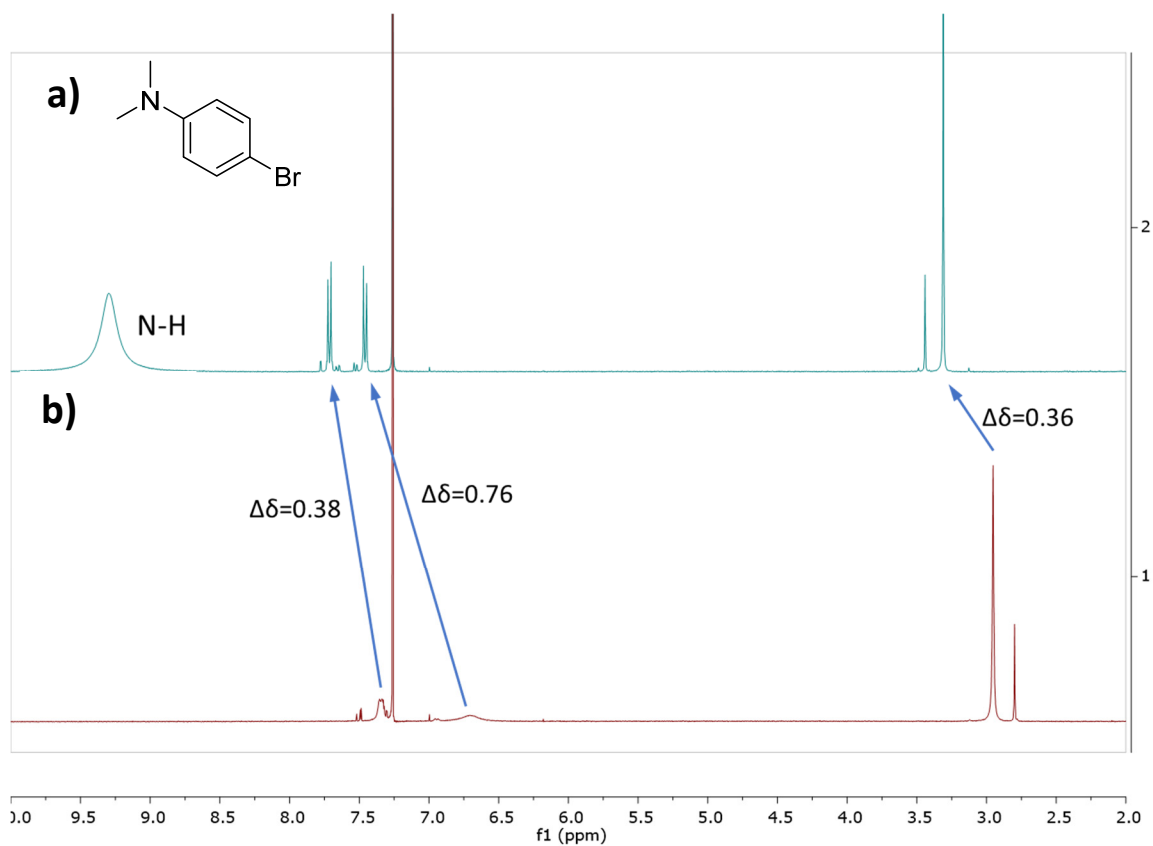
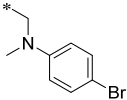
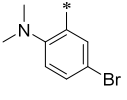
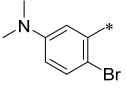


Table S1. Chemical shift table for TFA addition to 4-bromo-*N,N*-dimethylaniline

Signal Assignment	Shift $\delta_1 \rightarrow \delta_2$	Change $\Delta\delta$
	2.95 \rightarrow 3.31	0.36
	6.71 \rightarrow 7.47	0.76
	7.35 \rightarrow 7.73	0.38

^1H NMR (400 MHz, CDCl_3) of aromatic region of phenanthro[4,5-*abc*]phenazine **H₂quin** a) with and b) without TFA.

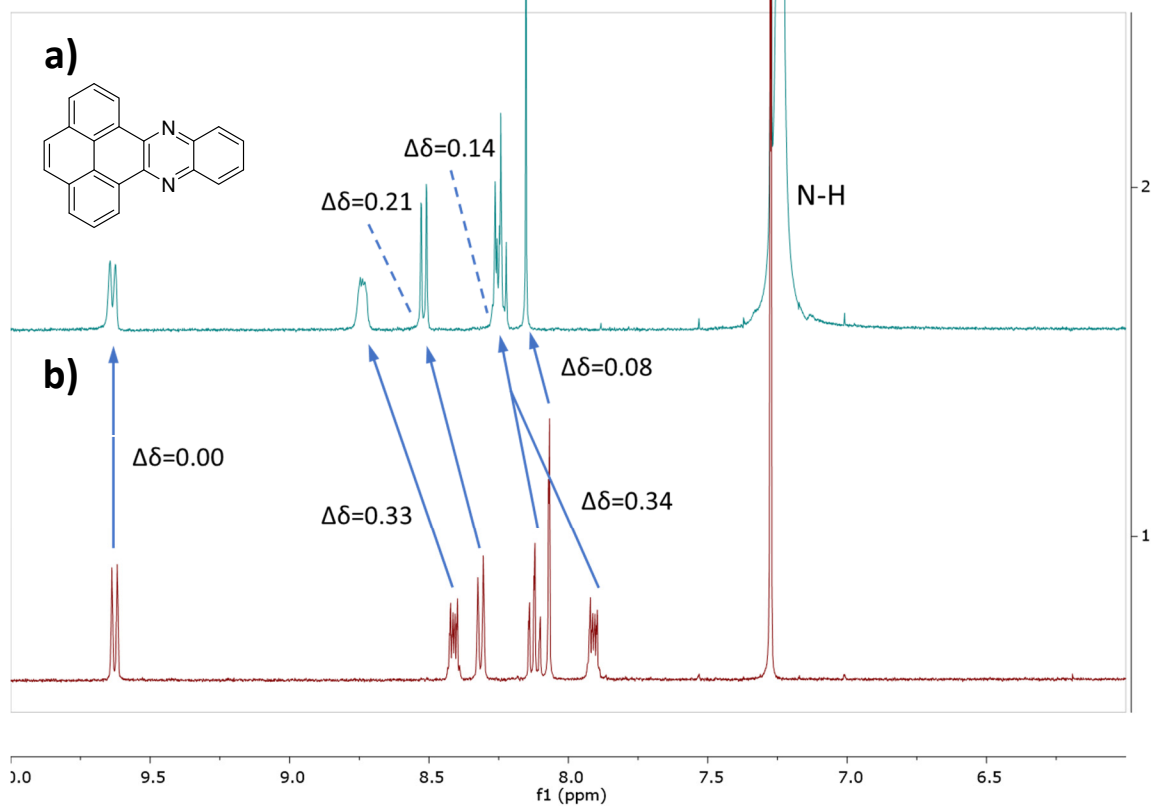


Table S2. Chemical shift table for TFA addition to **H₂quin**

Signal Assignment	Shift $\delta_1 \rightarrow \delta_2$	Change $\Delta\delta$
	7.91 \rightarrow 8.25	0.34
	8.06 \rightarrow 8.14	0.08
	8.13 \rightarrow 8.27	0.14
	8.31 \rightarrow 8.52	0.21
	8.41 \rightarrow 8.74	0.33
	9.63 \rightarrow 9.63	0.00

Full-spectrum ^1H NMR (400 MHz, CDCl_3 , top) of 1,8-bis(4-*N,N*-dimethylaminophenyl)phenanthro[4,5-*abc*]phenazine **NMe₂quin** a) with and b) without *minimal* TFA, and aromatic region ^1H NMR (400 MHz, CDCl_3 , bottom) of the same spectra.

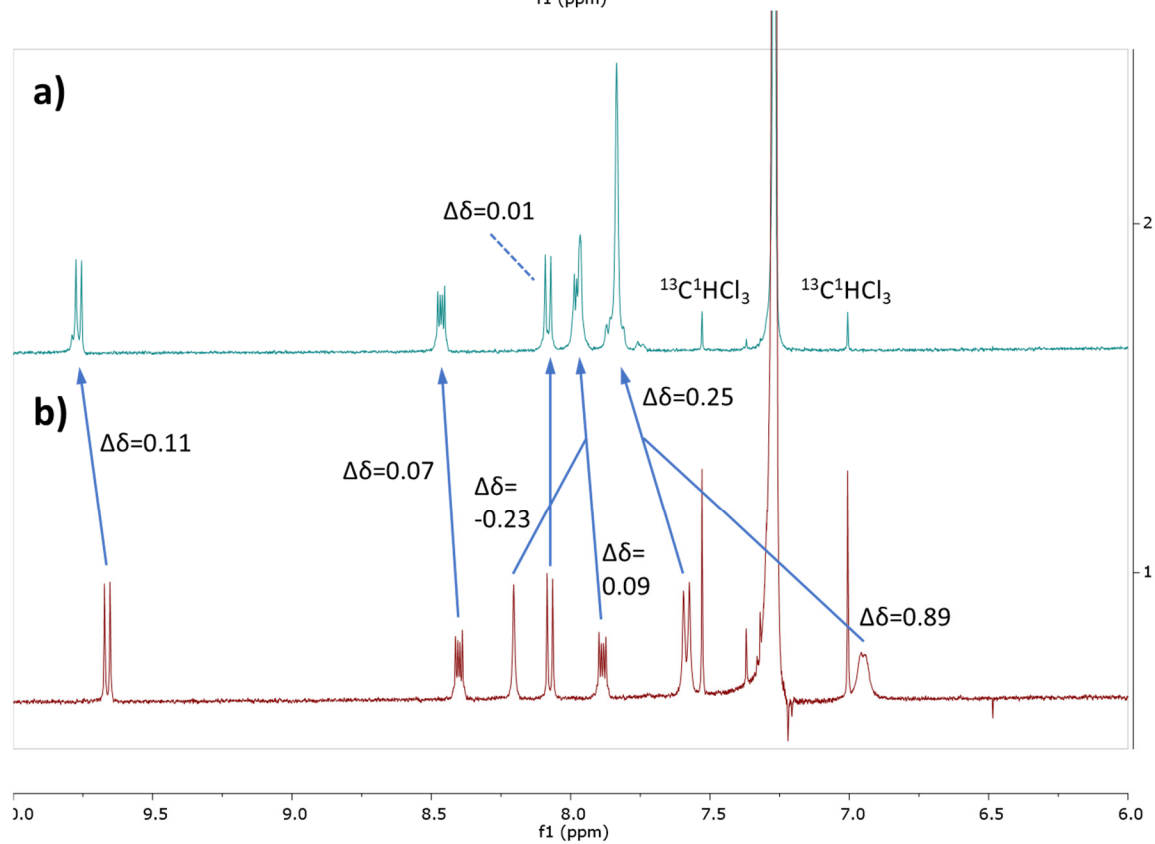
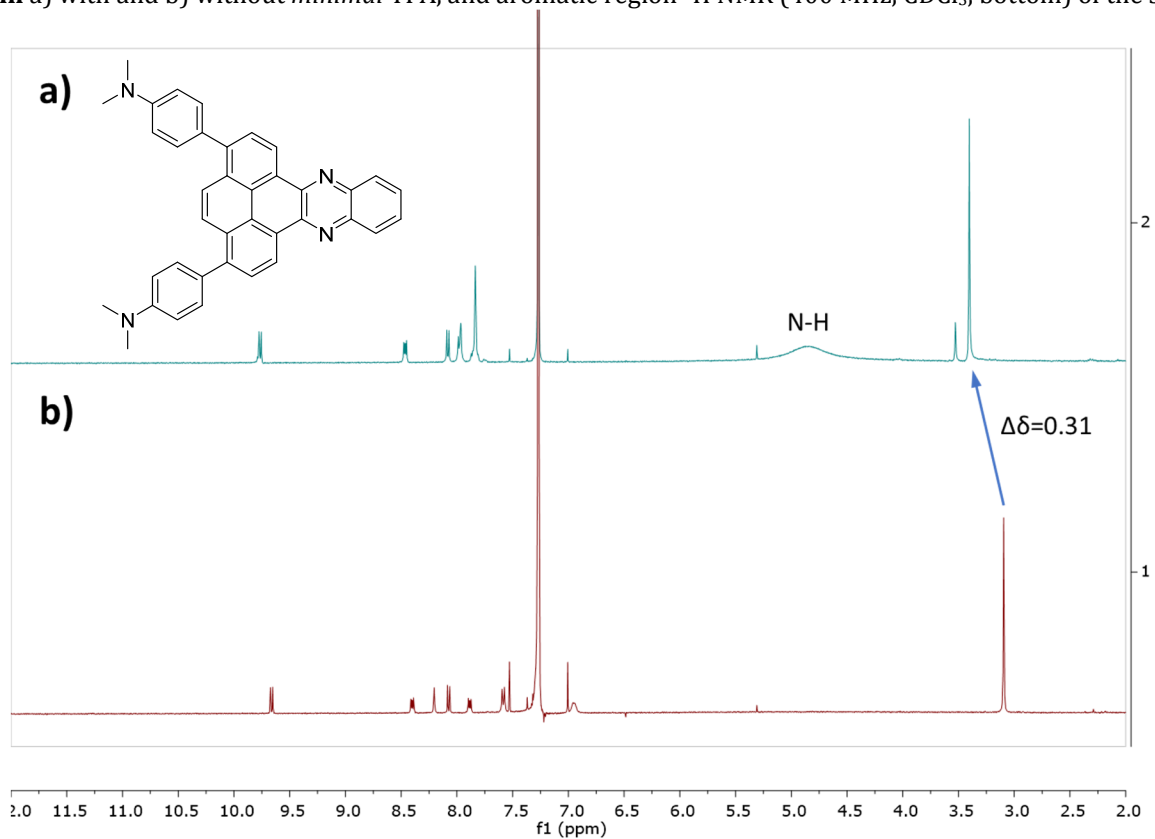
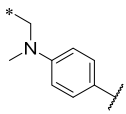
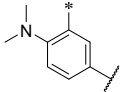
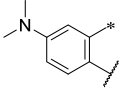
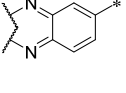
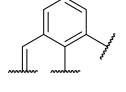
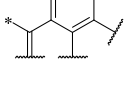
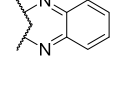
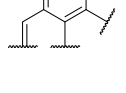


Table S3. Chemical shift table for *minimal* TFA addition to NMe₂quin

Signal Assignment	Shift $\delta_1 \rightarrow \delta_2$	Change $\Delta\delta$
	3.08 → 3.39	0.31
	6.95 → 7.84	0.89
	7.59 → 7.84	0.25
	7.89 → 7.98	0.09
	8.07 → 8.08	0.01
	8.19 → 7.96	-0.23
	8.40 → 8.47	0.07
	9.67 → 9.78	0.11

Full-spectrum ^1H NMR (400 MHz, CDCl_3 , top) of 1,8-bis(4-*N,N*-dimethylaminophenyl)phenanthro[4,5-*abc*]phenazine **NMe₂quin** a) with and b) without excess TFA, and aromatic region ^1H NMR (400 MHz, CDCl_3 , bottom) of the same spectrum.

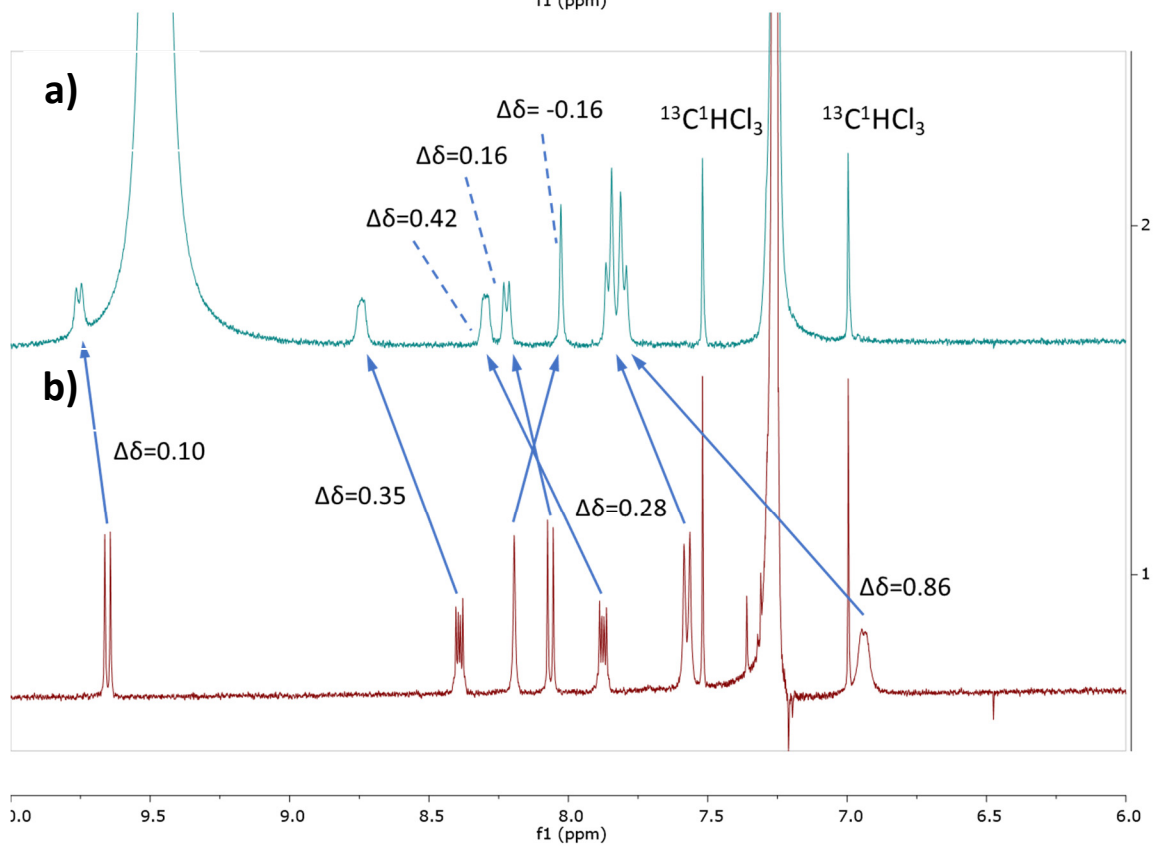
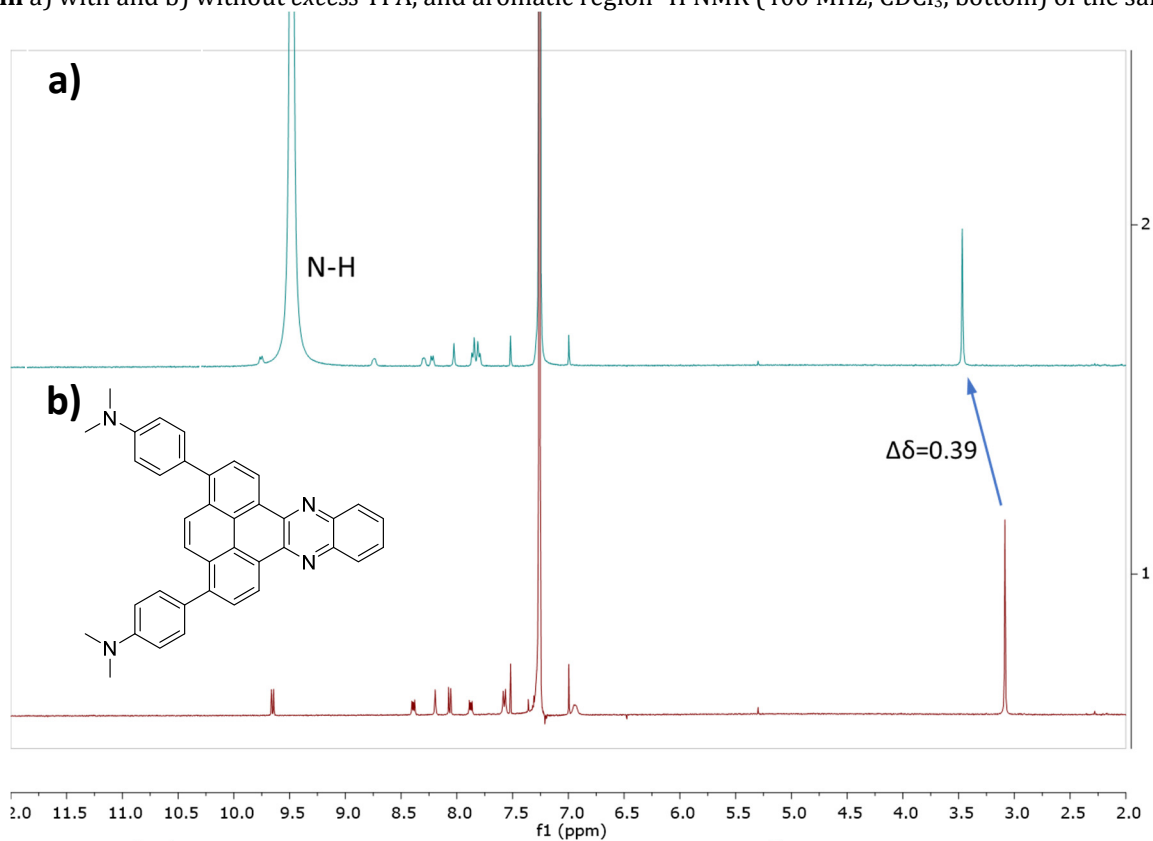
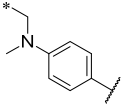
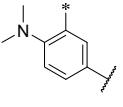
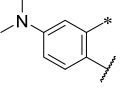
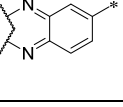
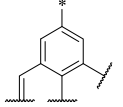
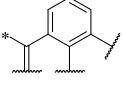
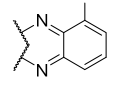
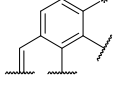
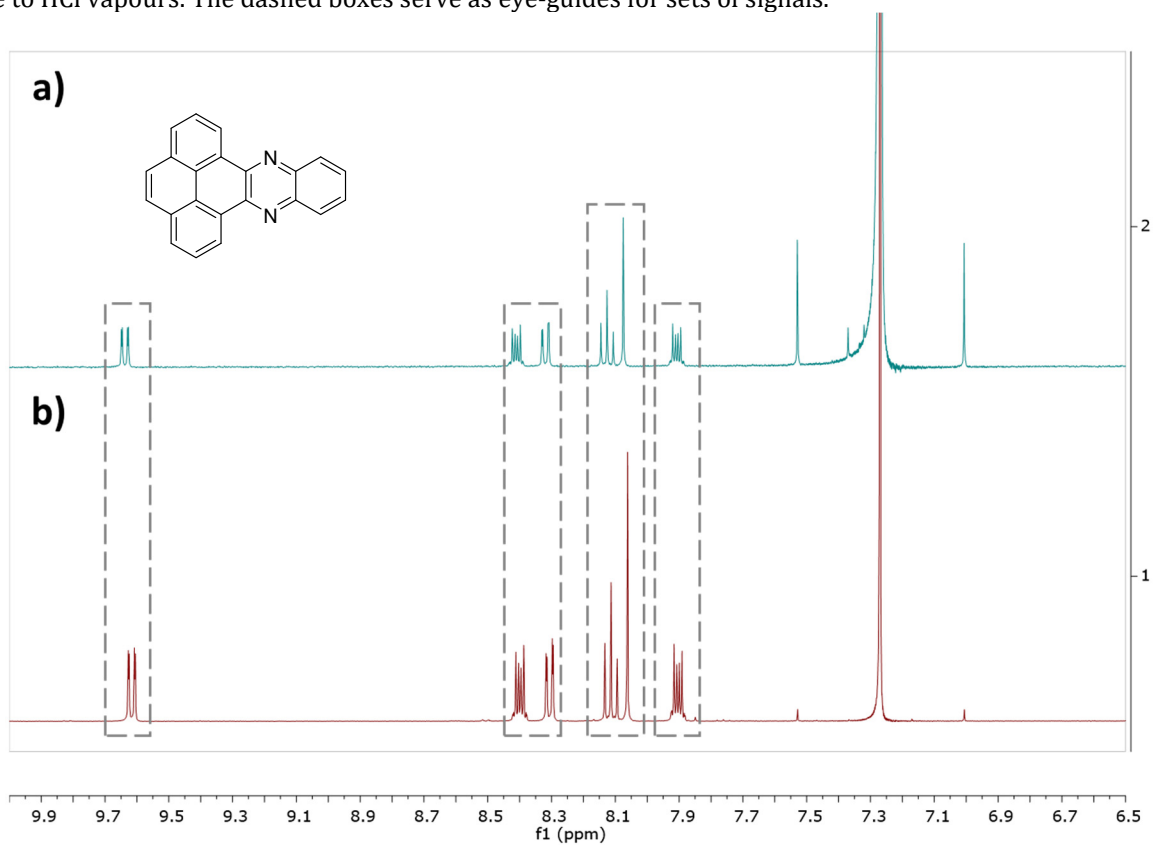


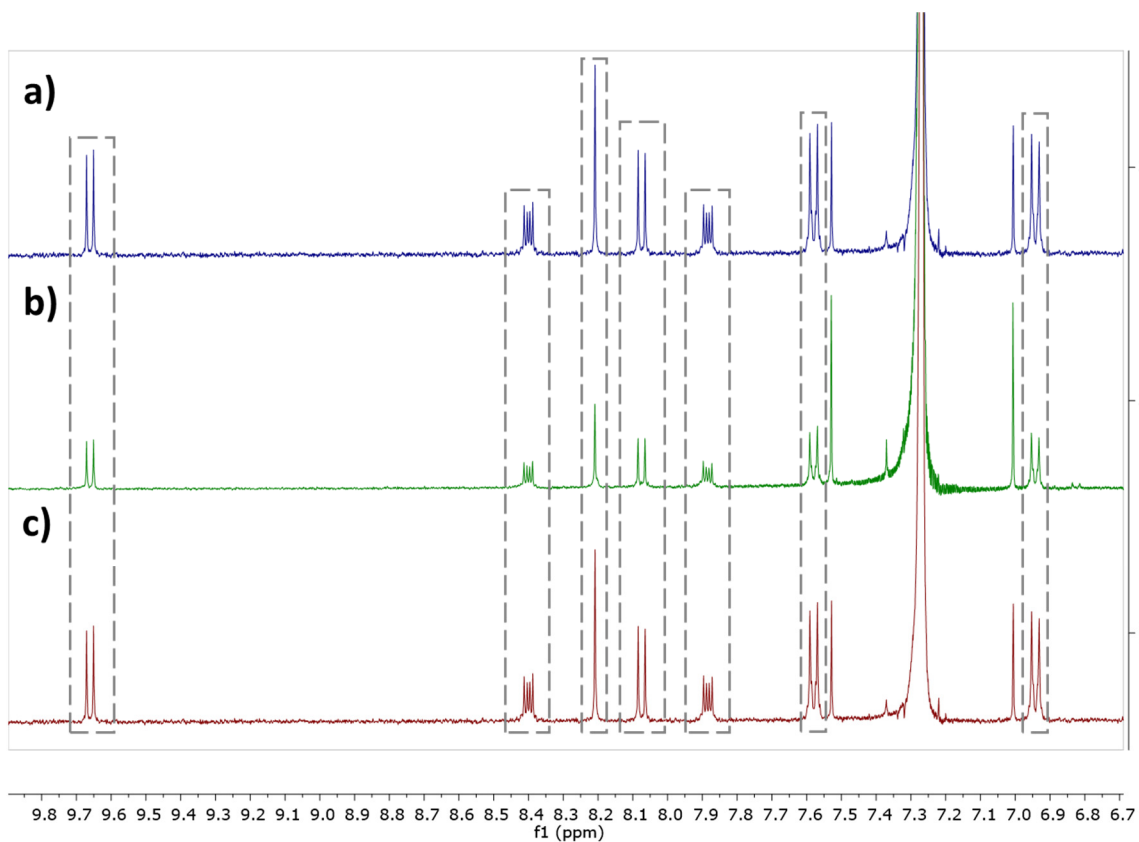
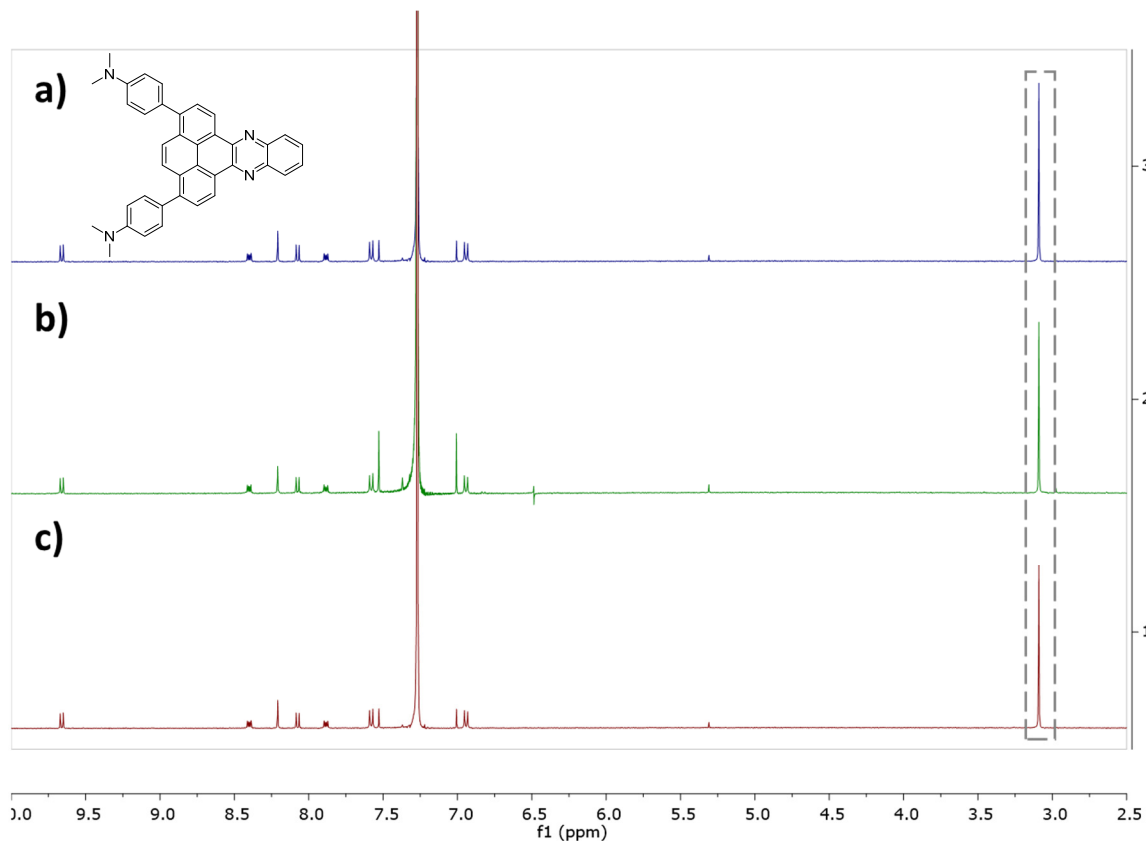
Table S4. Chemical shift table for *excess* TFA addition to **NMe₂quin**

Signal Assignment	Shift $\delta_1 \rightarrow \delta_2$	Change $\Delta\delta$
	3.08 → 3.47	0.39
	6.95 → 7.81	0.86
	7.59 → 7.87	0.28
	7.89 → 8.31	0.42
	8.07 → 8.23	0.16
	8.19 → 8.03	-0.16
	8.40 → 8.35	0.35
	9.67 → 9.77	0.10

^1H NMR (400 MHz, CDCl_3) of phenanthro[4,5-*abc*]phenazine **H₂quin** a) after allowing HCl vapours to dissipate and b) before exposure to HCl vapours. The dashed boxes serve as eye-guides for sets of signals.



Full-spectrum ^1H NMR (400 MHz, CDCl_3 , top) of 1,8-bis(4-*N,N*-dimethylaminophenyl)phenanthro[4,5-*abc*]phenazine **NMe₂quin** a) after allowing HCl vapours to dissipate b) after grinding the sample and c) as-prepared sample, and aromatic region ^1H NMR (400 MHz, CDCl_3 , bottom) of the same spectrum. The dashed boxes serve as eye-guides for sets of signals.



Section 5a Results of Single Molecule Calculations

Energy-minimized structures were calculated using density functional theory (DFT) with the B3LYP exchange-correlation functional²⁴⁻²⁶ and the cc-pVTZ basis sets²⁷ on the Gaussian 16 Version A01 software package,²⁸ solvated with the integral-equation formalism polarizable continuum model (IEFPCM)²⁹. The optimized atomic cartesian coordinates are shown on the left. On the right are images captured using GaussView 6 of the optimized structure with RB3LYP energy and lowest energy vibration. Images of Kohn-Sham HOMO and LUMO surfaces with an Isovalue of 0.015 are in numbered figures immediately below their list of optimized cartesian coordinates. No keywords were added to the job input, save in the case of **NMe₂quin** derivatives. A numerical instability was observed in frequency calculations with the B3LYP functional when jobs involved many basis functions, in this case near or over 1694. The observed error "OrtVc1 failed #1" was solved by applying the keyword "FMM=NoParallelCPHF" to the input.

Electronic absorption spectra were calculated using time-dependent density functional theory (TD-DFT) with the B3LYP exchange-correlation functional²⁴⁻²⁶ and the cc-pVTZ basis set,²⁷ solvated with the integral-equation formalism polarizable continuum model (IEFPCM)²⁹. Geometry optimized structures were used, calculated as described above. The first 10 singlet and triplet excited states were calculated. Given the possibility for intra-molecular charge transfer (ICT) states each geometry optimization, frequency, energy and time-dependent calculation was also performed using the long range-corrected functionals CAM-B3LYP³⁰ and ω B97X-D³¹. However, both failed to predict any absorption in the visible region, instead placing all transitions into the UV. Surprisingly, the B3LYP functional most accurately represented the positions of absorptions. Summary of calculated UV-visible absorption spectra are located in Section 8, with bandwidths of 0.15 eV for the Gaussian curves.

Kohn-Sham Orbitals of Phenanthro[4,5-*abc*]phenazine **H₂quin** in CH₂Cl₂

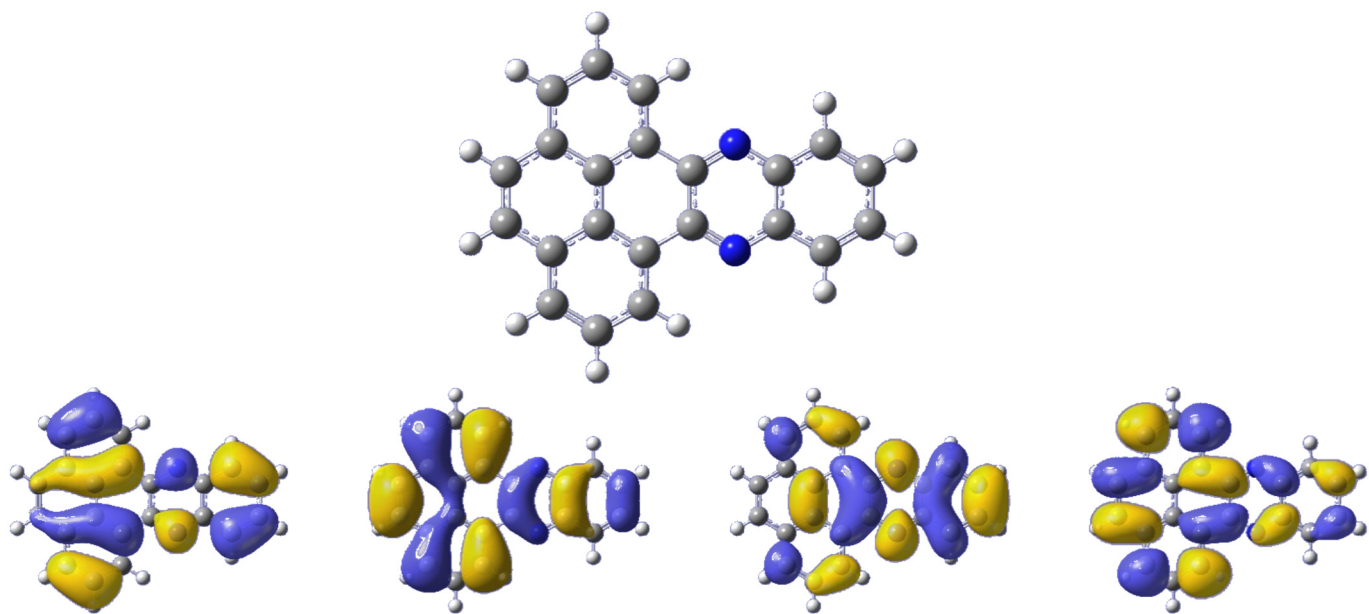


Figure S1. HOMO-1	HOMO	LUMO	LUMO+1
E CyH (eV) -0.23474	E CyH (eV) -0.21791	E CyH (eV) -0.09350	E CyH (eV) -0.06744
E CH ₂ Cl ₂ (eV) -0.23715	E CH ₂ Cl ₂ (eV) -0.22011	E CH ₂ Cl ₂ (eV) -0.09648	E CH ₂ Cl ₂ (eV) -0.06973

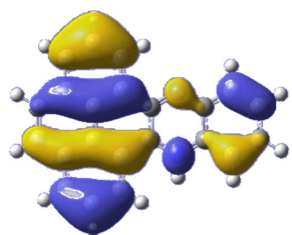
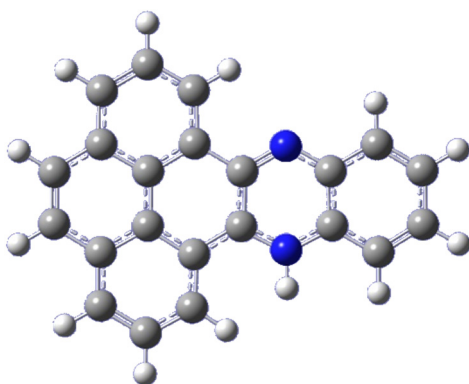
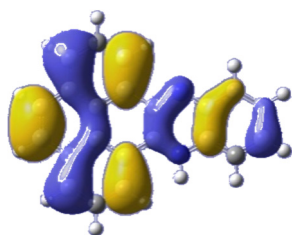
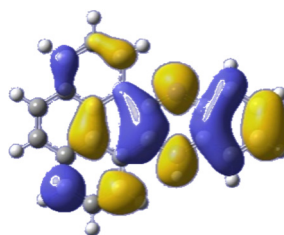


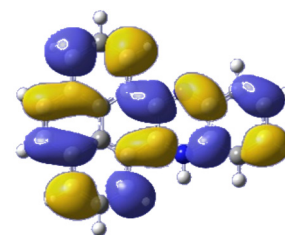
Figure S2. HOMO-1
E CH₂Cl₂ (eV) -0.26834



HOMO
E CH₂Cl₂ (eV) -0.24631



LUMO
E CH₂Cl₂ (eV) -0.15257



LUMO+1
E CH₂Cl₂ (eV) -0.10106

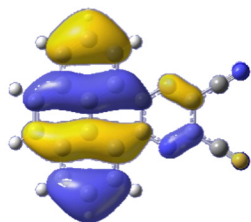
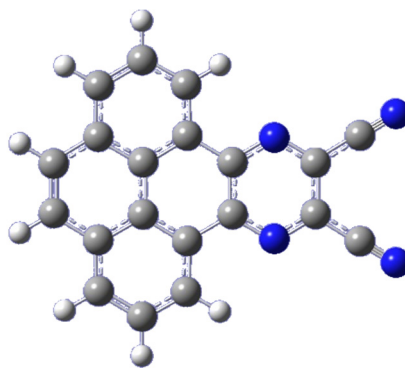
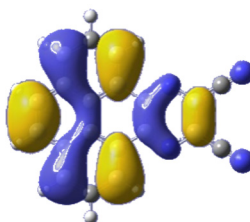
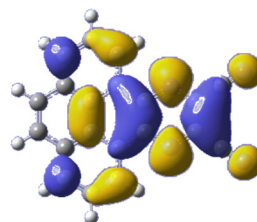


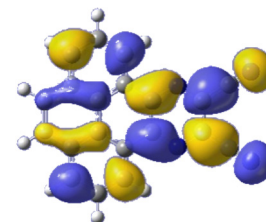
Figure S3. HOMO-1
E CyH (eV) -0.25908
E CH₂Cl₂ (eV) -0.25504



HOMO
E CyH (eV) -0.23845
E CH₂Cl₂ (eV) -0.23082

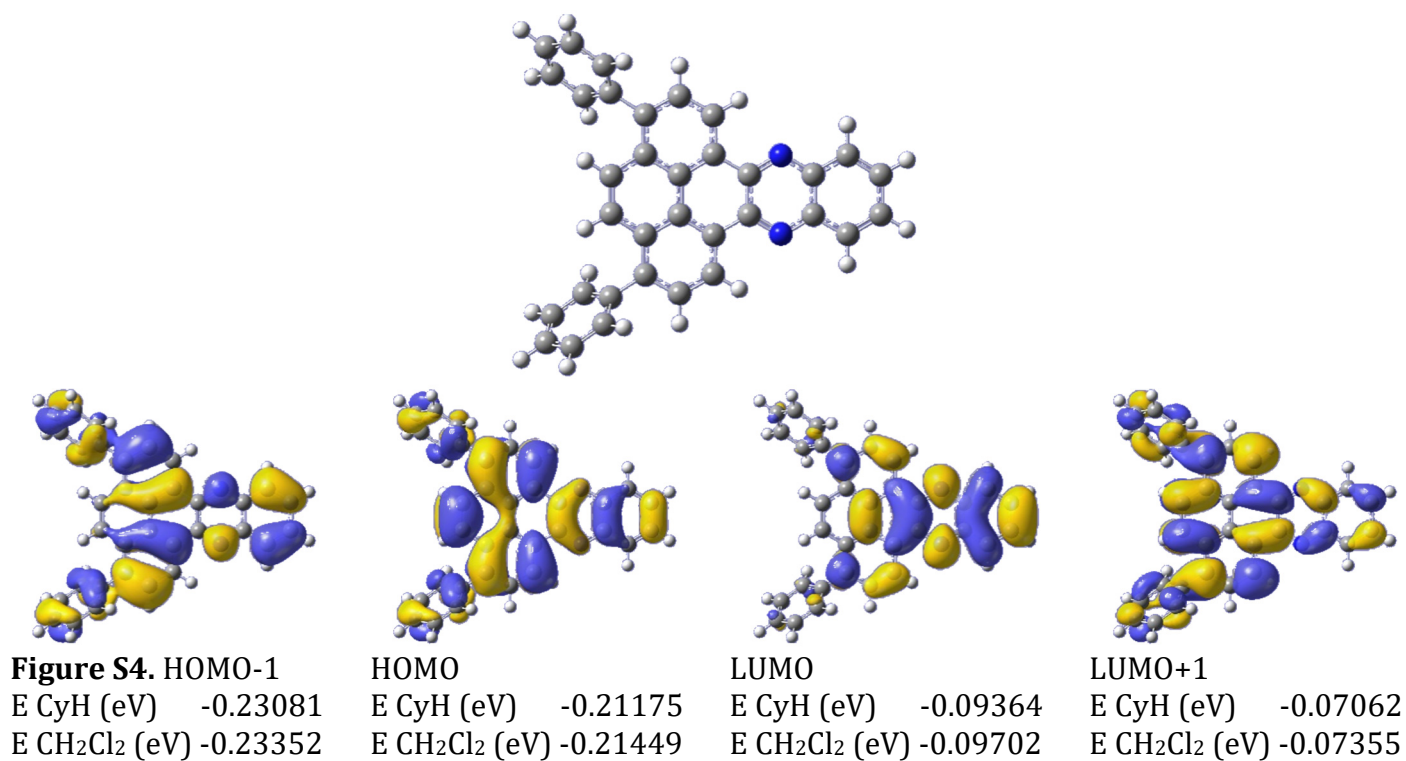


LUMO
E CyH (eV) -0.11474
E CH₂Cl₂ (eV) -0.11293

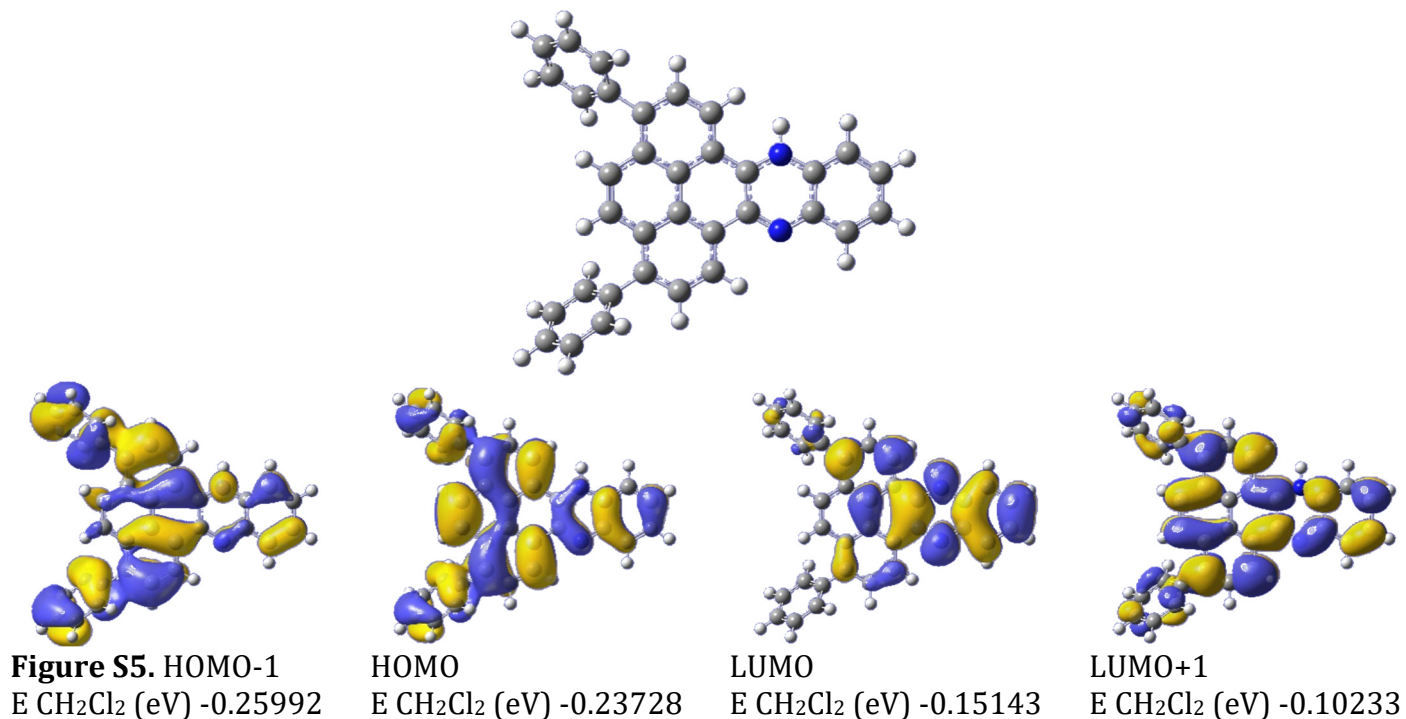


LUMO+1
E CyH (eV) -0.10752
E CH₂Cl₂ (eV) -0.10659

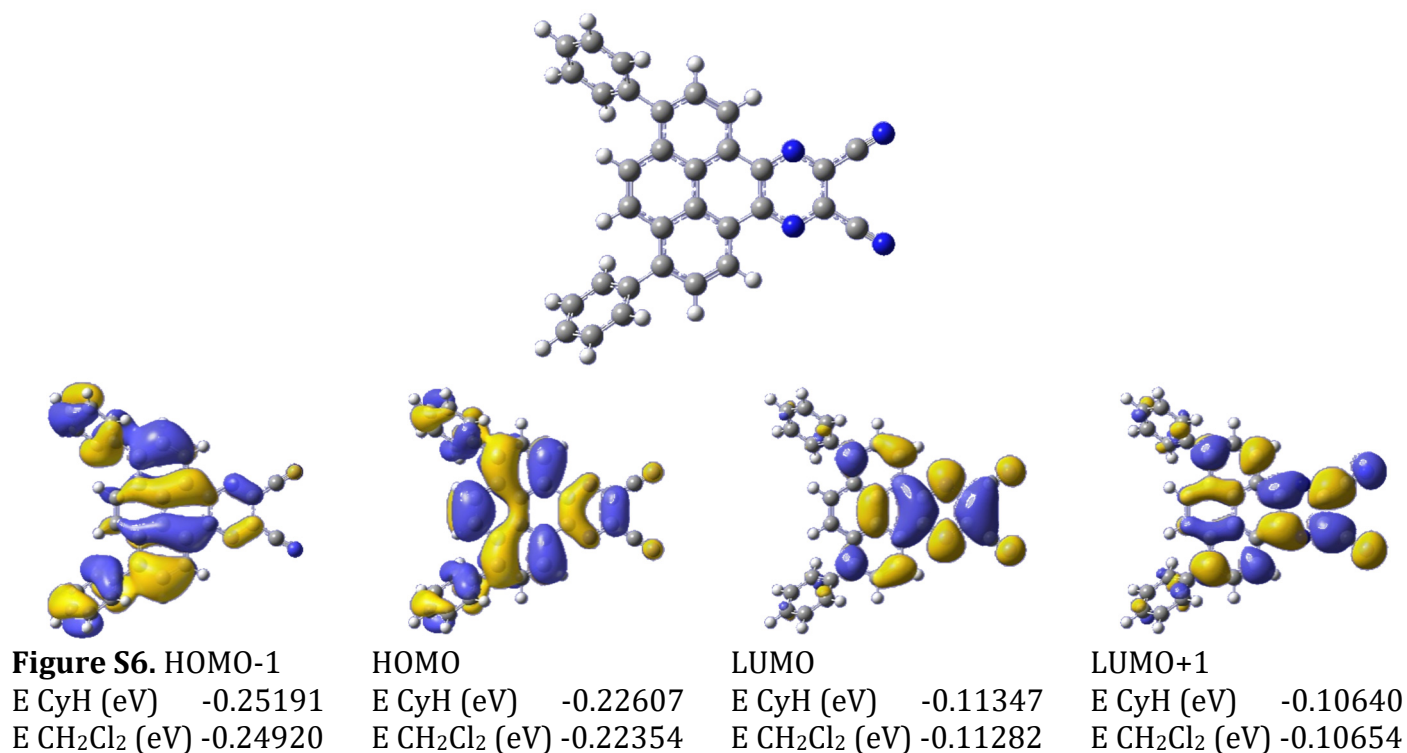
Kohn-Sham Orbitals of 1,8-Diphenylphenanthro[4,5-*abc*]phenazine **Ph₂quin** in CH₂Cl₂



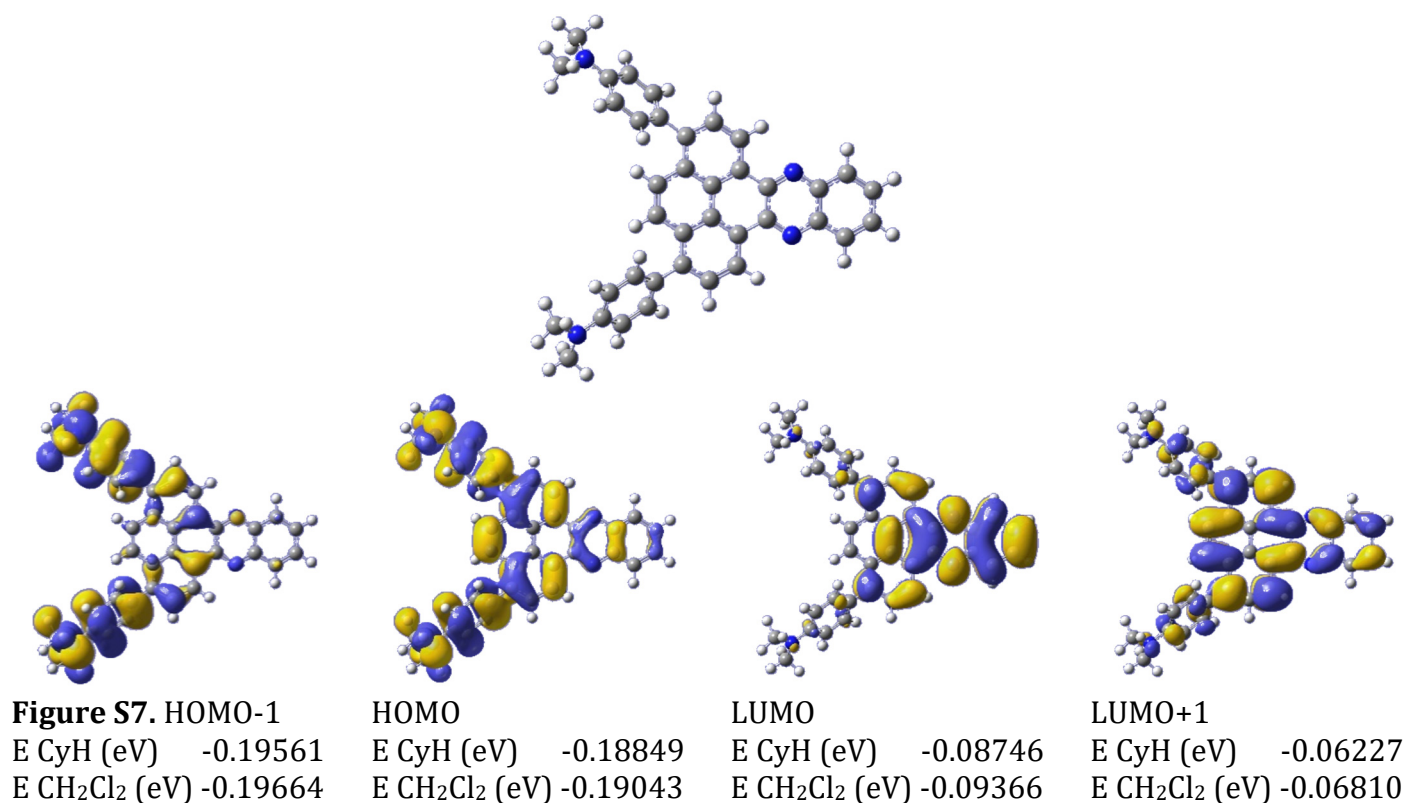
Kohn-Sham Orbitals of Protonated 1,8-Diphenylphenanthro[4,5-*abc*]phenazine **Ph₂quin** in CH₂Cl₂



Kohn-Sham Orbitals of 1,8-Diphenylphenanthro[4,5-*fg*h]quinoxaline-10,11-dicarbonitrile **Ph₂pyr** in CH₂Cl₂



Kohn-Sham Orbitals of 1,8-Bis(4-*N,N*-dimethylaminophenyl)phenanthro[4,5-*abc*]phenazine **NMe₂quin** in CH₂Cl₂



Kohn-Sham Orbitals of Aniline-Protonated 1,8-Bis(4-*N,N*-dimethylaminophenyl) phenanthro[4,5-*abc*]phenazine **NMe₂quin** in CH₂Cl₂

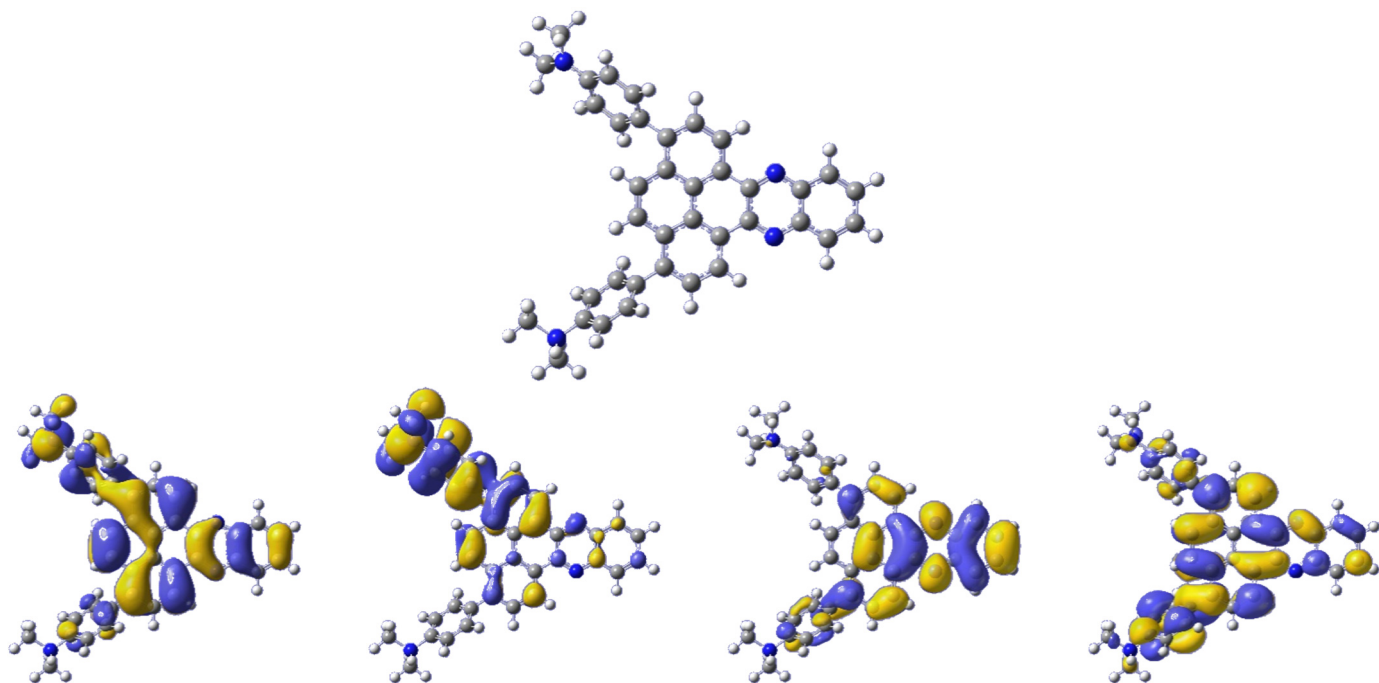


Figure S8. HOMO-1
E CH₂Cl₂ (eV) -0.22681

HOMO
E CH₂Cl₂ (eV) -0.19969

LUMO
E CH₂Cl₂ (eV) -0.10241

LUMO+1
E CH₂Cl₂ (eV) -0.08187

Kohn-Sham Orbitals of Quinoxaline-Protonated 1,8-Bis(4-*N,N*-dimethylaminophenyl) phenanthro[4,5-*abc*]phenazine **NMe₂quin** in CH₂Cl₂

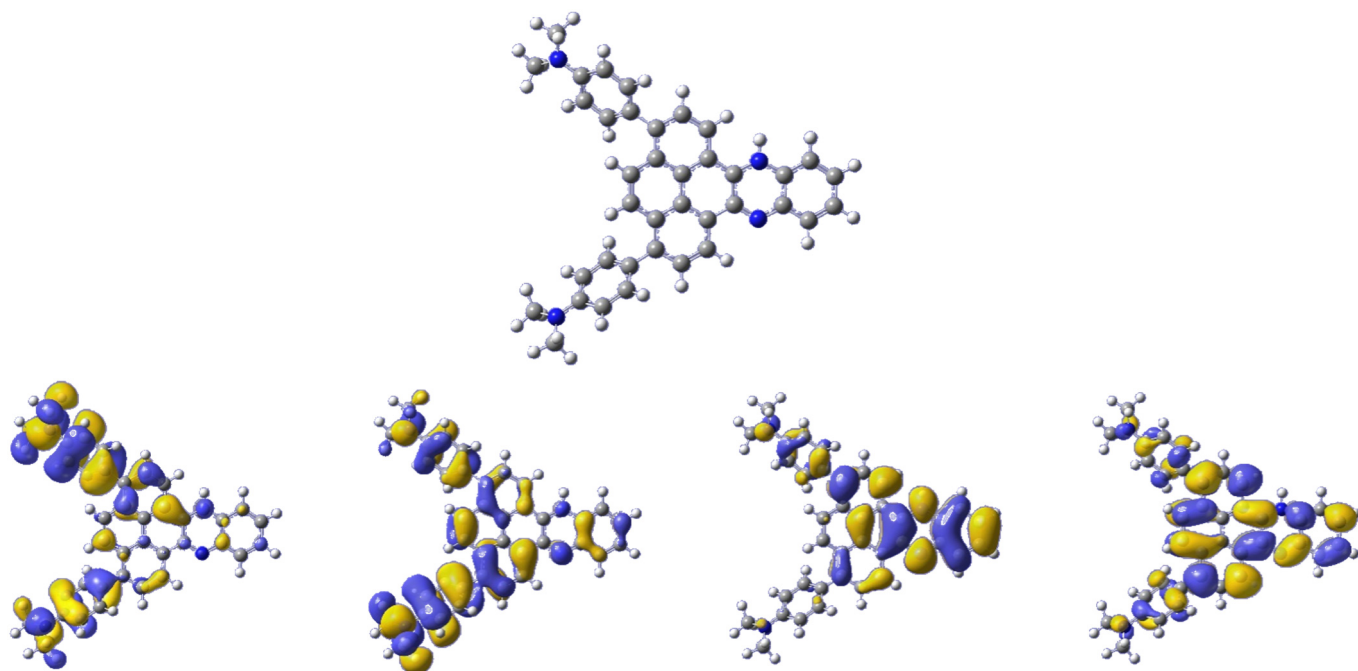


Figure S9. HOMO-1
E CH₂Cl₂ (eV) -0.20898

HOMO
E CH₂Cl₂ (eV) -0.20188

LUMO
E CH₂Cl₂ (eV) -0.14441

LUMO+1
E CH₂Cl₂ (eV) -0.09509

Section 5b Calculated and Experimental ^1H NMR Comparisons

Nuclear magnetic resonance (NMR) spectra were DFT-simulated using the gauge-independent atomic orbital (GIAO) method^{32,33} with the B3LYP exchange-correlation functional²⁴⁻²⁶ and the cc-pVTZ basis set,²⁷ solvated in CHCl_3 with the integral-equation formalism polarizable continuum model (IEFPCM)²⁹. Geometry optimized structures were used, calculated as described above and the spectra are referenced to TMS calculated at the B3LYP/6-311G++(2d,p) level which is available in GaussView6. Spin-spin couplings were not calculated because only chemical shift information was required to identify the site of protonation of **NMe₂quin**. The predicted spectra are provided below, using a FWHM of 0.003 ppm and degeneracy tolerance of 0.05 ppm. Also provided are tabulated values of δ and $\Delta\delta$ between the neutral and protonated versions, compared to the experimental ^1H NMR results on pages S36-S39.

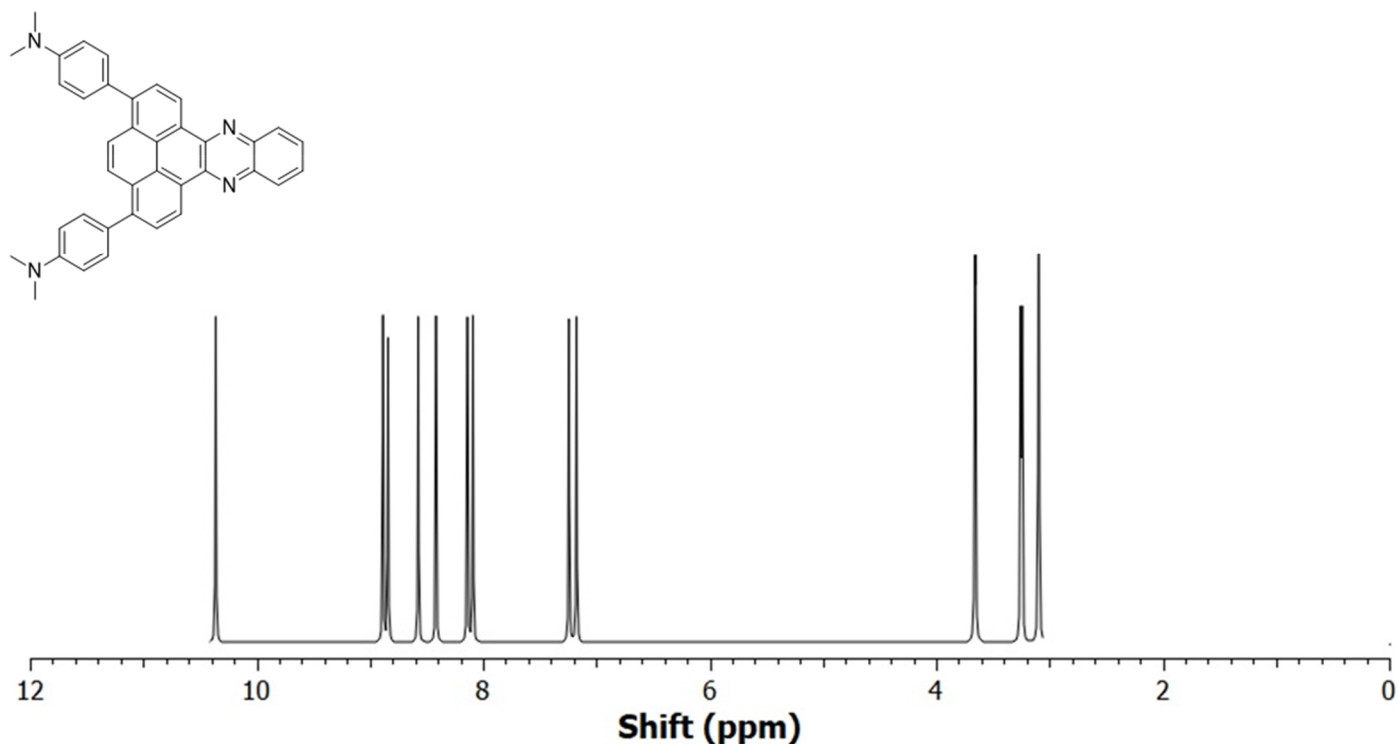


Figure S10. GIAO-simulated ^1H NMR of neutral **NMe₂quin** from 0-12 ppm.

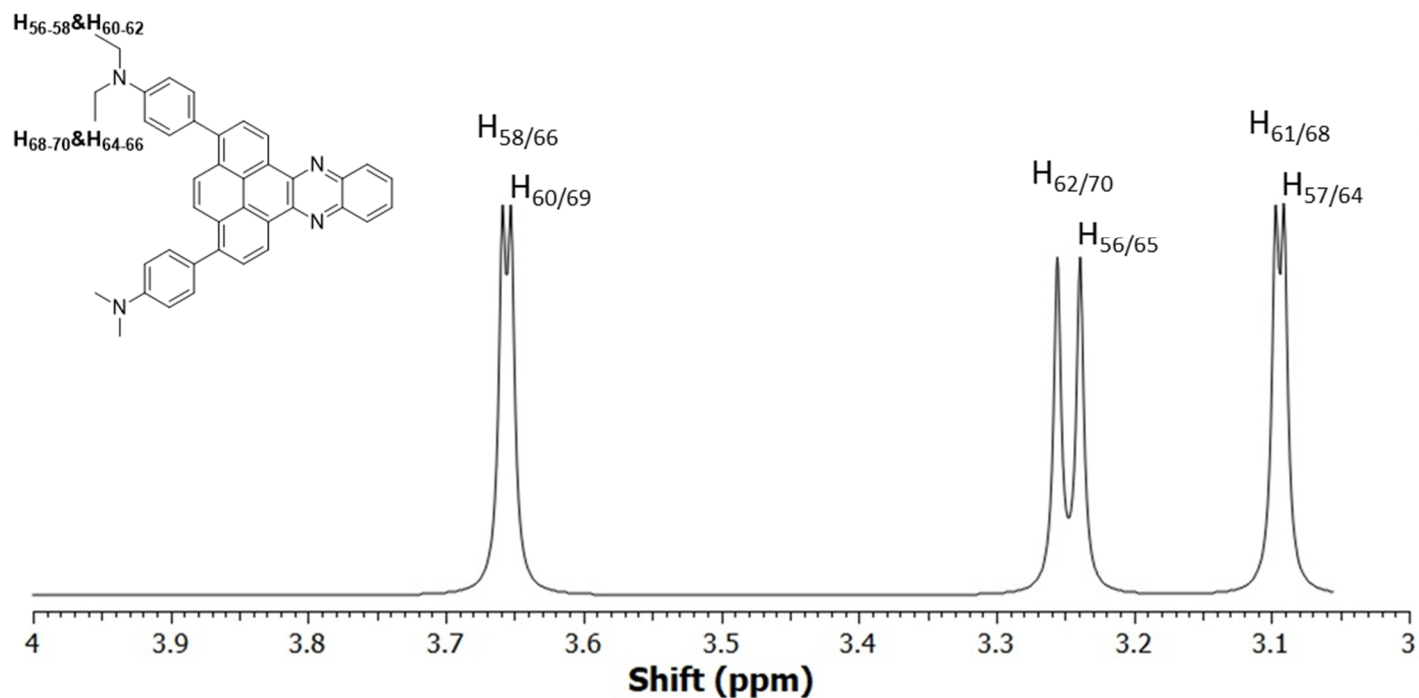


Figure S11. GIAO-simulated ^1H NMR of neutral NMe_2quin from 3-4 ppm.

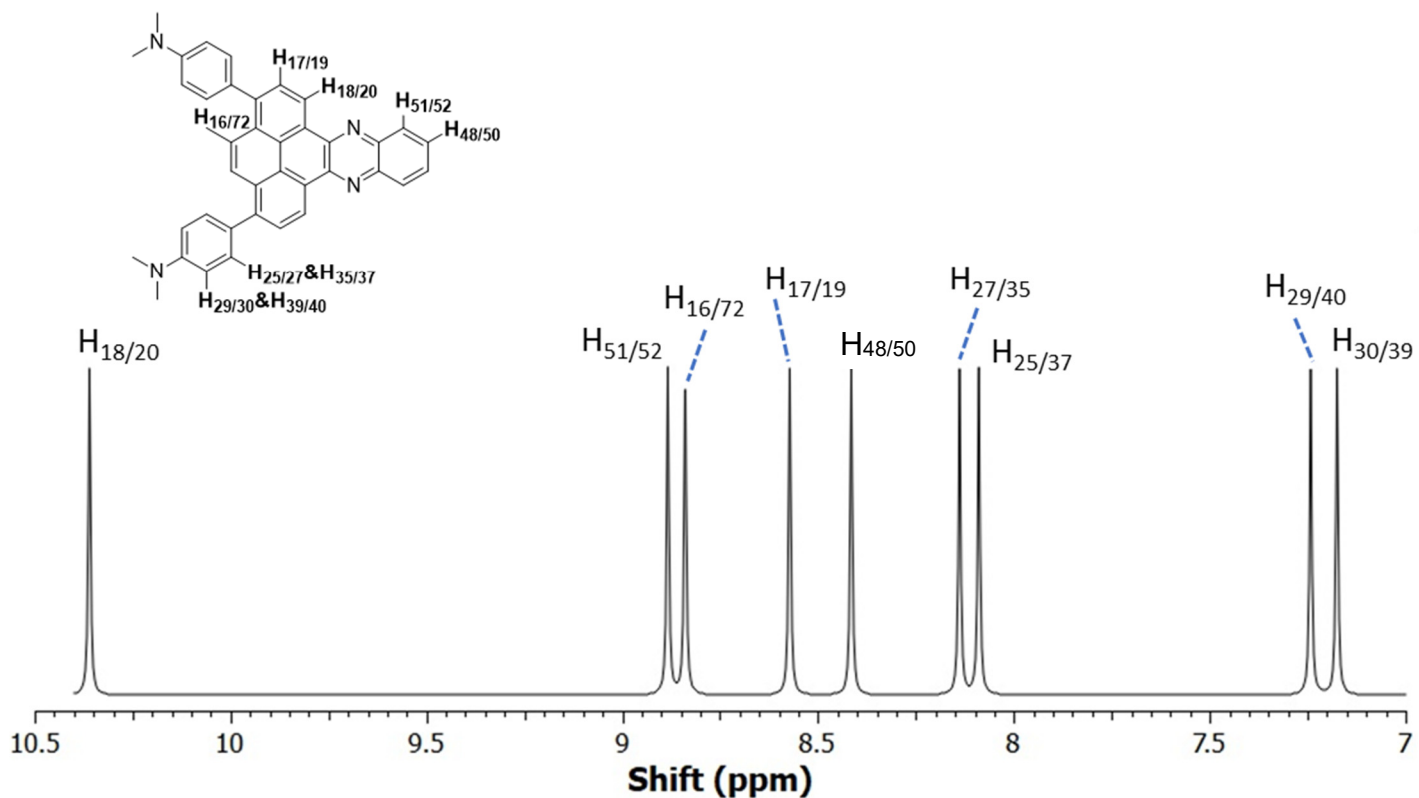


Figure S12. GIAO-simulated ^1H NMR of neutral NMe_2quin from 7-10.5 ppm.

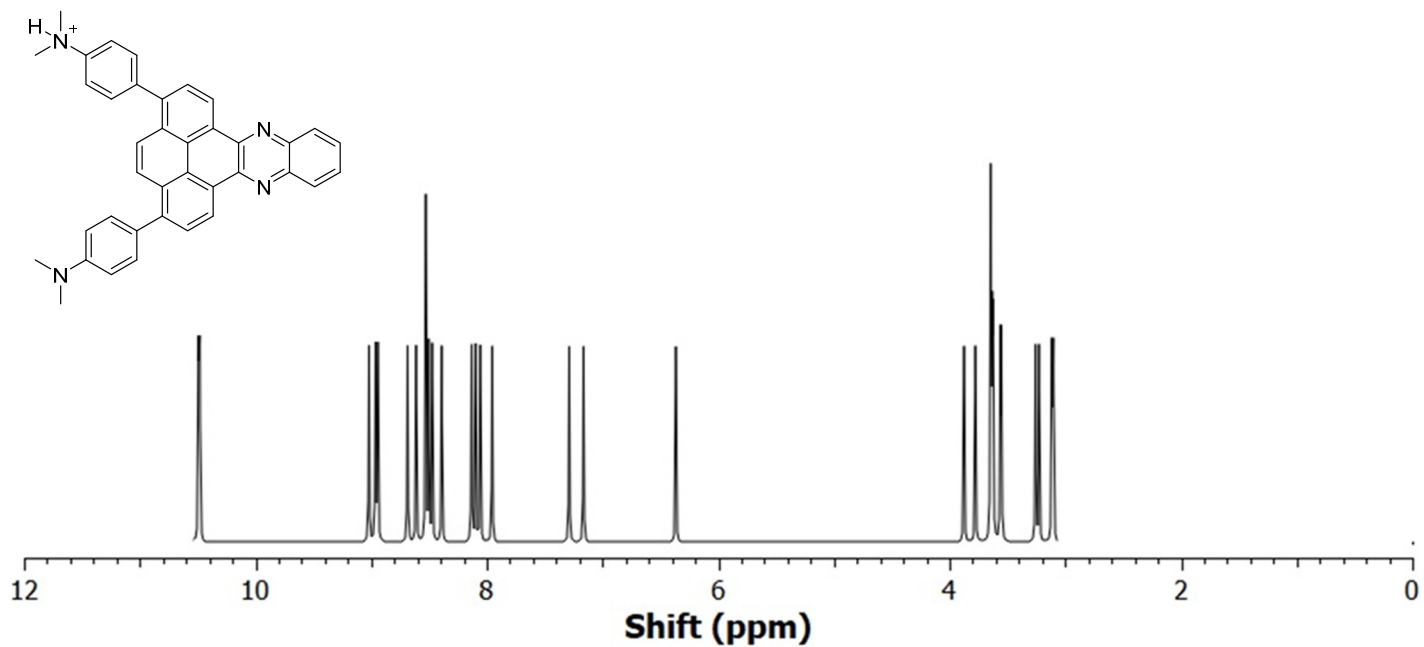


Figure S13. GIAO-simulated ^1H NMR of aniline-protonated NMe_2quin from 0-12 ppm.

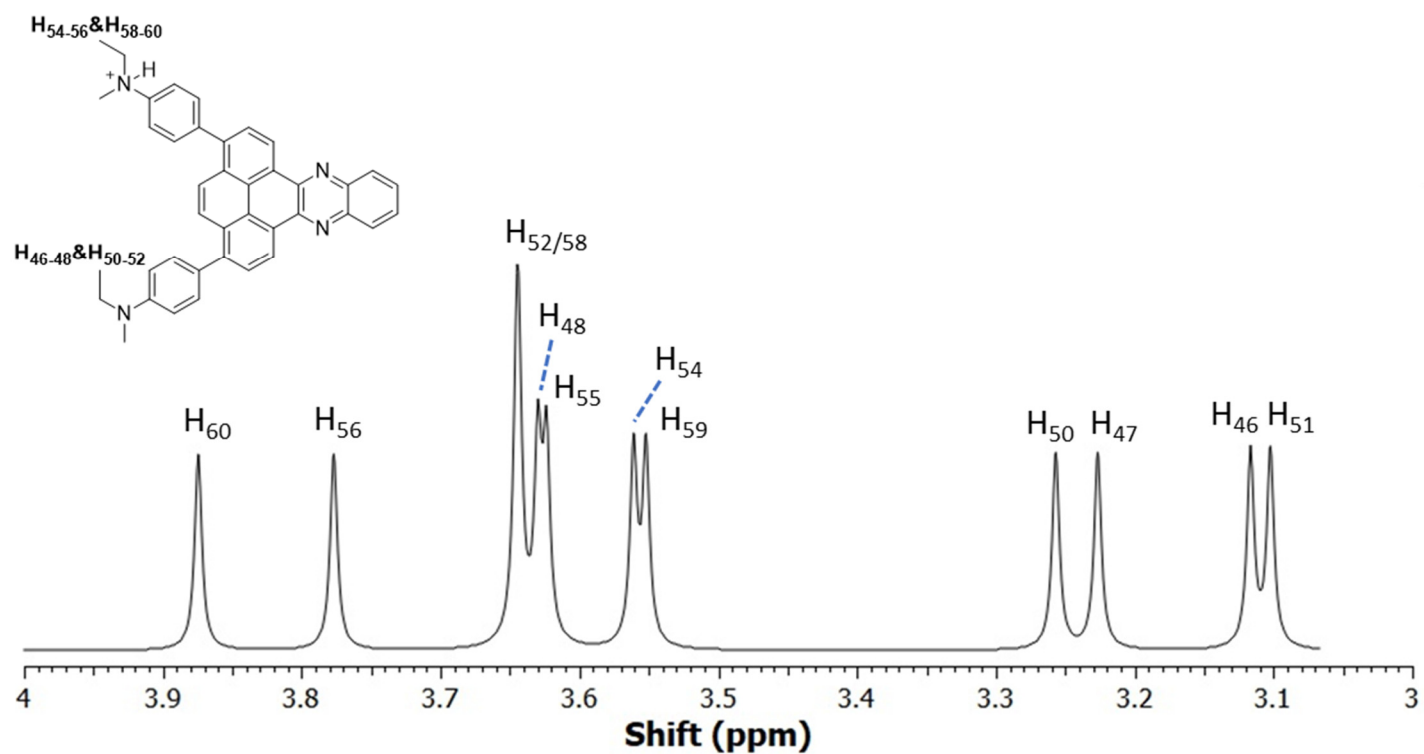


Figure S14. GIAO-simulated ^1H NMR of aniline-protonated NMe_2quin from 3-4 ppm.

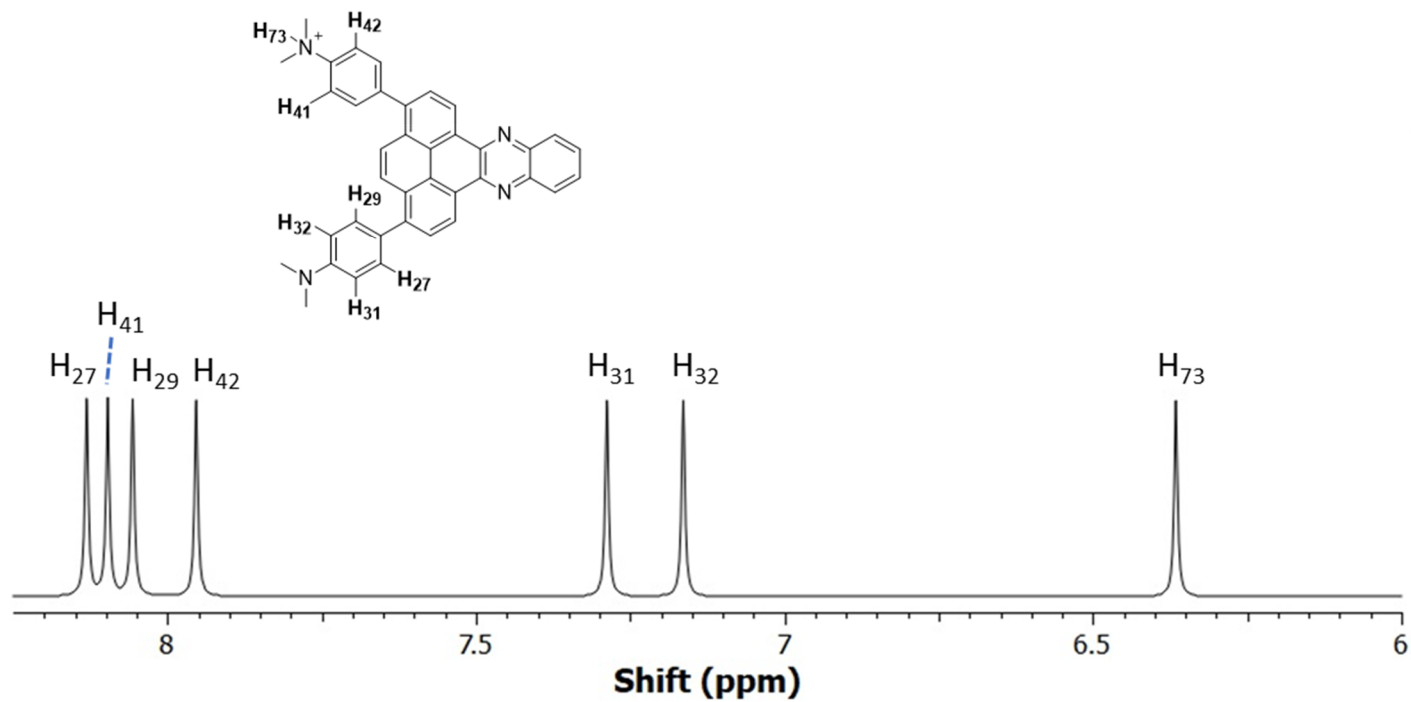


Figure S15. GIAO-simulated ^1H NMR of aniline-protonated NMe_2quin from 6-8.25 ppm.

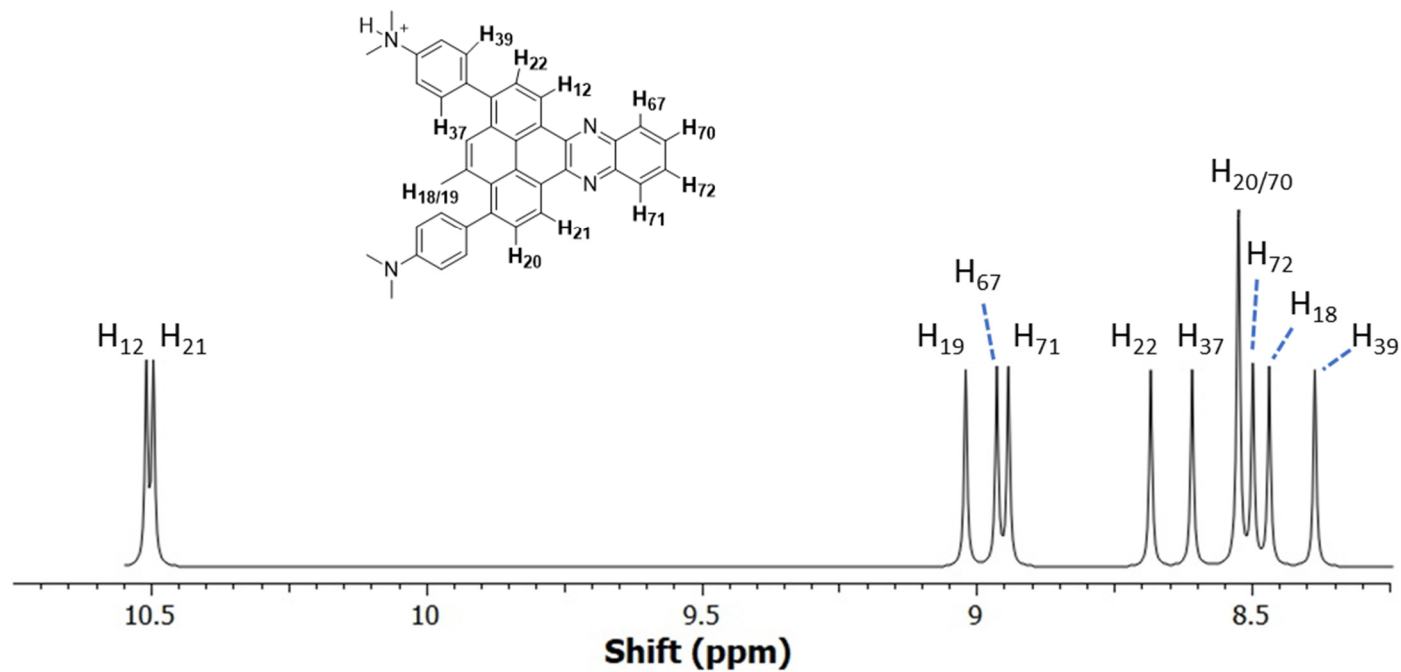
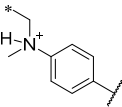
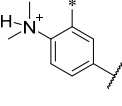
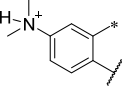
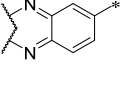
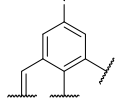
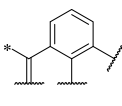
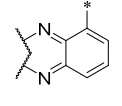
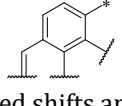


Figure S16. GIAO-simulated ^1H NMR of aniline-protonated NMe_2quin from 8.25-10.75 ppm.

Table S5. Chemical shift changes of calculated aniline-protonated **NMe₂quin** versus experimental *minimal* TFA-addition

Signal Assignment	Calculated Shift $\delta_1 \rightarrow \delta_2$	Calculated Change $\Delta\delta$	Experimental Shift $\delta_1 \rightarrow \delta_2^*$	Experimental Change $\Delta\delta^*$
	3.34 \rightarrow 3.67 ¹	0.32	3.08 \rightarrow 3.39	0.31
	7.21 \rightarrow 8.02 ¹	0.81	6.95 \rightarrow 7.84	0.89
	8.11 \rightarrow 8.50 ¹	0.39	7.59 \rightarrow 7.84	0.25
	8.42 \rightarrow 8.52	0.10	7.89 \rightarrow 7.98	0.09
	8.57 \rightarrow 8.61	0.04	8.07 \rightarrow 8.08	0.01
	8.84 \rightarrow 8.61	-0.23	8.19 \rightarrow 7.96	-0.23
	8.88 \rightarrow 8.75	-0.13	8.40 \rightarrow 8.47	0.07
	10.36 \rightarrow 10.49	0.19	9.67 \rightarrow 9.78	0.11

¹ Calculated shifts are from protons on the anilinium group.

* Experimental values come from addition of *minimal* TFA, as found on pages S36-S37.

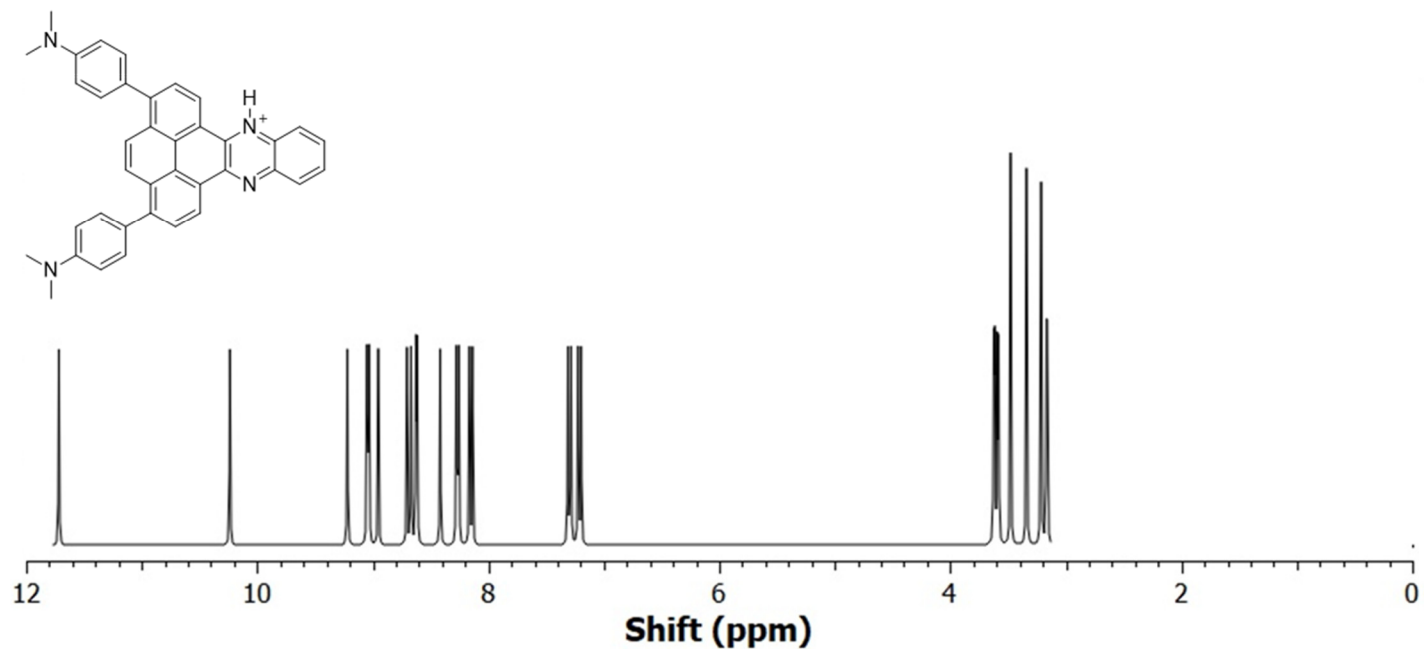


Figure S17. GIAO-simulated 1H NMR of quinoxaline-protonated NMe_2 quin from 0-12 ppm.

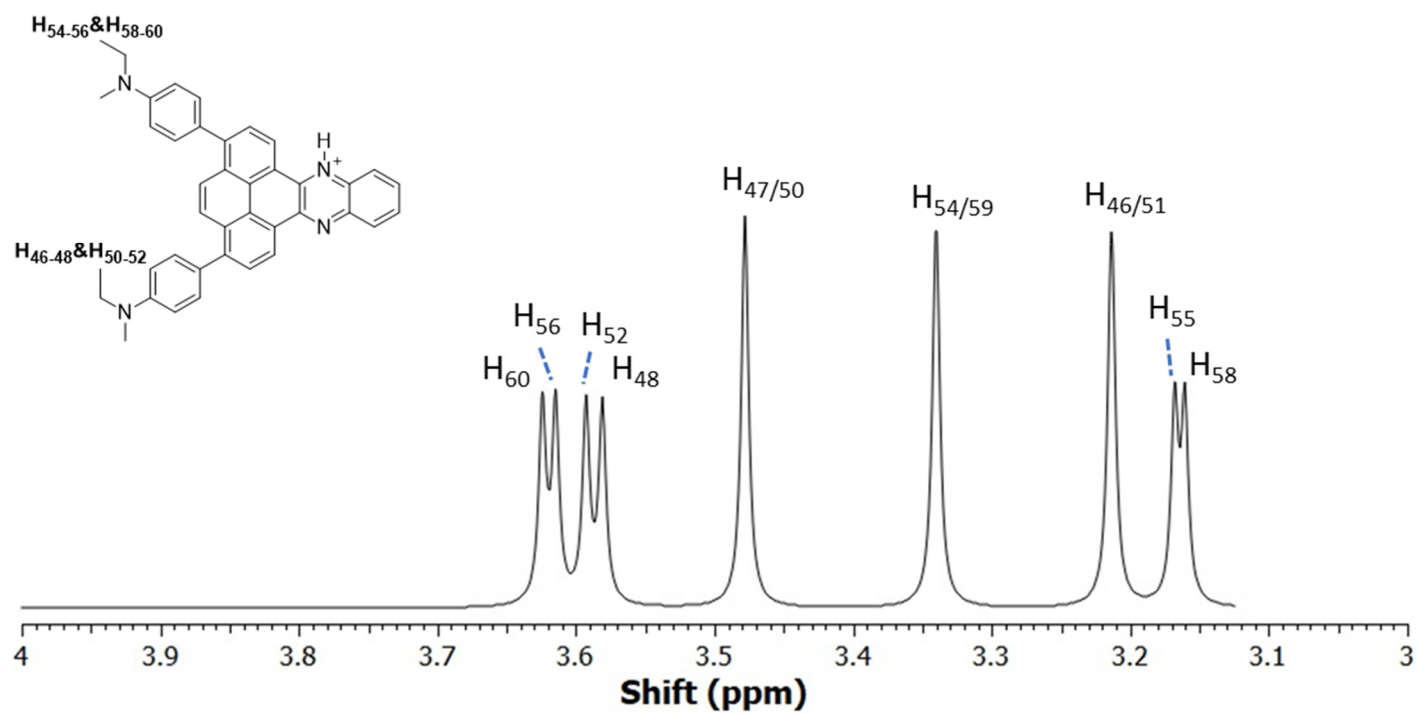


Figure S18. GIAO-simulated 1H NMR of quinoxaline-protonated NMe_2 quin from 3-4 ppm.

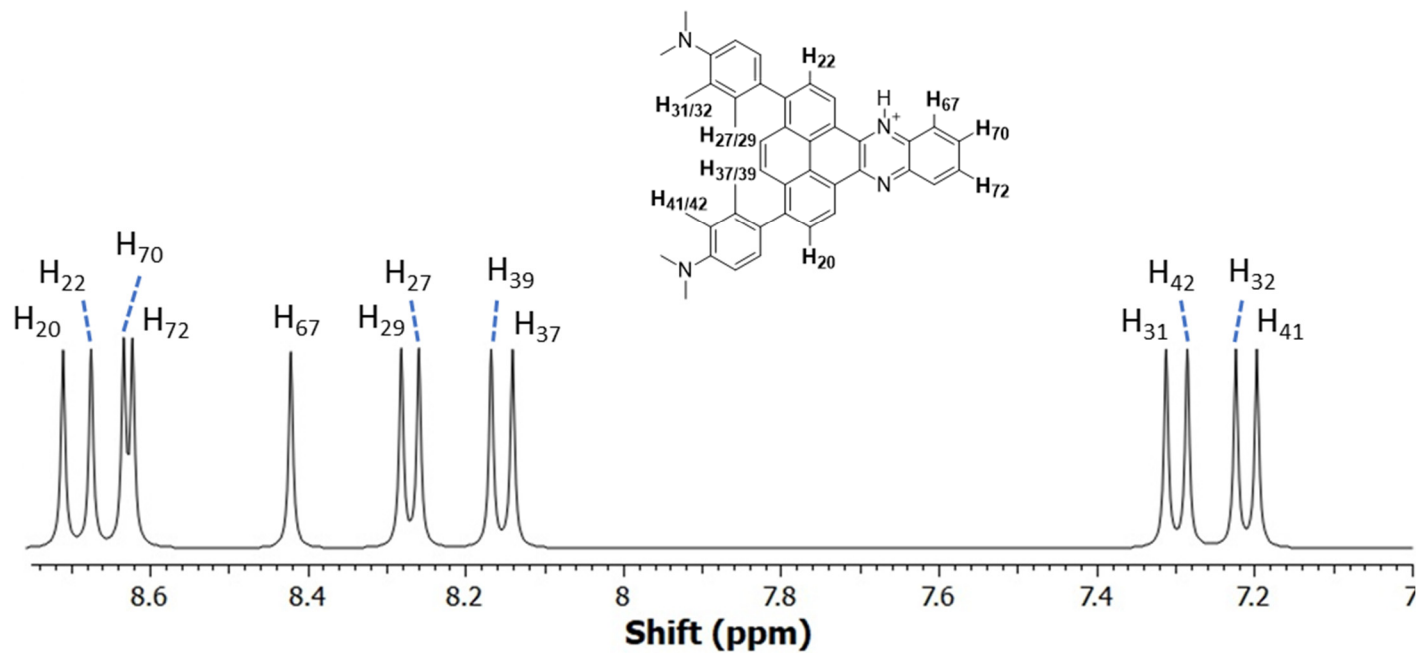


Figure S19. GIAO-simulated ^1H NMR of quinoxaline-protonated NMe_2quin from 7-8.75 ppm.

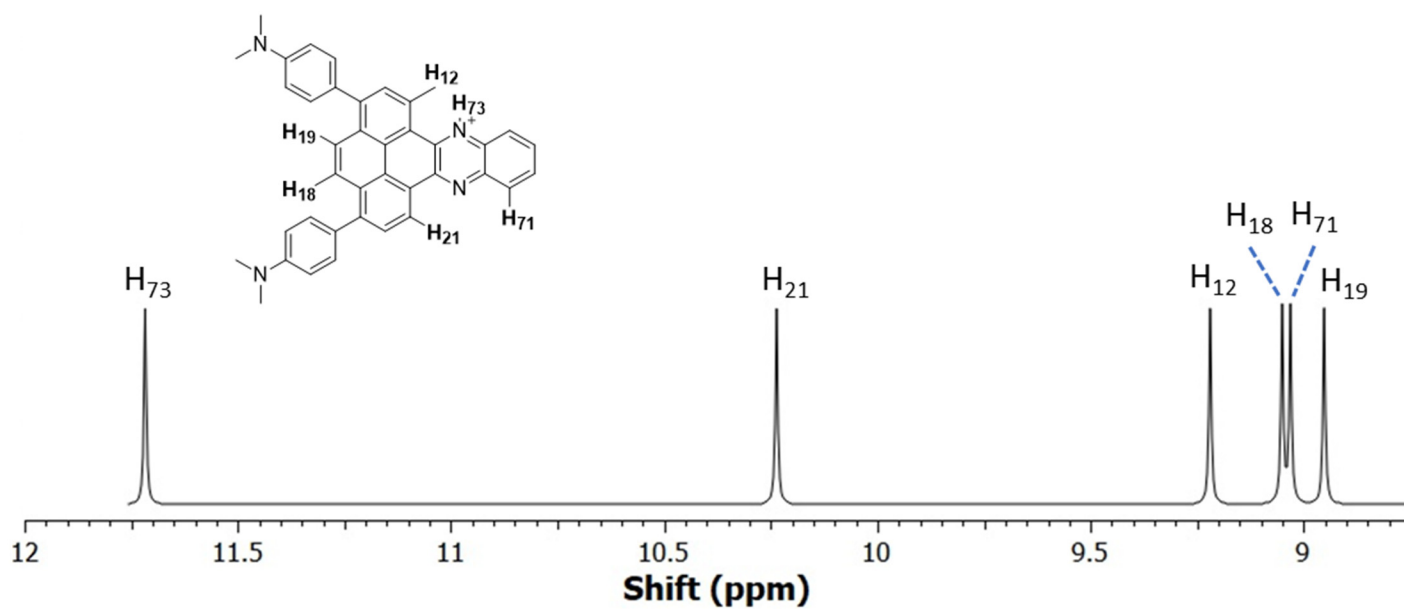
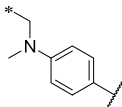
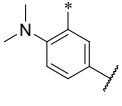
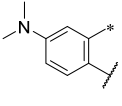
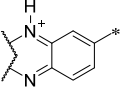
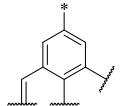
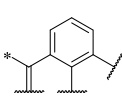
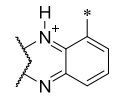
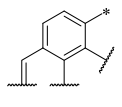


Figure S20. GIAO-simulated ^1H NMR of quinoxaline-protonated NMe_2quin from 8.75-12 ppm.

Table S6. Chemical shift changes of calculated quinoxaline-protonated **NMe₂quin** versus experimental *minimal* TFA-addition

Signal Assignment	Calculated Shift $\delta_1 \rightarrow \delta_2$	Calculated Change $\Delta\delta$	Experimental Shift $\delta_1 \rightarrow \delta_2^*$	Experimental Change $\Delta\delta^*$
	3.34 \rightarrow 3.40	0.06	3.08 \rightarrow 3.39	0.31
	7.21 \rightarrow 7.25	0.04	6.95 \rightarrow 7.84	0.89
	8.11 \rightarrow 8.21	0.10	7.59 \rightarrow 7.84	0.25
	8.42 \rightarrow 8.62 ¹	0.20	7.89 \rightarrow 7.98	0.09
	8.57 \rightarrow 8.69	0.12	8.07 \rightarrow 8.08	0.01
	8.84 \rightarrow 9.00	0.06	8.19 \rightarrow 7.96	-0.23
	8.88 \rightarrow 9.03 ¹	0.15	8.40 \rightarrow 8.47	0.07
	10.36 \rightarrow 9.70	-0.66	9.67 \rightarrow 9.78	0.11

¹ Calculated shift is based upon the proton closest to the quinoxalinium nitrogen.

* Experimental values come from addition of *minimal* TFA, as found on pages S36-S37.

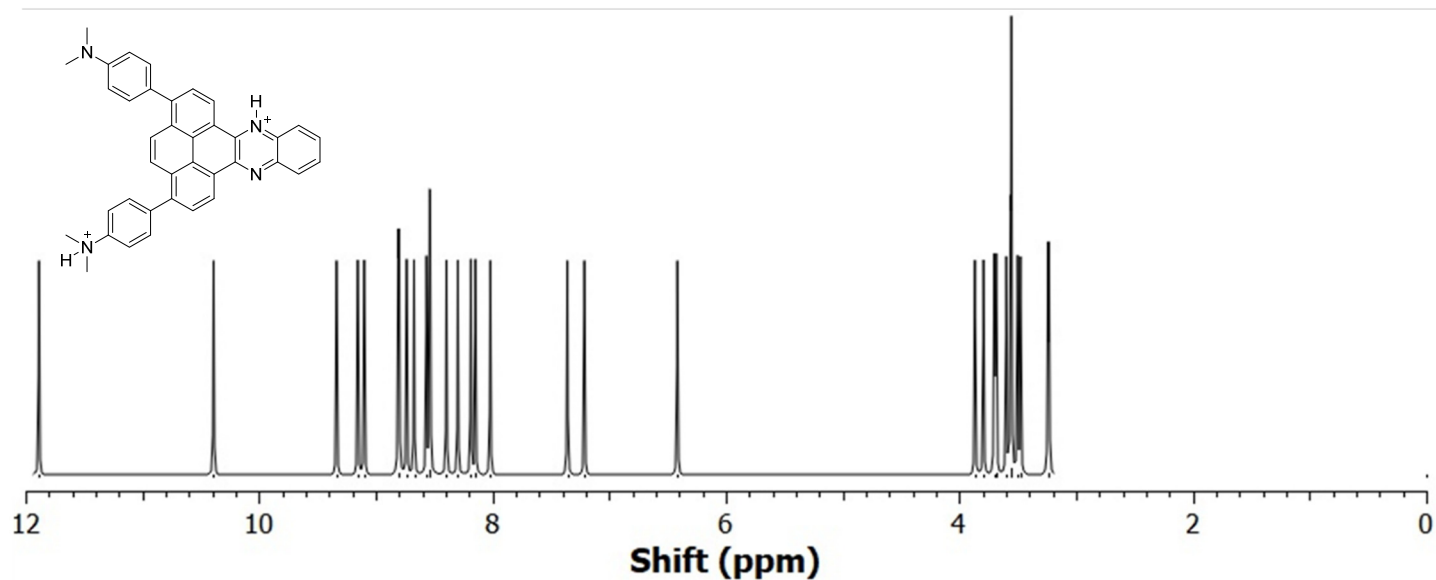


Figure S21. GIAO-simulated ^1H NMR of quinoxaline & aniline-protonated NMe_2quin from 0-12 ppm.

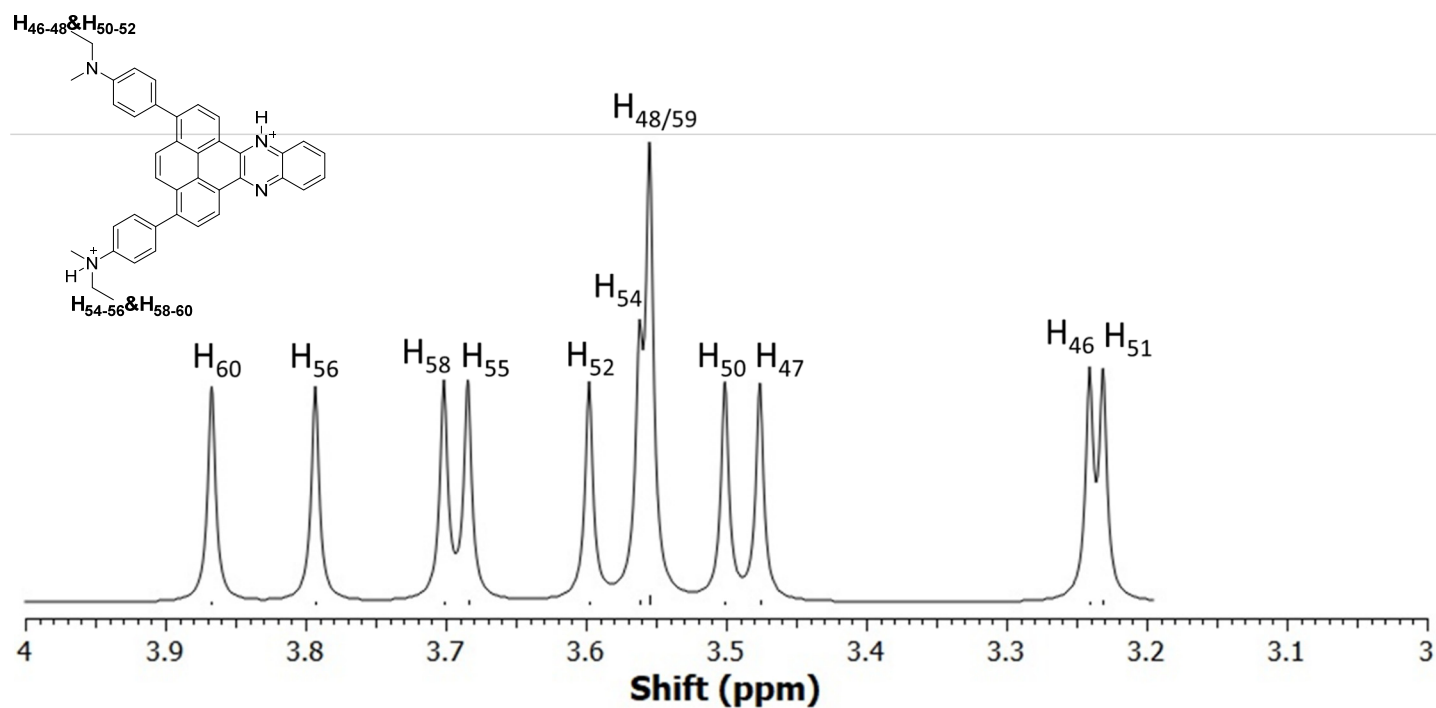


Figure S22. GIAO-simulated ^1H NMR of quinoxaline & aniline-protonated NMe_2quin from 3-4 ppm.

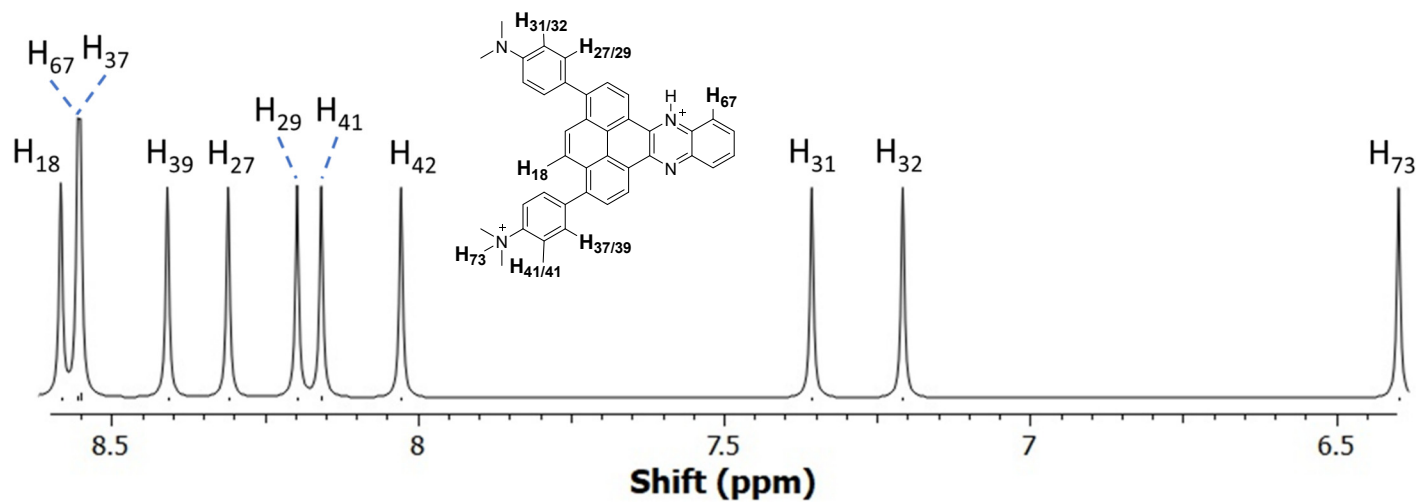


Figure S23. GIAO-simulated ^1H NMR of quinoxaline & aniline-protonated NMe_2quin from 6.4-8.6 ppm.

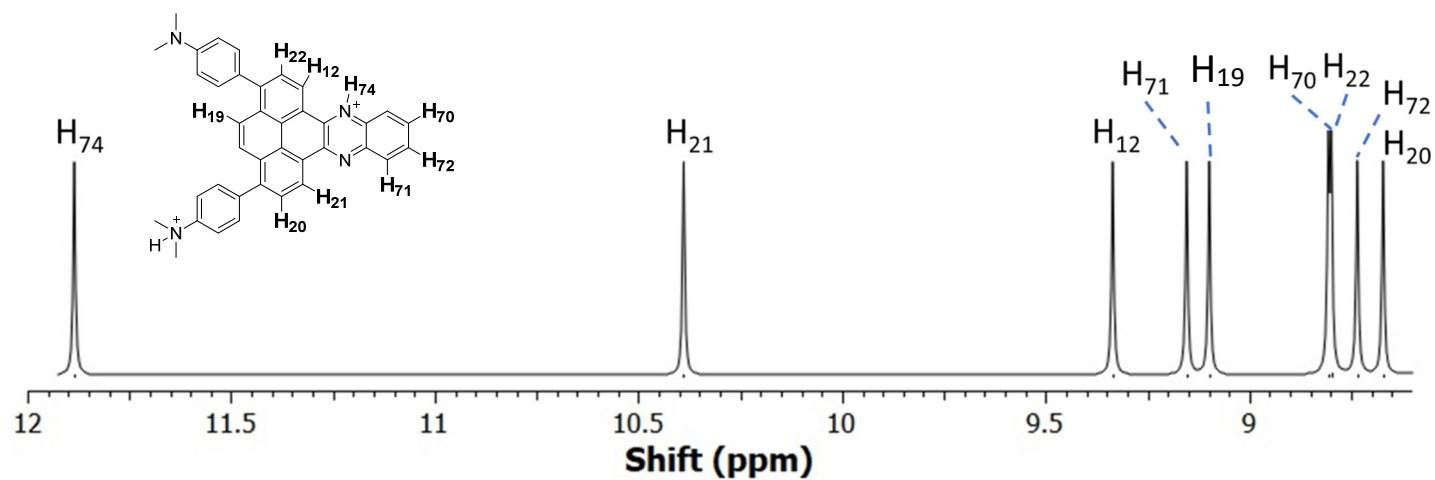
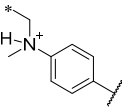
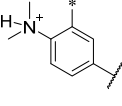
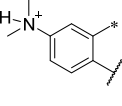
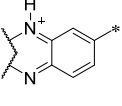
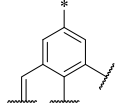
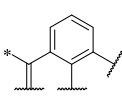
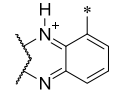
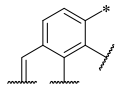


Figure S24. GIAO-simulated ^1H NMR of quinoxaline & aniline-protonated NMe_2quin from 8.6-12 ppm.

Table S7. Chemical shift changes of calculated quinoxaline & aniline-protonated **NMe₂quin** versus experimental excess TFA-addition

Signal Assignment	Calculated Shift $\delta_1 \rightarrow \delta_2$	Calculated Change $\Delta\delta$	Experimental Shift $\delta_1 \rightarrow \delta_2^*$	Experimental Change $\Delta\delta^*$
	3.34 \rightarrow 3.69 ¹	0.35	3.08 \rightarrow 3.47	0.39
	7.21 \rightarrow 8.09 ¹	0.88	6.95 \rightarrow 7.81	0.86
	8.11 \rightarrow 8.47 ¹	0.36	7.59 \rightarrow 7.87	0.28
	8.42 \rightarrow 8.81 ¹	0.39	7.89 \rightarrow 8.31	0.42
	8.57 \rightarrow 8.66	0.09	8.07 \rightarrow 8.23	0.16
	8.84 \rightarrow 8.56	-0.28	8.19 \rightarrow 8.03	-0.16
	8.88 \rightarrow 9.15 ¹	0.27	8.40 \rightarrow 8.35	0.35
	10.36 \rightarrow 10.40	0.04	9.67 \rightarrow 9.77	0.10

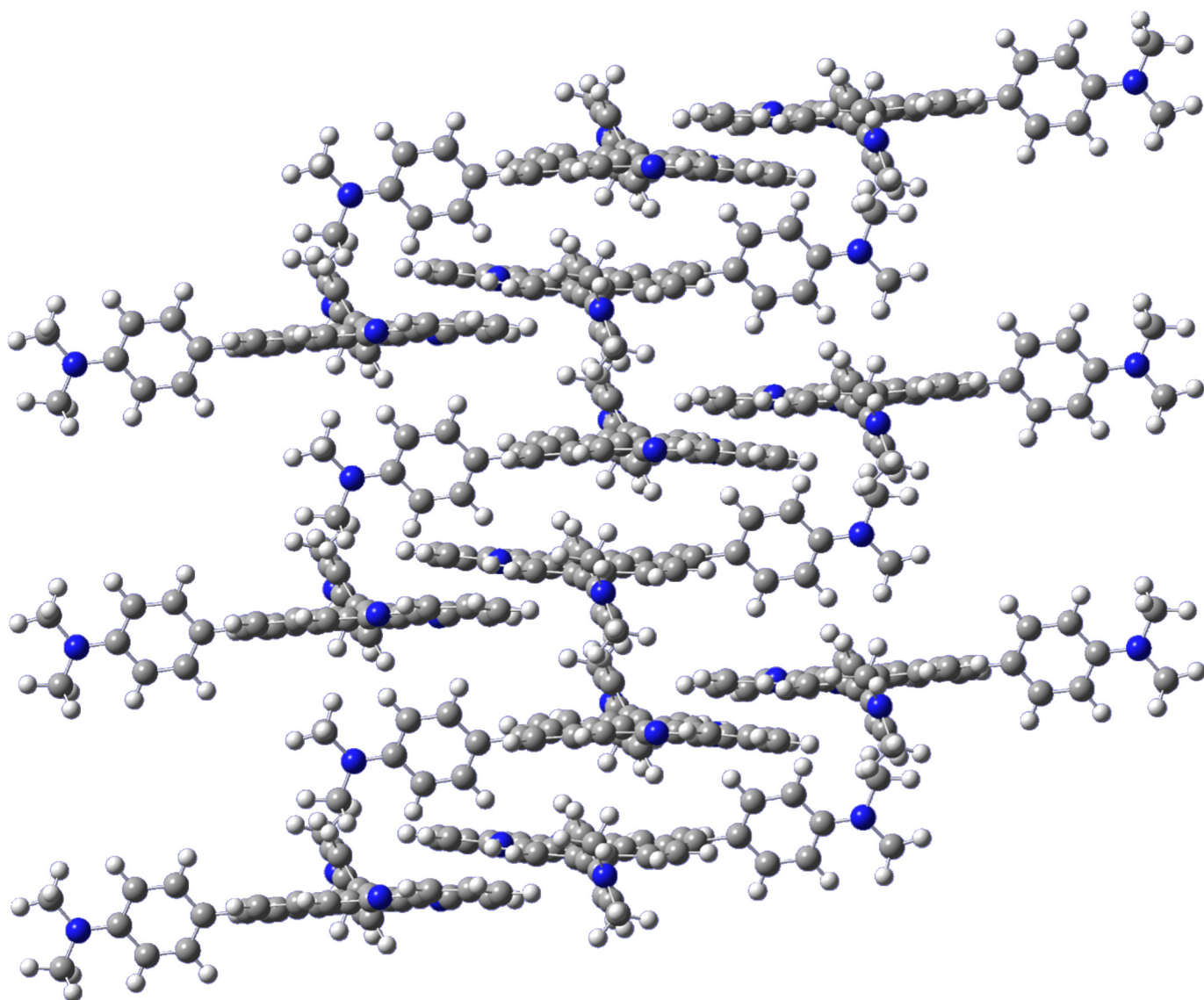
¹Calculated shift is based upon the proton closest to the protonated nitrogen, either anilinium or quinoxalinium.

* Experimental values come from addition of *excess* TFA, as found on pages S38-S39.

Section 5c Results of Crystal Packing Calculations

DFT Simulations were performed on the crystal structures of the two polymorphs of **NMe₂quin** to compare the relative energies of intermolecular (i.e. dispersive) interactions. Cartesian coordinates were extracted from the crystal structures and all C-H bonds lengths were manually set to those obtained of a single molecule of **NMe₂quin** at the B3LYP/cc-pVTZ level. The structures were not optimized *in-silico* but left frozen to acquire the best simulation of a collective of molecules in the crystal structures. Energy calculations were performed using the 6-311G++(d,p) basis sets^{34,35} to adequately model dispersive interactions with lesser computational cost than cc-pVTZ. The energies of the crystal structures were obtained using multiple functionals that include Grimme's empirical dispersion³⁶ with Becke-Johnson damping,³⁷ if implemented: B3LYP-D3(BJ),²⁴⁻²⁶ B97-D3(BJ),³⁸ ω B97X-D2,³¹ and M06-2X-D2³⁹. The crystal structure energies were then compared to multiple times the individual molecule energies, at the same level of theory, and the difference was assumed to represent the stabilization incurred from dispersive intermolecular interactions. Such comparison is summed in a Table S8, below.

1,8-Bis(4-*N,N*-dimethylaminophenyl)phenanthro[4,5-*abc*]phenazine in Polymorph **NMe₂quin-grou**



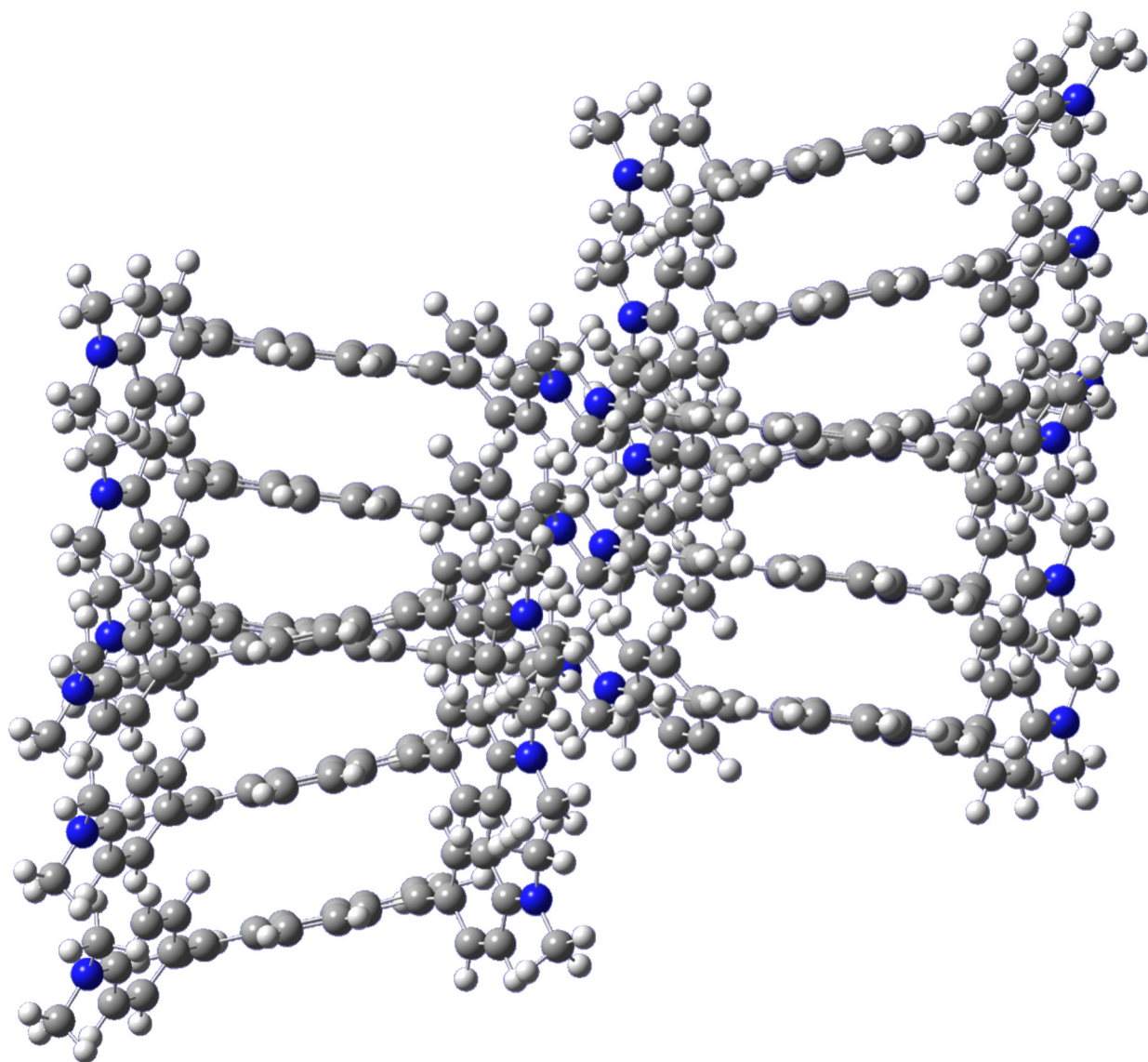


Table S8. Dispersion energy comparison between molecules in **NMe₂quin-grou** and **NMe₂quin-pris**

	Energy from Exchange-Correlation Functional (kcal/mol)			
	B3LYP-D3(BJ)	B97-D3(BJ)	ωB97X-D2	M06-2X-D3
Polymorph NMe₂quin-grou				
Single Molecule	-1057830.172	-1057022.659	-1057348.597	-1057288.595
12 \times Single Molecules	-12693962.07	-12684271.91	-12688183.16	-12687463.14
12 Molecules in Crystal	-12694247.77	-12684577.24	-12688482.65	-12687736.82
<i>ΔE of Dispersive Interaction (crystal – 12 \times single-molecules)</i>	<i>-285.702</i>	<i>-305.324</i>	<i>-299.49</i>	<i>-273.677</i>
Polymorph NMe₂quin-pris				
Single Molecule	-1057828.834	-1057020.878	-1057347.321	-1057287.215
12 \times Single Molecules	-12693946.01	-12684250.54	-12688167.86	-12687446.57
12 Molecules in Crystal	-12694300.21	-12684624.96	-12688537.87	-12687780.39
<i>ΔE of Dispersive Interaction (crystal – 12 \times single-molecules)</i>	<i>-354.203</i>	<i>-374.417</i>	<i>-370.015</i>	<i>-333.819</i>
ΔE in Crystal Energies (Interaction Energy of pris minus grou)	-68.500	-69.093	-70.523	-60.142

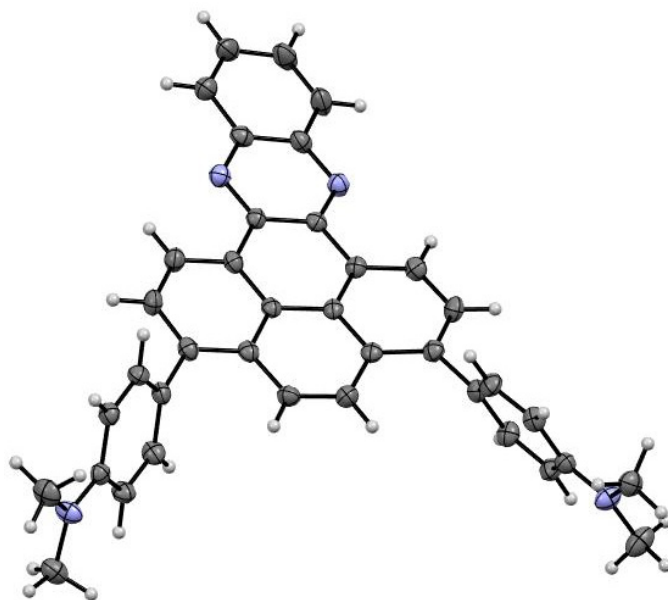


Figure S25. ORTEP representation of **NMe₂quin-grou** with 50% thermal ellipsoids.

Table S9. Crystal data and structural refinement for **NMe₂quin-grou**

Identification code	DTH6-96A
Empirical formula	C ₃₈ H ₃₀ N ₄
Formula weight	542.66
Temperature/K	173
Crystal system	monoclinic
Space group	P2 ₁ /c
a/Å	9.3641(9)
b/Å	17.2562(17)
c/Å	17.3647(16)
α/°	90
β/°	101.383(3)
γ/°	90
Volume/Å ³	2750.7(5)
Z	4
ρ _{calc} /g/cm ³	1.310
μ/mm ⁻¹	0.078
F(000)	1144.0
Crystal size/mm ³	0.34 × 0.27 × 0.26
Radiation	MoKα (λ = 0.71073)
2θ range for data collection/°	3.36 to 51.5
Index ranges	-11 ≤ h ≤ 11, -21 ≤ k ≤ 21, -21 ≤ l ≤ 21
Reflections collected	39971
Independent reflections	5233 [R _{int} = 0.0530, R _{sigma} = 0.0349]

Data/restraints/parameters 5233/0/383
Goodness-of-fit on F^2 1.103
Final R indexes [$I \geq 2\sigma(I)$] $R_1 = 0.0683$, $wR_2 = 0.1742$
Final R indexes [all data] $R_1 = 0.0985$, $wR_2 = 0.1919$
Largest diff. peak/hole / $e \text{ \AA}^{-3}$ 0.28/-0.28

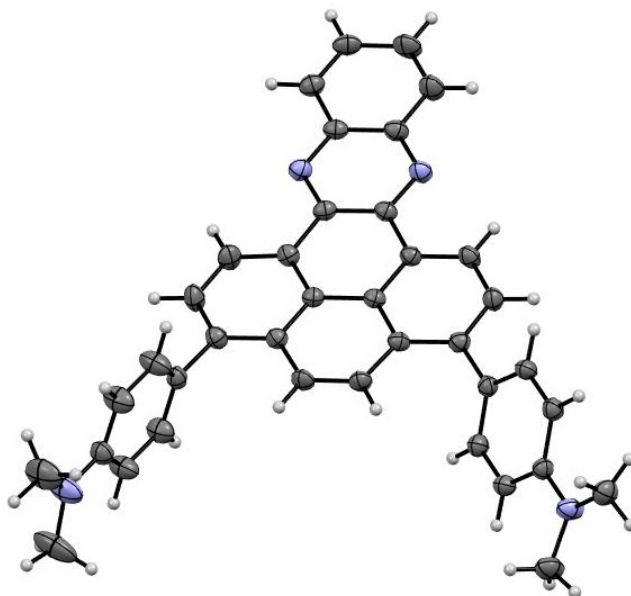


Figure S26. ORTEP representation of **NMe₂quin-pris** with 50% thermal ellipsoids.

Table S10. Crystal data and structural refinement for **NMe₂quin-pris**

Identification code	DTH6-96B
Empirical formula	C ₃₈ H ₃₀ N ₄
Formula weight	542.66
Temperature/K	173
Crystal system	monoclinic
Space group	P2 ₁ /n
a/Å	8.14050(10)
b/Å	27.7632(5)
c/Å	12.0061(2)
$\alpha/^\circ$	90
$\beta/^\circ$	91.3970(10)
$\gamma/^\circ$	90
Volume/Å ³	2712.65(7)
Z	4
$\rho_{\text{calc}}/\text{cm}^3$	1.329
μ/mm^{-1}	0.609
F(000)	1144.0
Crystal size/mm ³	0.3 × 0.3 × 0.2
Radiation	CuK α ($\lambda = 1.54178$)
2 θ range for data collection/ $^\circ$	6.366 to 140.134

Index ranges	$-9 \leq h \leq 9, -31 \leq k \leq 33, -11 \leq l \leq 14$
Reflections collected	20606
Independent reflections	5112 [$R_{\text{int}} = 0.0334, R_{\text{sigma}} = 0.0311$]
Data/restraints/parameters	5112/0/383
Goodness-of-fit on F^2	1.013
Final R indexes [$I \geq 2\sigma(I)$]	$R_1 = 0.0475, wR_2 = 0.1249$
Final R indexes [all data]	$R_1 = 0.0643, wR_2 = 0.1381$
Largest diff. peak/hole / $e \text{ \AA}^{-3}$	0.23/-0.20

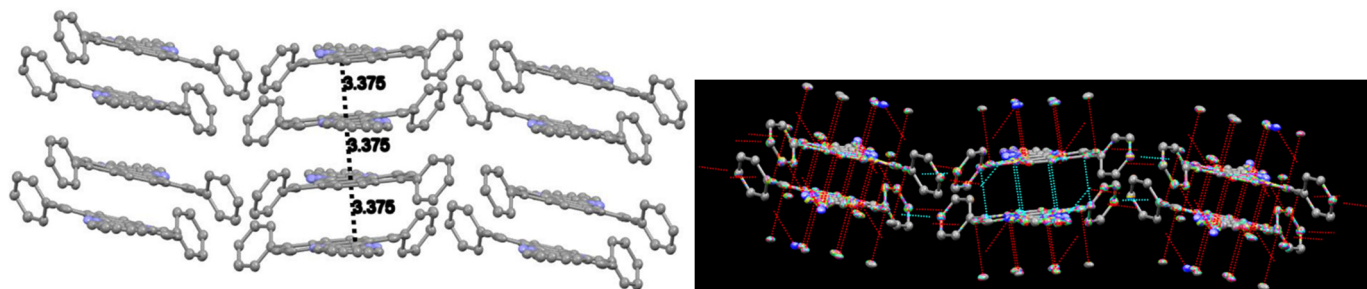


Figure S27. Packing of **Ph₂quin** viewed along the b-axis, showing the intermolecular distances and the vertically dominant short-contacts in the unit cell. Cyan contacts indicate those between molecules fully within the unit cell.

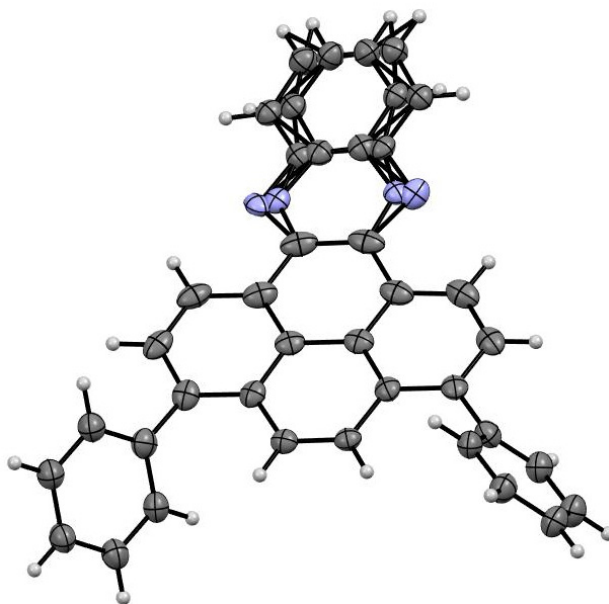
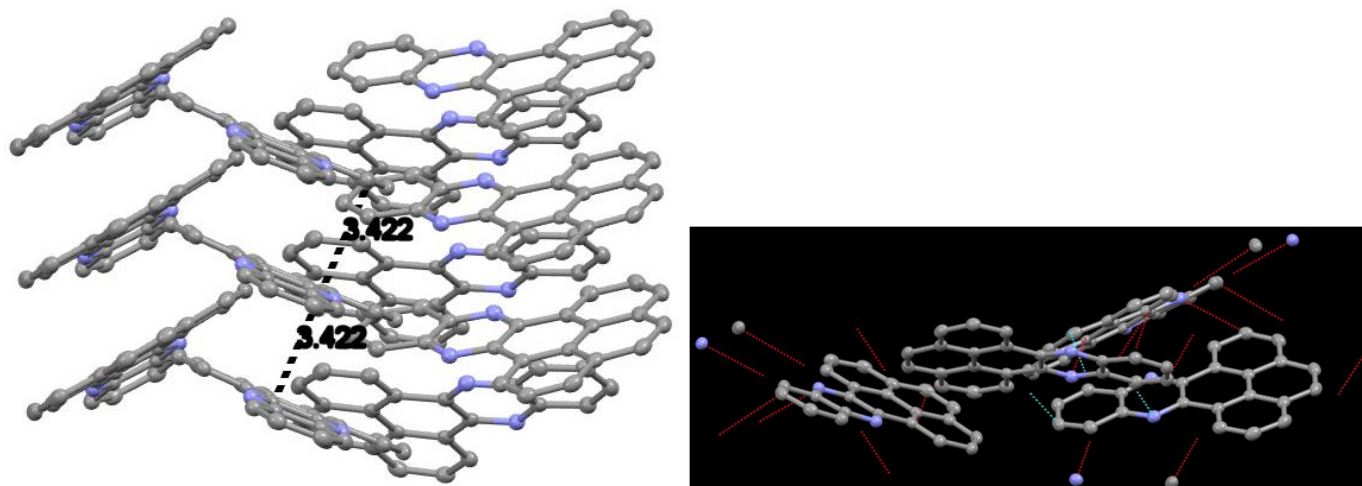


Figure S28. ORTEP representation of **Ph₂quin** with 50% thermal ellipsoids.

Table S11. Crystal data and structural refinement for **Ph₂quin**

chemical formula	C ₆₈ H ₄₀ N ₄ (disordered chemical formula)
crystal colour	Yellow
<i>F</i> _w ; <i>F</i> (000)	913.04; 952
<i>T</i> (K)	100
wavelength (Å)	0.7749
space group	Pbcn
<i>a</i> (Å)	23.746(5)
<i>b</i> (Å)	13.717(3)
<i>c</i> (Å)	6.8210(14)
α (deg)	90
β (deg)	90
γ (deg)	90
<i>Z</i>	2
<i>V</i> (Å ³)	2221.8(8)
ρ_{calcd} (g·cm ⁻³)	1.365
μ (mm ⁻¹)	0.080
θ range (deg); completeness	3.238 – 26.752; 0.996
collected reflections; <i>R</i> _{σ}	23076; 0.0371
unique reflections; <i>R</i> _{int}	23076; 0.1016
<i>R</i> 1 ^a ; <i>wR</i> 2 ^b [<i>I</i> > 2 σ (<i>I</i>)]	0.1236; 0.3559
<i>R</i> 1; <i>wR</i> 2 [all data]	0.1441; 0.3687
GOF	1.141
largest diff peak and hole	0.445 and -0.375

**Figure S29.** Packing of **H₂quin** viewed along the *c*-axis, showing the intermolecular distances and short contacts in the unit cell. Cyan contacts indicate those between molecules fully within the unit cell.

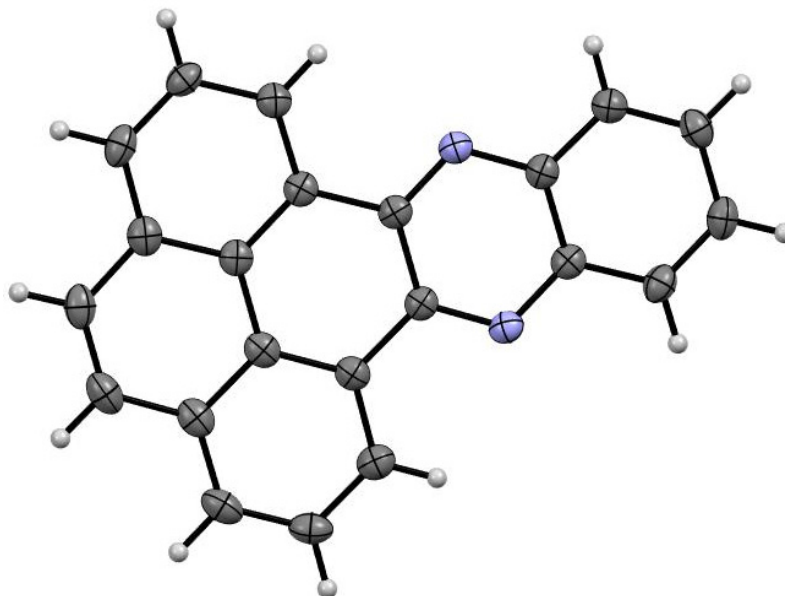


Figure S30. ORTEP representation of **H₂quin** with 50% thermal ellipsoids.

Table S12. Crystal data and structural refinement for **H₂quin**

Identification code	DTH6-79A
Empirical formula	C ₂₂ H ₁₂ N ₂
Formula weight	304.34
Temperature/K	173
Crystal system	orthorhombic
Space group	P2 ₁ 2 ₁ 2 ₁
a/Å	3.8365(2)
b/Å	18.0157(8)
c/Å	20.0105(9)
α/°	90
β/°	90
γ/°	90
Volume/Å ³	1383.07(11)
Z	4
ρ _{calc} /cm ³	1.462
μ/mm ⁻¹	0.674
F(000)	632.0
Crystal size/mm ³	0.384 × 0.045 × 0.044
Radiation	CuKα (λ = 1.54178)
2θ range for data collection/°	6.602 to 140.068
Index ranges	-4 ≤ h ≤ 4, -21 ≤ k ≤ 21, -24 ≤ l ≤ 20
Reflections collected	7153
Independent reflections	2615 [R _{int} = 0.0364, R _{sigma} = 0.0423]
Data/restraints/parameters	2615/0/218
Goodness-of-fit on F ²	1.034
Final R indexes [I ≥ 2σ (I)]	R ₁ = 0.0419, wR ₂ = 0.0984

Final R indexes [all data] $R_1 = 0.0525$, $wR_2 = 0.1042$
Largest diff. peak/hole / $e \text{ \AA}^{-3}$ 0.14/-0.24
Flack parameter -0.5(9)

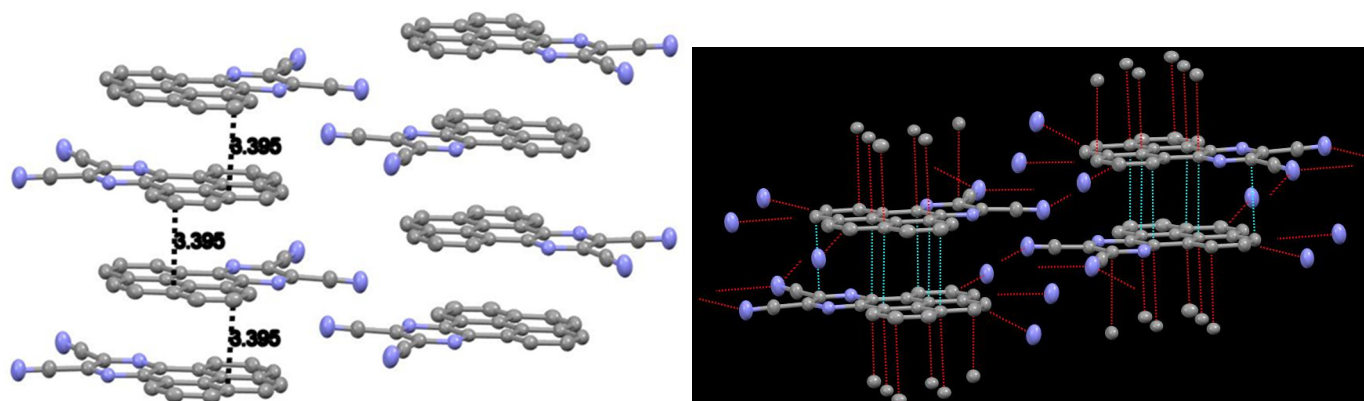


Figure S32. Packing of **H₂pyr** viewed along the a-axis, showing the intermolecular distances and short contacts in the unit cell. Cyan contacts indicate those between molecules fully within the unit cell.

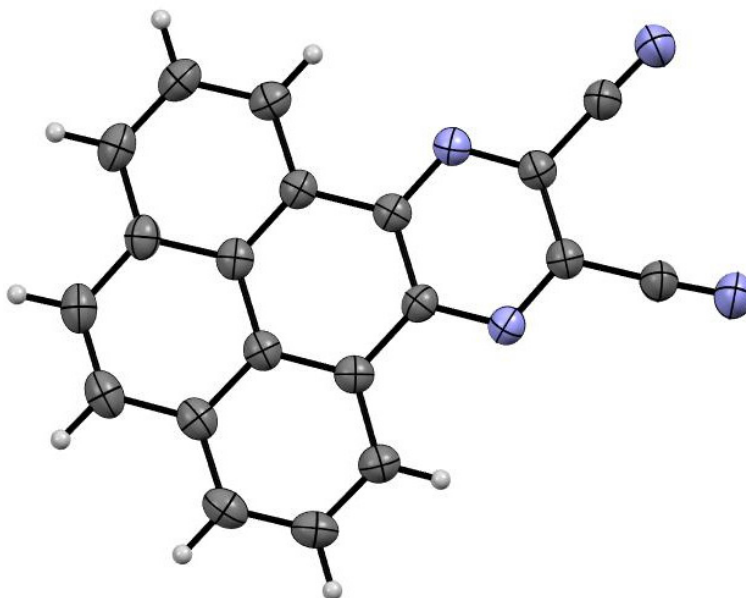


Figure S33. ORTEP representation of **H₂pyr** with 50% thermal ellipsoids.

Table S13. Crystal data and structural refinement for **H₂pyr**

Identification code	20190309DH
Empirical formula	C ₂₀ H ₈ N ₄
Formula weight	304.30
Temperature/K	173
Crystal system	monoclinic
Space group	P2 ₁ /c

a/Å	9.0269(3)
b/Å	21.7465(7)
c/Å	7.1992(2)
α /°	90
β /°	94.579(2)
γ /°	90
Volume/Å ³	1408.72(8)
Z	4
ρ_{calc} /cm ³	1.435
μ /mm ⁻¹	0.709
F(000)	624.0
Crystal size/mm ³	0.151 × 0.084 × 0.046
Radiation	CuK α (λ = 1.54178)
2 θ range for data collection/°	8.132 to 140.064
Index ranges	-10 ≤ h ≤ 8, -26 ≤ k ≤ 25, -8 ≤ l ≤ 8
Reflections collected	11402
Independent reflections	2657 [R _{int} = 0.0316, R _{sigma} = 0.0281]
Data/restraints/parameters	2657/0/217
Goodness-of-fit on F ²	1.081
Final R indexes [I >= 2 σ (I)]	R ₁ = 0.0490, wR ₂ = 0.1282
Final R indexes [all data]	R ₁ = 0.0616, wR ₂ = 0.1384
Largest diff. peak/hole / e Å ⁻³	0.21/-0.29

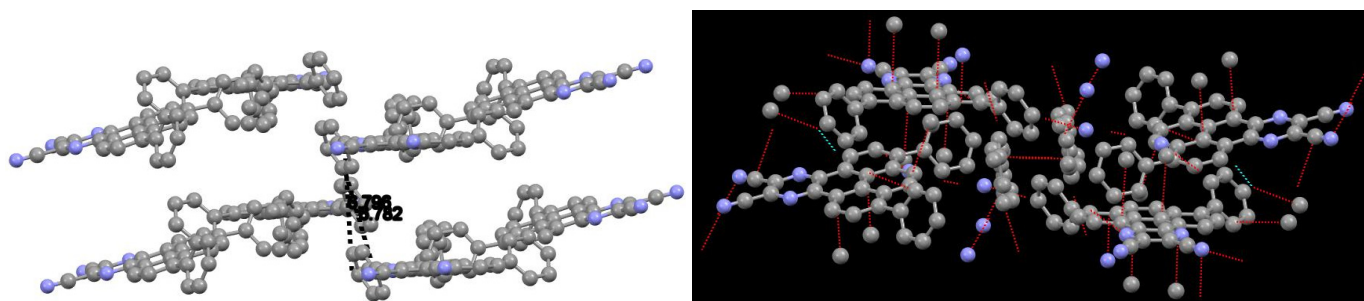


Figure S34. Packing of **Ph₂pyr** viewed along the b-axis, showing the intermolecular distances and short contacts in the unit cell. Cyan contacts indicate those between molecules fully within the unit cell.

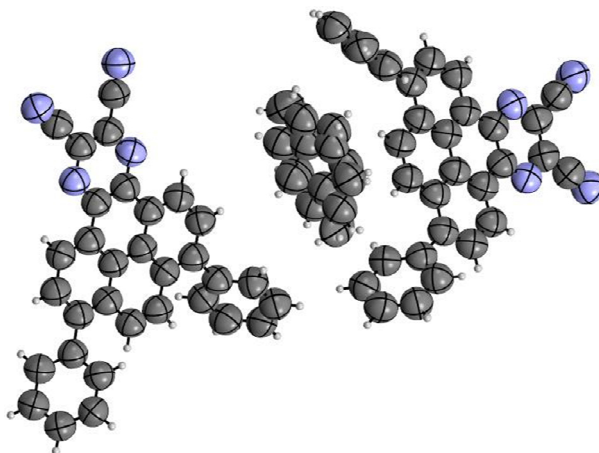


Figure S35. ORTEP representation of **Ph₂pyr** toluene solvate with 50% thermal ellipsoids.

Table S14. Crystal data and structural refinement for **H₂pyr**

Chemical formula	C ₇₁ H ₄₀ N ₈ (toluene solvate, 2 Ph ₂ pyr molecules)
Molecular weight	1005.11
Temperature	100
Wavelength	0.6889
Crystal system ; space group	triclinic ; P -1
Unit cell dimensions	a = 6.9190(14) Å ; α = 98.88(3) ° b = 17.346(3) Å ; β = 90.98(3) ° c = 21.688(4) Å ; γ = 95.88(3) °
Volume	2556.8(9) Å ³
Z, Calculated density	2, 1.306 g/cm ³
Absorption coefficient	0.072 1/mm
F(000)	1044
Theta range for data collection	0.922° to 23.757°
Limiting indices	-8 ≤ h ≤ 8 ; -20 ≤ k ≤ 20 ; -6 ≤ l ≤ 25
Reflection collected / unique	8485 / 8485 [R(int) = ?]
Completeness to theta max	99.1 %
Refinement method	Full-matrix least-square on F ²
Data / restraints / parameters	8485 / 194 / 753
Goodness of fit on F ²	1.069

Final R indices [$I > 2\sigma(I)$] R1 = 0.0938 ; wR2 = 0.2675

Final R indices [all data] R1 = 0.1356 ; wR2 = 0.3489

Absolute structure parameter

Largest diff peak and hole 0.233 and -0.186 e/Å³

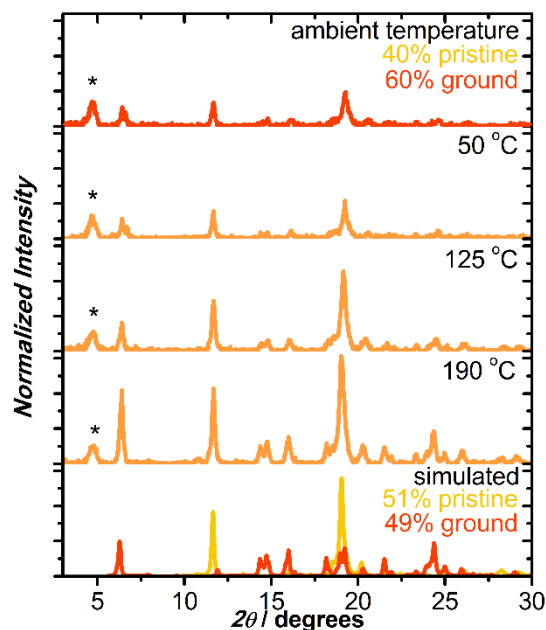


Figure S36. Variable temperature PXRD of ground NMe₂quin, with temperatures chosen following thermal events by DSC. Rough Reitveld refinement yielded the mass fractions from ground (red) and pristine (yellow) material. The asterisks mark a reflection from the sample container.

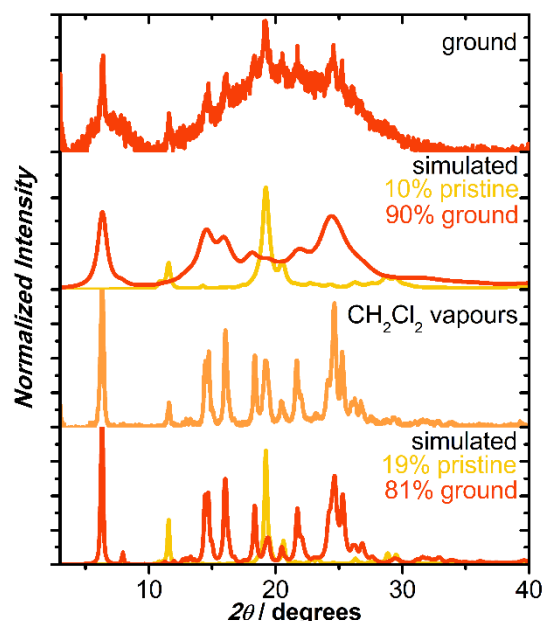


Figure S37. PXRD of ground material before (top) and after (bottom) exposure to dichloromethane vapour. Rough Reitveld refinements yielded the mass fractions from ground (red) and pristine (yellow) material.

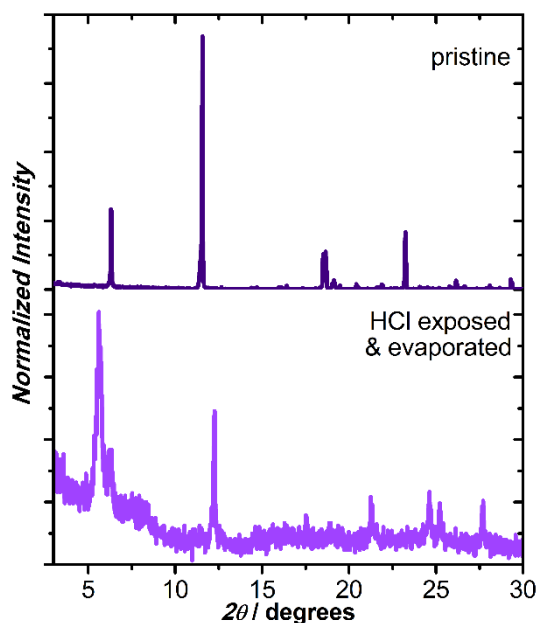


Figure S38. PXRD of NMe₂quin before (top) and after (bottom) exposure and off-gassing HCl vapours.

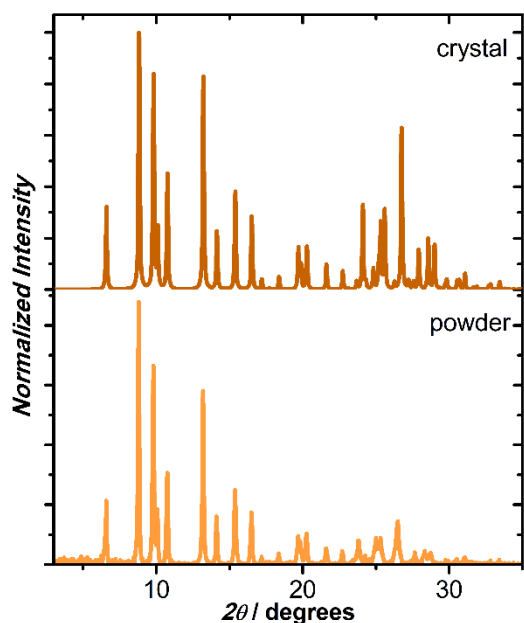


Figure S39. Comparison of the simulated PXRD from single-crystalline H₂quin (top) and the experimental powdered sample (bottom).

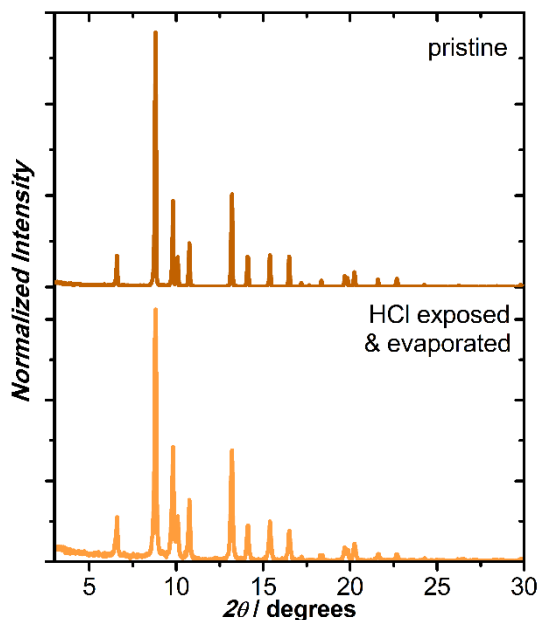


Figure S40. PXR D of **H₂quin** before (top) and after (bottom) exposure and off-gassing HCl vapours.

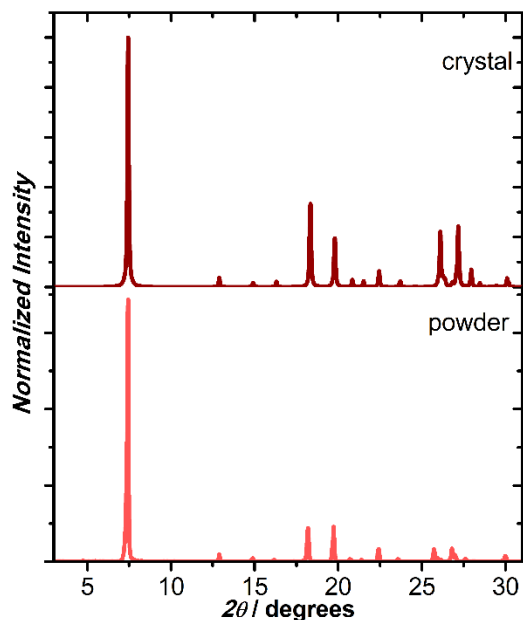


Figure S41. Comparison of the PXR D from simulated single-crystalline **Ph₂quin** (top) and the experimental powdered sample (bottom).

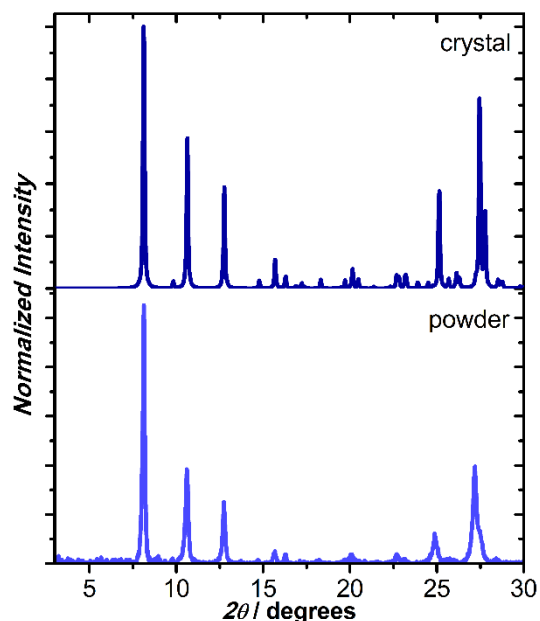


Figure S42. Comparison of the PXR D from simulated single-crystalline **H₂pyr** (top) and the experimental powdered sample (bottom).

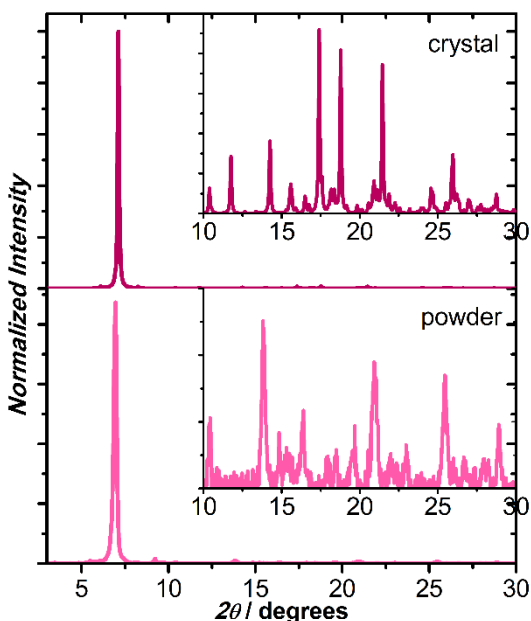


Figure S43. Comparison of the PXR D from simulated single-crystalline **Ph₂pyr** (top) and the experimental powdered sample (bottom). Due to included toluene in the crystal, there is no match between the two patterns.

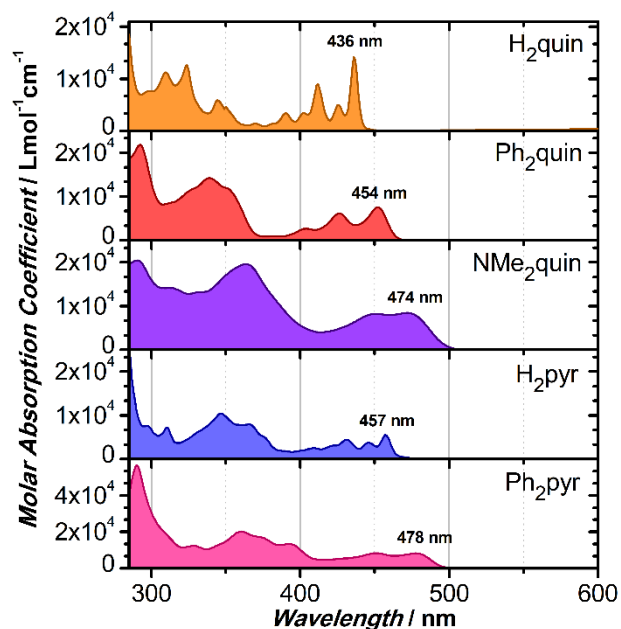


Figure S44. UV-visible absorption spectra of all core-expanded pyrenes in 10 μM cyclohexane solution.

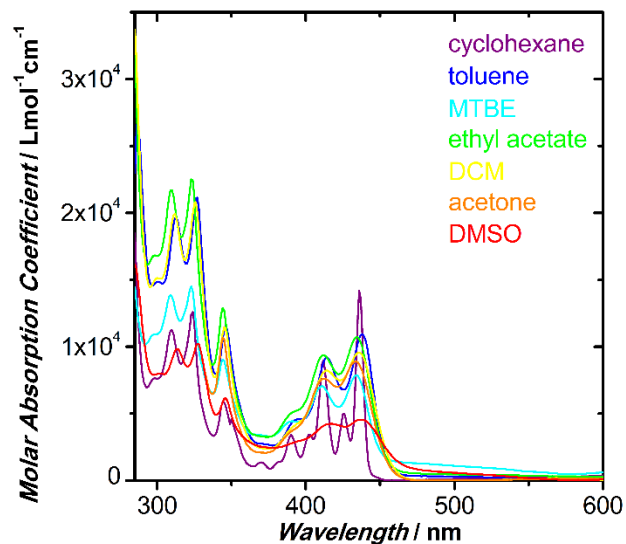


Figure S45. UV-visible absorption spectra of 10 μM **H₂quin** in solvents of increasing polarity.

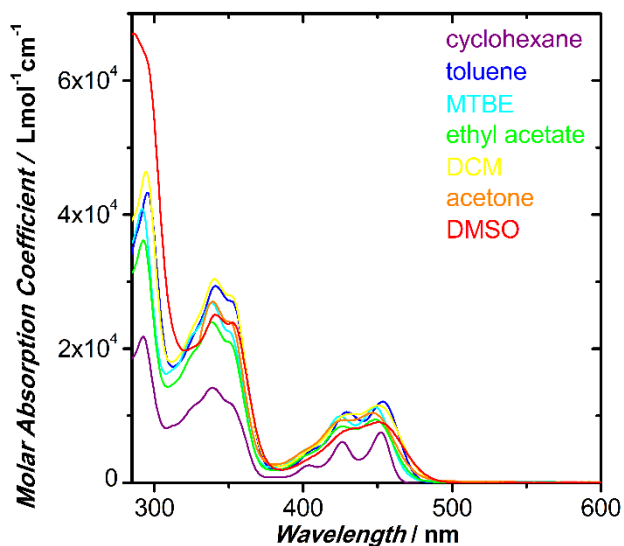


Figure S46. UV-visible absorption spectra of 10 μM **Ph₂quin** in solvents of increasing polarity.

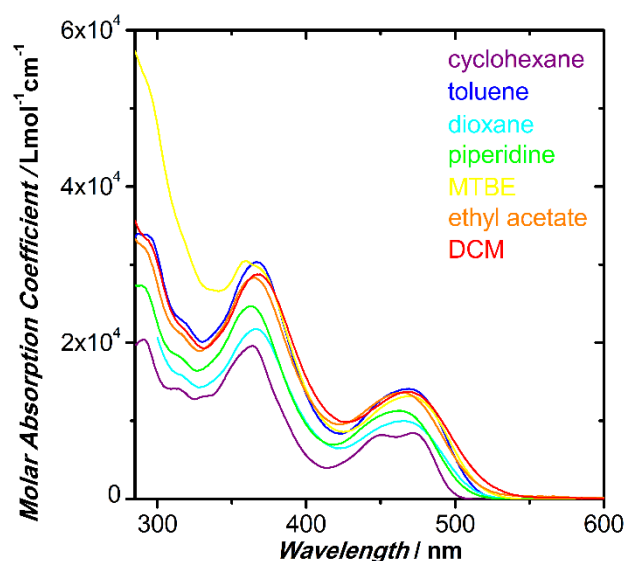


Figure S47. UV-visible absorption spectra of 10 μM **NMe₂quin** in solvents of increasing polarity.

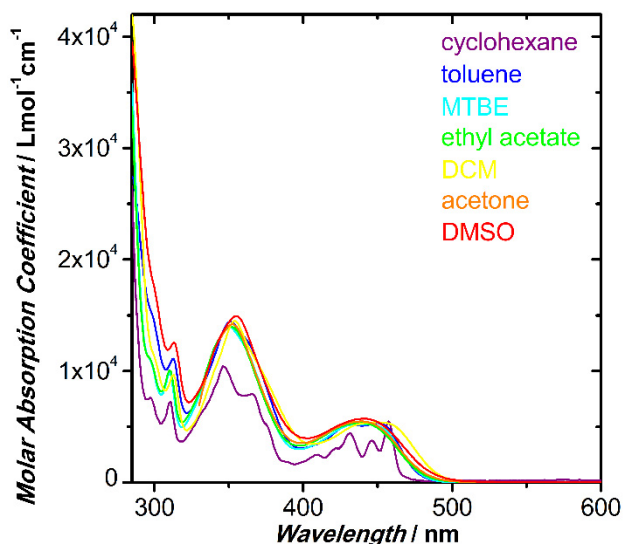


Figure S48. UV-visible absorption spectra of 10 μM H_2pyr in solvents of increasing polarity.

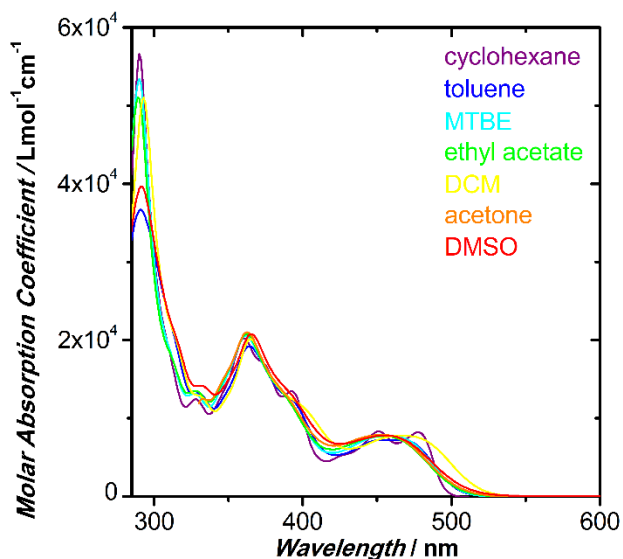


Figure S49. UV-visible absorption spectra of 10 μM Ph_2pyr in solvents of increasing polarity.

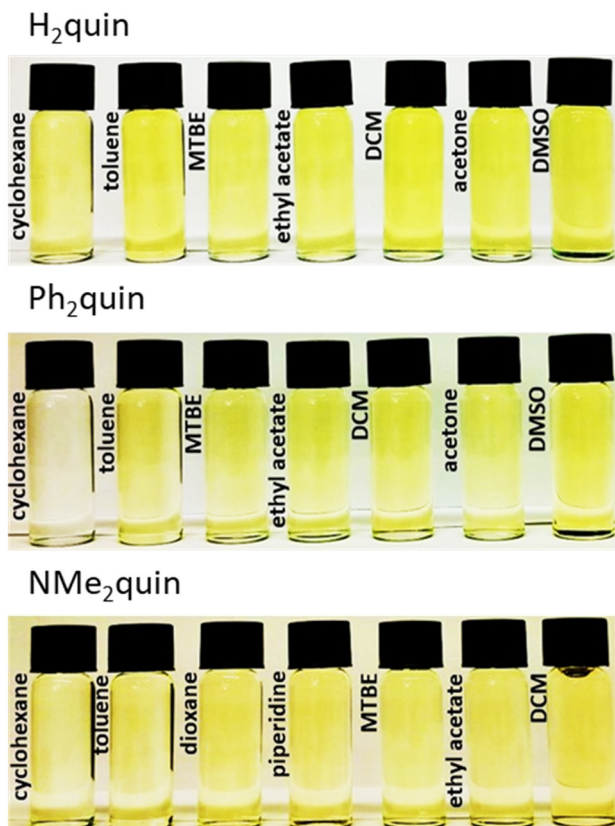


Figure S50. Photograph of quinoxaline-fused pyrenes in solutions of varying polarity under ambient lighting.

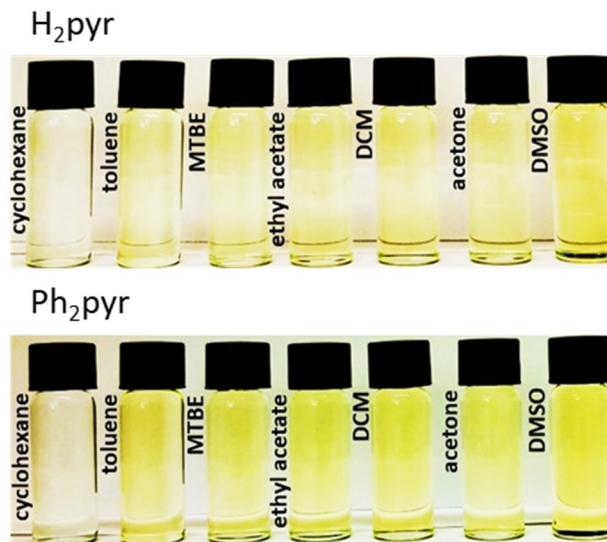


Figure S51. Photograph of dicyanopyrazine-fused pyrenes in solutions of varying polarity under ambient lighting.

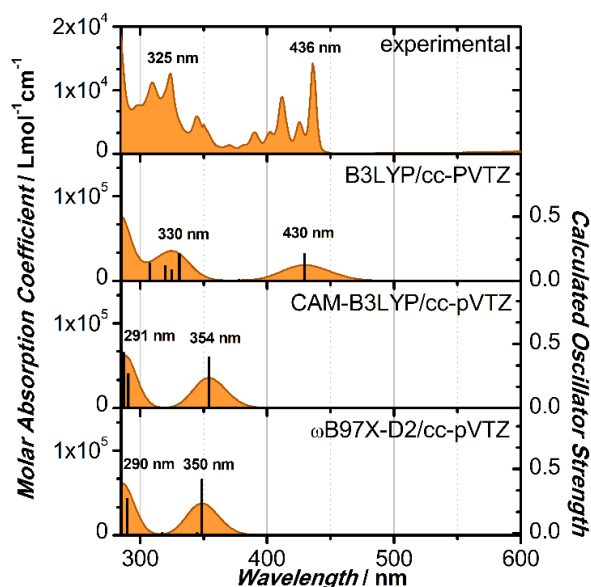


Figure S52. Experimental UV-visible absorption spectrum of 10 μM **H₂quin** in cyclohexane (top) compared to DFT-calculated spectra (bottom) with different functionals. The matching to B3LYP is superior to either of the range-corrected functionals. Black lines indicate the positions of predicted transitions.

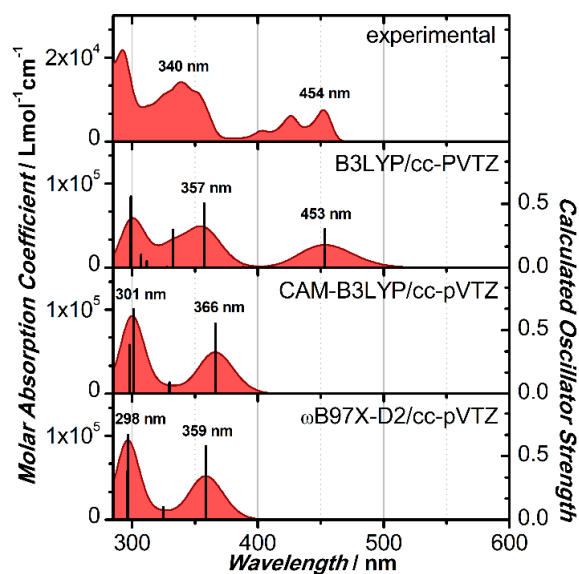


Figure S53. Experimental UV-visible absorption spectrum of 10 μM **Ph₂quin** in cyclohexane (top) compared to DFT-calculated spectra (bottom) with different functionals. The matching to B3LYP is superior to either of the range-corrected functionals. Black lines indicate the positions of predicted transitions.

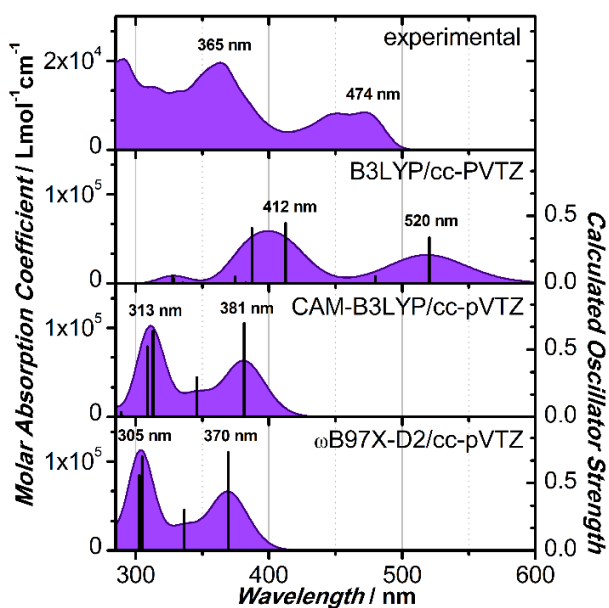


Figure S54. Experimental UV-visible absorption spectrum of 10 μM **NMe₂quin** in cyclohexane (top) compared to DFT-calculated spectra (bottom) with different functionals. The matching to B3LYP is superior to either of the range-corrected functionals. Black lines indicate the positions of predicted transitions.

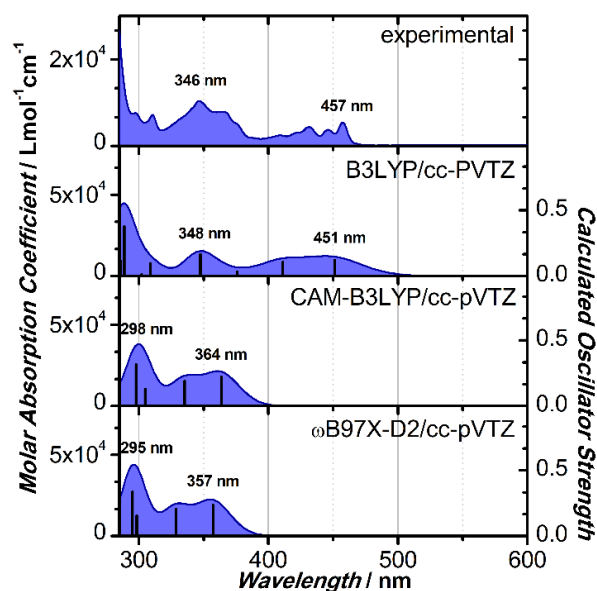


Figure S55. Experimental UV-visible absorption spectrum of 10 μM **H₂pyr** in cyclohexane (top) compared to DFT-calculated spectra (bottom) with different functionals. The matching to B3LYP is superior to either of the range-corrected functionals. Black lines indicate the positions of predicted transitions.

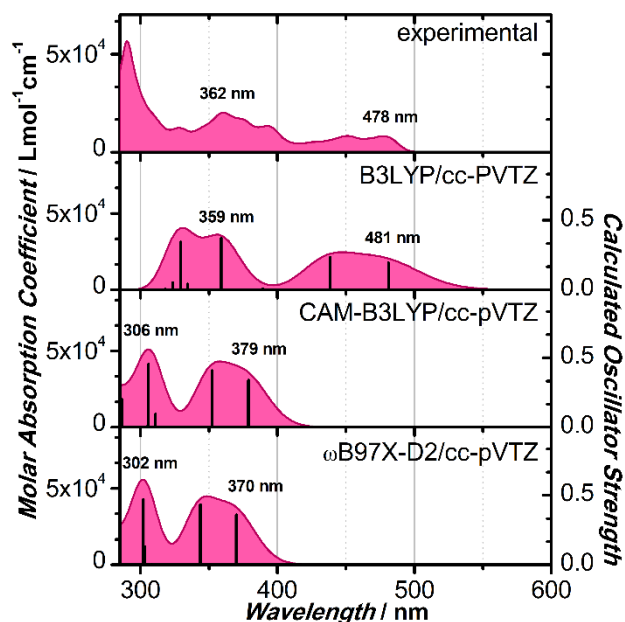


Figure S56. Experimental UV-visible absorption spectrum of 10 μM **Ph₂pyr** in cyclohexane (top) compared to DFT-calculated spectra (bottom) with different functionals. The matching to B3LYP is superior to either of the range-corrected functionals. Black lines indicate the positions of predicted transitions.

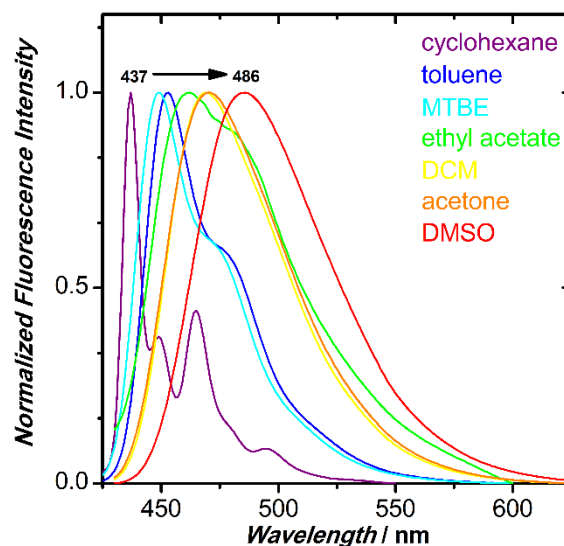


Figure S57. Fluorescence spectra of 10 μM **H₂quin** in solvents of varying polarity, with the peak wavelength shift marked. $\lambda_{\text{exc}} = 420$ nm.

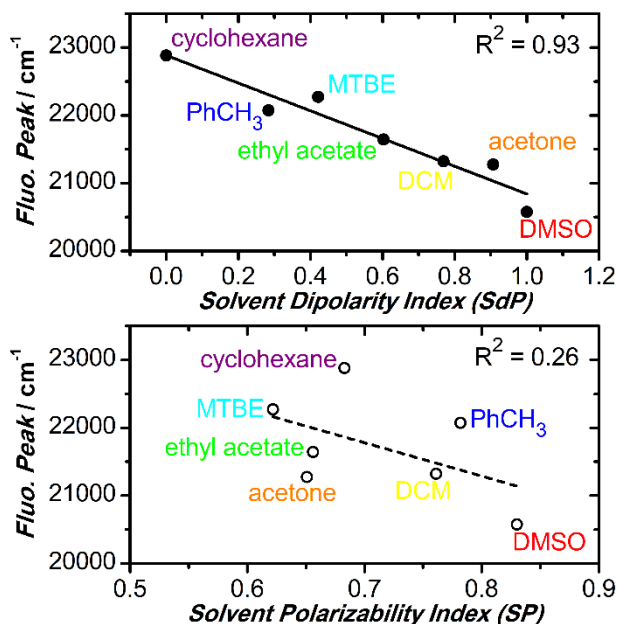


Figure S58. Catalán's solvent dipolarity (filled circles) and solvent polarizability (open circles) versus fluorescence peak wavelength for **H₂quin** solutions. The least-squares fitting is shown in solid and dashed lines, along with the linear R^2 fit.

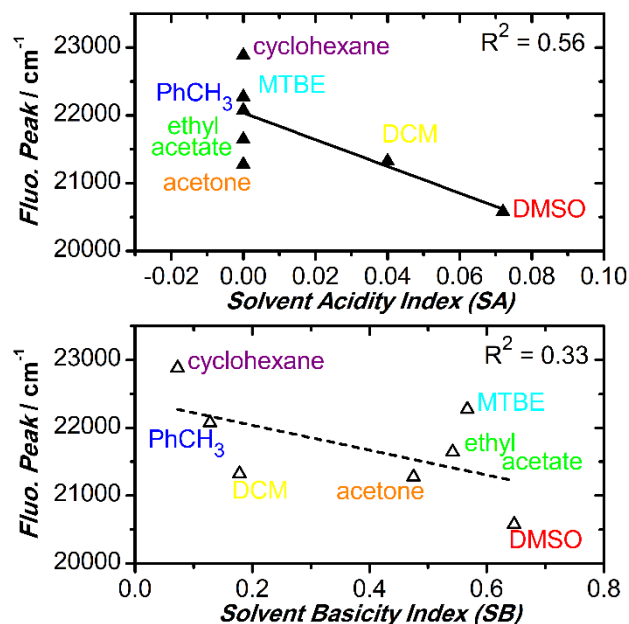


Figure S59. Catalán's solvent acidity (filled triangles) and solvent basicity (open triangles) versus fluorescence peak wavelength for **H₂quin** solutions. The least-squares fitting is shown in solid and dashed lines, along with the linear R^2 fit.

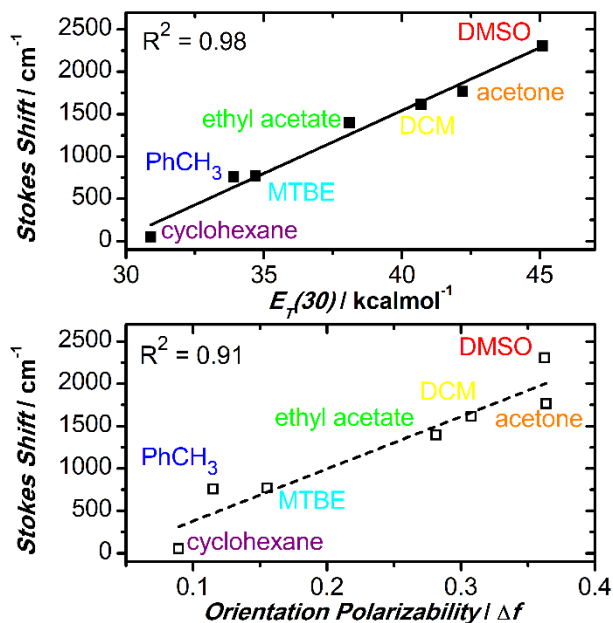


Figure S60. Reichardt's $E_T(30)$ (closed squares) & Lippert and Mataga's orientation polarizability (open squares) plotted against the Stokes shift of **H₂quin** in solvents of varying polarity. The least-squares fitting is shown in solid and dashed lines, along with the linear R^2 fit.

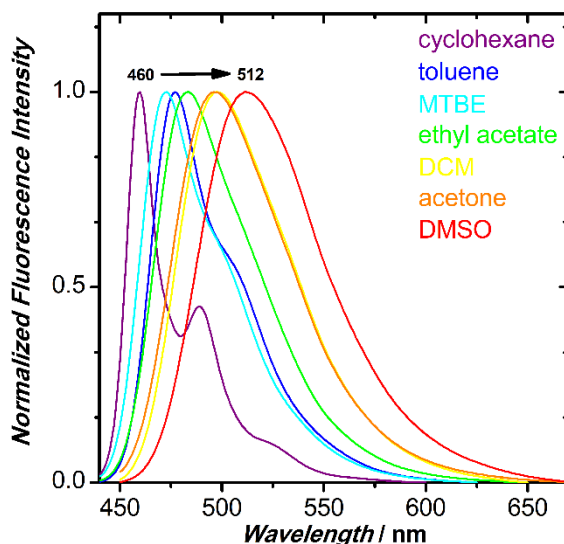


Figure S61. Fluorescence spectra of 10 μM **Ph₂quin** in solvents of varying polarity, with the peak wavelength shift marked. $\lambda_{\text{exc}} = 430 \text{ nm}$.

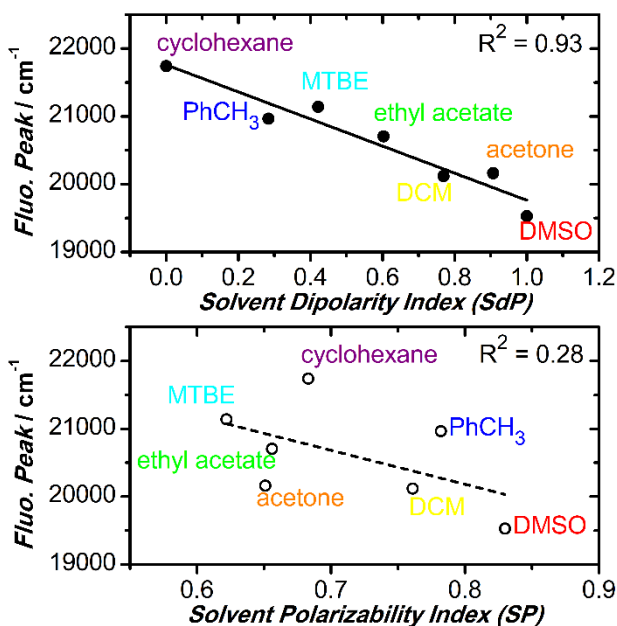


Figure S62. Catalán's solvent dipolarity (filled circles) and solvent polarizability (open circles) versus fluorescence peak wavelength for **Ph₂quin** solutions. The least-squares fitting is shown in solid and dashed lines, along with the linear R^2 fit.

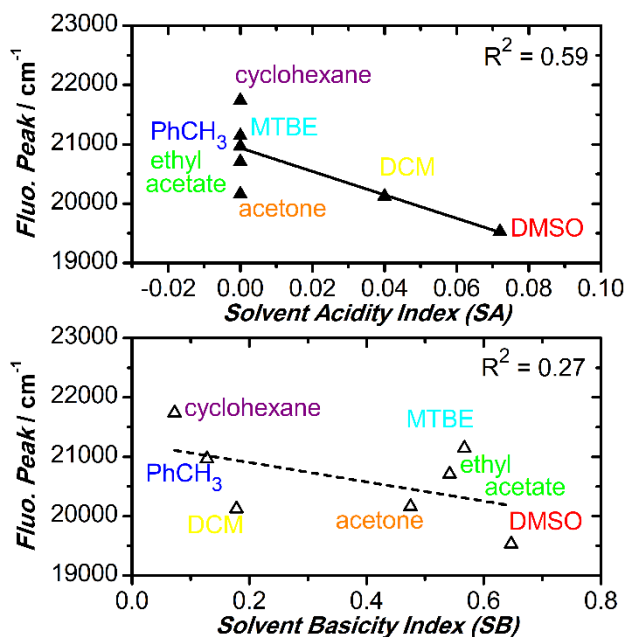


Figure S63. Catalán's solvent acidity (filled triangles) and solvent basicity (open triangles) versus fluorescence peak wavelength for **Ph₂quin** solutions. The least-squares fitting is shown in solid and dashed lines, along with the linear R^2 fit.

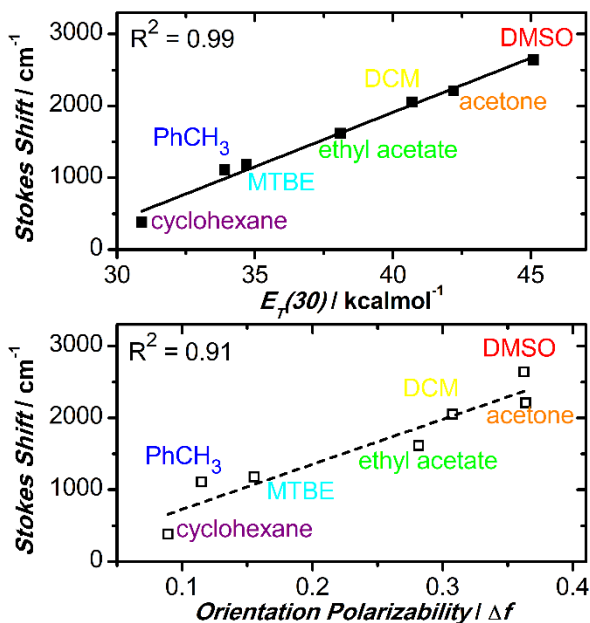


Figure S64. Reichardt's $E_T(30)$ (closed squares) & Lippert and Mataga's orientation polarizability (open squares) plotted against the Stokes shift of **Ph₂quin** in solvents of varying polarity. The least-squares fitting is shown in solid and dashed lines, along with the linear R^2 fit.

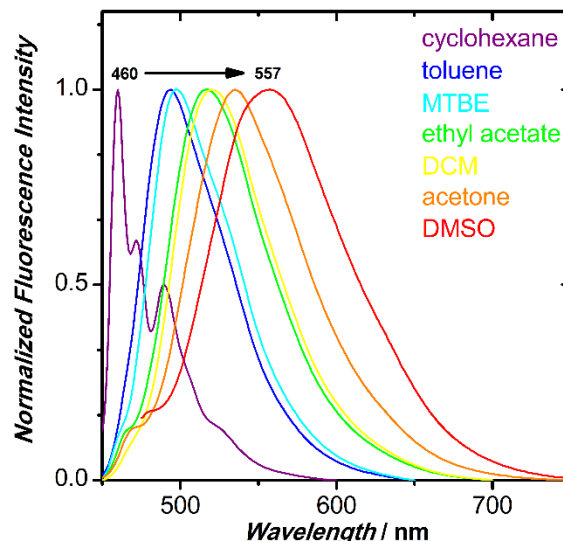


Figure S65. Fluorescence spectra of 10 μM **H₂pyr** in solvents of varying polarity, with the peak wavelength shift marked. $\lambda_{\text{exc}} = 440$ nm.

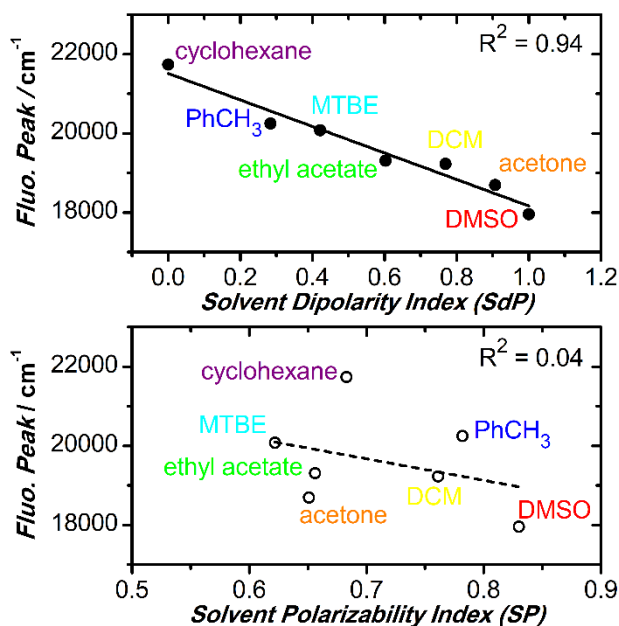


Figure S66. Catalán's solvent dipolarity (filled circles) and solvent polarizability (open circles) versus fluorescence peak wavelength for **H₂pyr** solutions. The least-squares fitting is shown in solid and dashed lines, along with the linear R^2 fit.

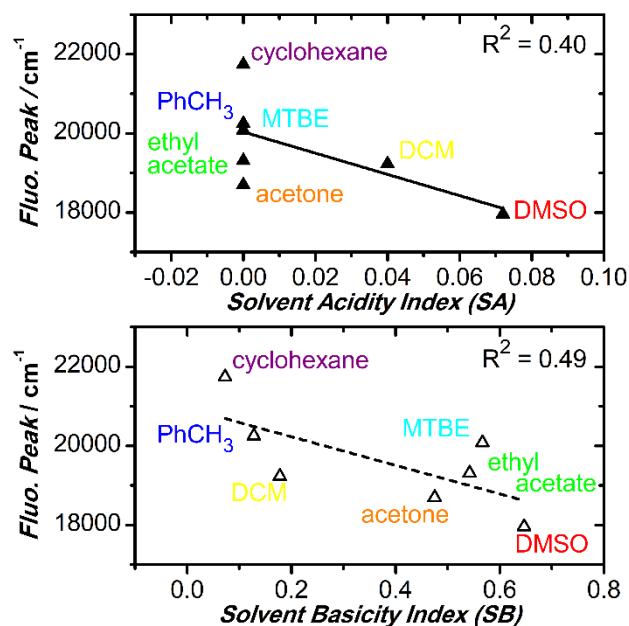


Figure S67. Catalán's solvent acidity (filled triangles) and solvent basicity (open triangles) versus fluorescence peak wavelength for **H₂pyr** solutions. The least-squares fitting is shown in solid and dashed lines, along with the linear R^2 fit.

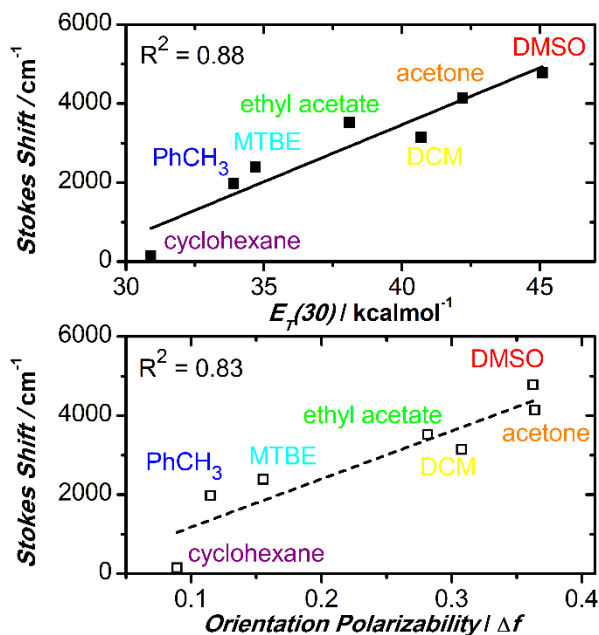


Figure S68. Reichenardt's $E_T(30)$ (closed squares) & Lippert and Mataga's orientation polarizability (open squares) plotted against the Stokes shift of **H₂pyr** in solvents of varying polarity. The least-squares fitting is shown in solid and dashed lines, along with the linear R^2 fit.

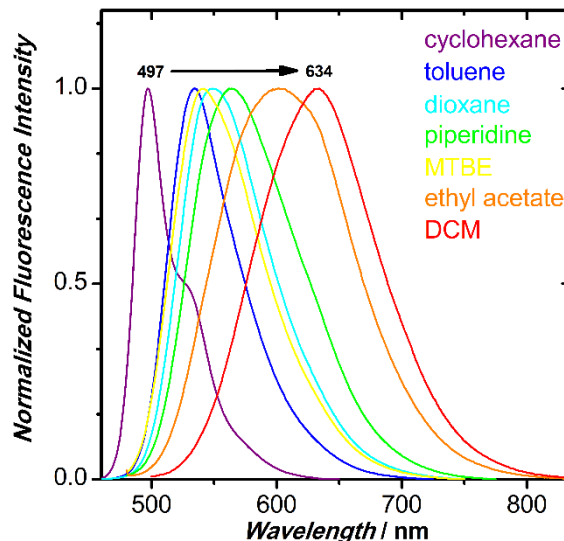


Figure S69. Fluorescence spectra of 10 μM **NMe₂quin** in solvents of varying polarity, with the peak wavelength shift marked. $\lambda_{\text{exc}} = 460 \text{ nm}$.

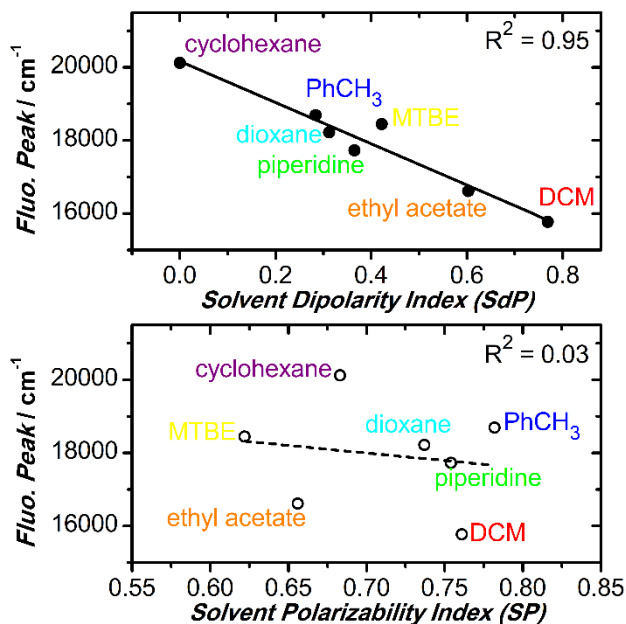


Figure S70. Catalán's solvent dipolarity (filled circles) and solvent polarizability (open circles) versus fluorescence peak wavelength for **NMe₂quin** solutions. The least-squares fitting is shown in solid and dashed lines, along with the linear R^2 fit.

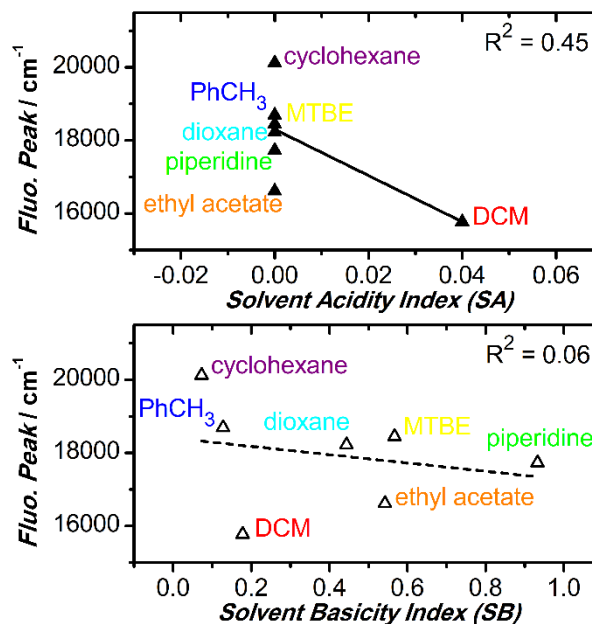


Figure S71. Catalán's solvent acidity (filled triangles) and solvent basicity (open triangles) versus fluorescence peak wavelength for **NMe₂quin** solutions. The least-squares fitting is shown in solid and dashed lines, along with the linear R^2 fit.

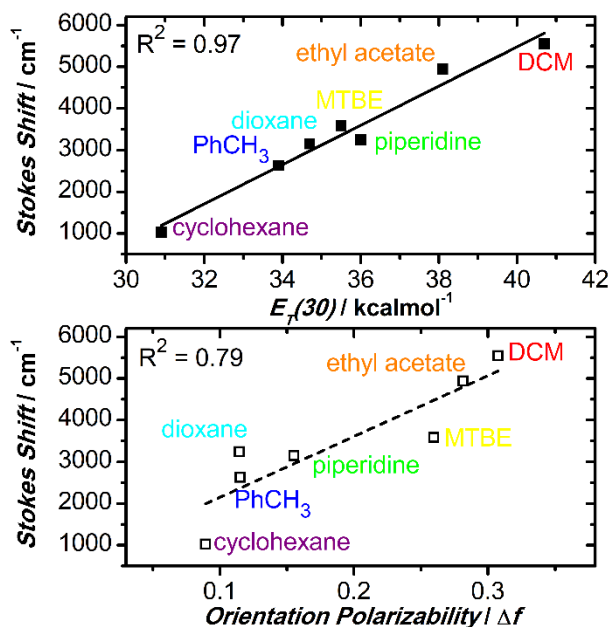


Figure S72. Reichardt's $E_T(30)$ (closed squares) & Lippert and Mataga's orientation polarizability (open squares) plotted against the Stokes shift of **NMe₂quin** in solvents of varying polarity. The least-squares fitting is shown in solid and dashed lines, along with the linear R^2 fit.

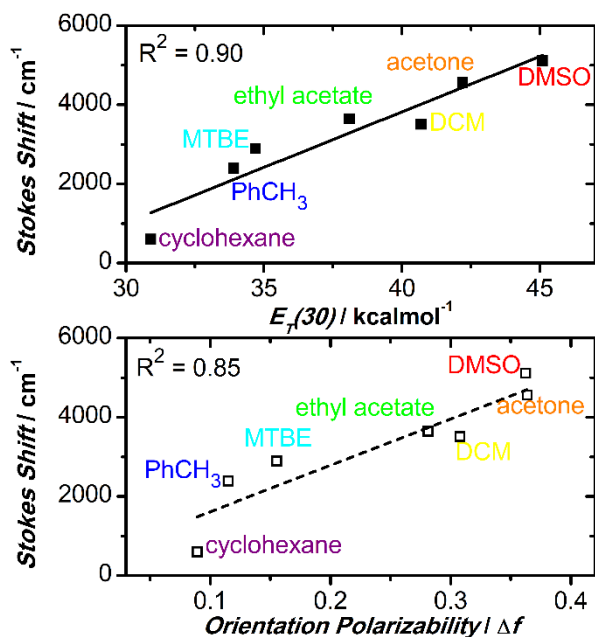


Figure S74. Reichardt's $E_T(30)$ (closed squares) & Lippert and Mataga's orientation polarizability (open squares) plotted against the Stokes shift of **Ph₂pyr** in solvents of varying polarity. The least-squares fitting is shown in solid and dashed lines, along with the linear R^2 fit.

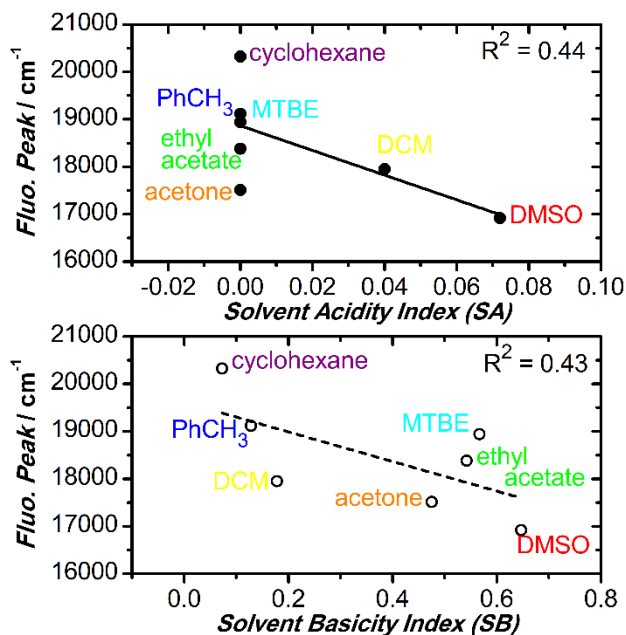


Figure S73. Catalán's solvent acidity (filled circles) and solvent basicity (open circles) versus fluorescence peak wavelength for **Ph₂pyr** in solutions. The least-squares fitting is shown in solid and dashed lines, along with the linear R^2 fit.

Table S15. Fluorescence quantum yields for core-expanded pyrenes

Compound	Solvent	Quantum Yield (Φ_f)
H₂quin	Cyclohexane ^a	0.19 +/- 0.02
	Ethyl acetate ^a	0.08 +/- 0.01
	Dimethylsulfoxide ^b	0.31 +/- 0.03
Ph₂quin	Cyclohexane ^a	0.07 +/- 0.01
	Ethyl acetate ^b	0.40 +/- 0.04
	Dimethylsulfoxide ^b	0.19 +/- 0.02
NMe₂quin	Cyclohexane ^a	0.35 +/- 0.04
	Piperidine ^d	0.22 +/- 0.02
	Dichloromethane ^d	0.12 +/- 0.01
H₂pyr	Cyclohexane ^a	0.33 +/- 0.03
	Ethyl acetate ^b	0.03 +/- 0.01
	Dimethylsulfoxide ^c	0.41 +/- 0.04
Ph₂pyr	Cyclohexane ^b	0.18 +/- 0.02
	Ethyl acetate ^c	0.16 +/- 0.02
	Dimethylsulfoxide ^c	0.40 +/- 0.04

^a relative to quinine sulfate in 0.05 M H₂SO₄ ($\Phi_f=0.55$)⁴⁰

^b relative coumarin 6 in ethanol ($\Phi_f=0.78$)⁴¹

^c relative rhodamine 6G in ethanol ($\Phi_f=0.94$)⁴²

^d relative to rhodamine B in ethanol ($\Phi_f=0.50$)⁴³

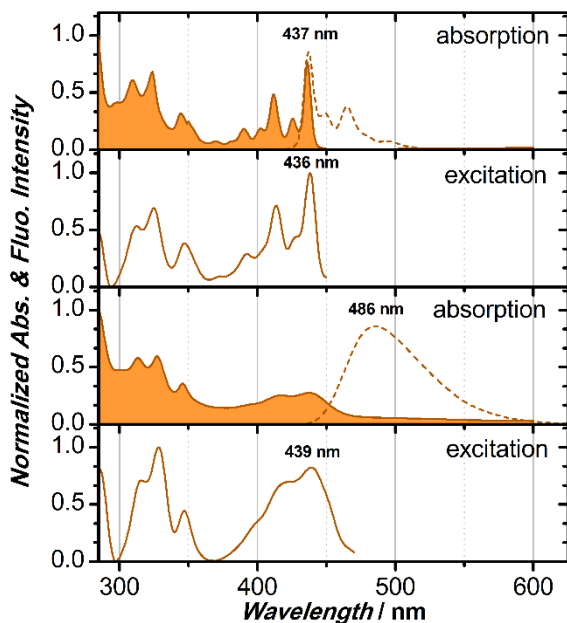


Figure S75. Overlaid UV-visible absorption and fluorescence spectra of 10 μM **H₂quin** against the excitation spectrum in cyclohexane (top, $\lambda_{\text{exc}} = 420$ nm, $\lambda_{\text{em}} = 460$ nm) and DMSO (bottom, $\lambda_{\text{exc}} = 420$ nm, $\lambda_{\text{em}} = 490$ nm.).

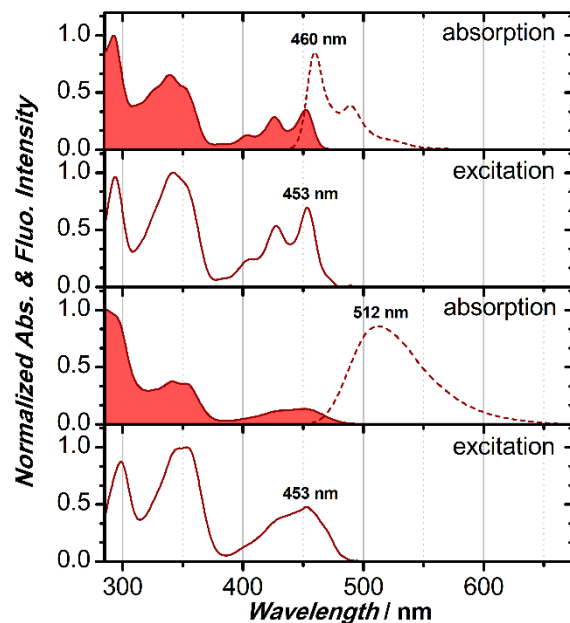


Figure S76. Overlaid UV-visible absorption and fluorescence spectra of 10 μM **Ph₂quin** against the excitation spectrum in cyclohexane (top, $\lambda_{\text{exc}} = 430$ nm, $\lambda_{\text{em}} = 510$ nm) and DMSO (bottom, $\lambda_{\text{exc}} = 430$ nm, $\lambda_{\text{em}} = 510$ nm).

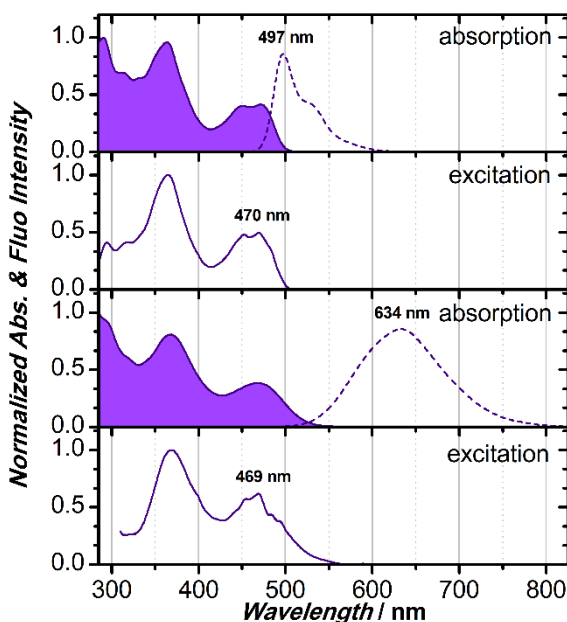


Figure S77. Overlaid UV-visible absorption and fluorescence spectra of 10 μM **NMe₂quin** against the excitation spectrum in cyclohexane (top, $\lambda_{\text{exc}} = 460$ nm, $\lambda_{\text{em}} = 510$ nm) and DMSO (bottom, $\lambda_{\text{exc}} = 460$ nm, $\lambda_{\text{em}} = 600$ nm).

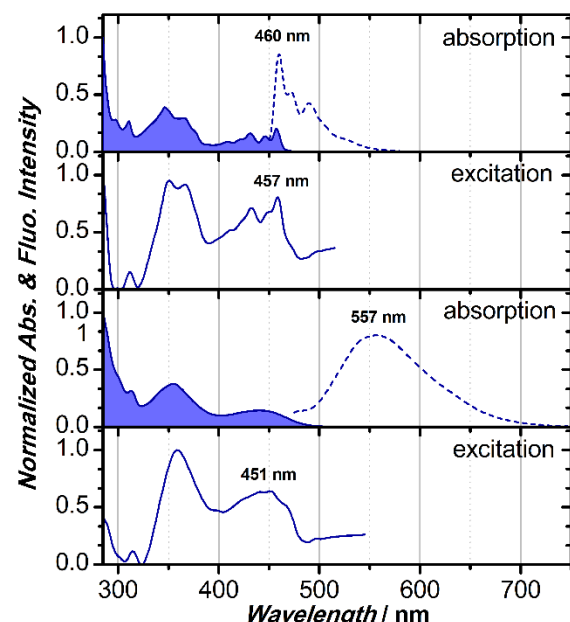


Figure S78. Overlaid UV-visible absorption and fluorescence spectra of 10 μM **H₂pyr** against the excitation spectrum in cyclohexane (top, $\lambda_{\text{exc}} = 440$ nm, $\lambda_{\text{em}} = 520$ nm) and DMSO (bottom, $\lambda_{\text{exc}} = 440$ nm, $\lambda_{\text{em}} = 560$ nm).

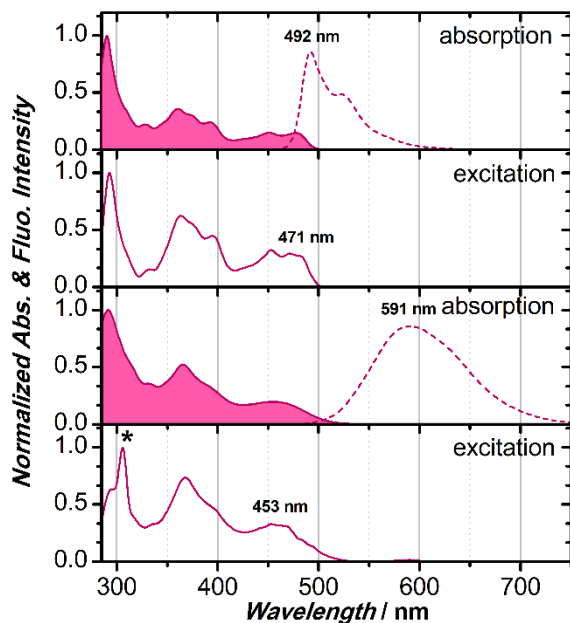


Figure S79. Overlaid UV-visible absorption and fluorescence spectra of 10 μM **Ph₂pyr** against the excitation spectrum in cyclohexane (top, $\lambda_{\text{exc}} = 460$ nm, $\lambda_{\text{em}} = 510$ nm) and DMSO (bottom, $\lambda_{\text{exc}} = 460$ nm, $\lambda_{\text{em}} = 600$ nm.).

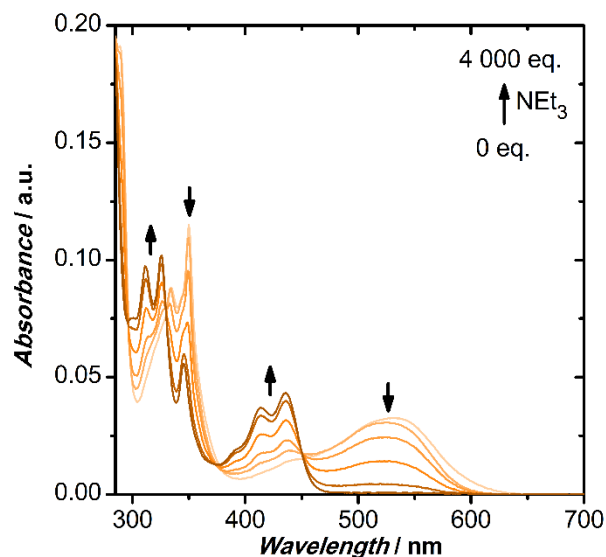


Figure S80. UV-visible absorption spectrum of 4 μM **H₂quin** in CH_2Cl_2 as $\text{NEt}_3/\text{CH}_2\text{Cl}_2$ is titrated to regenerate the non-protonated species. Arrows indicate the direction of peak growth/decay; initial traces are coloured light orange and final traces are coloured dark orange.

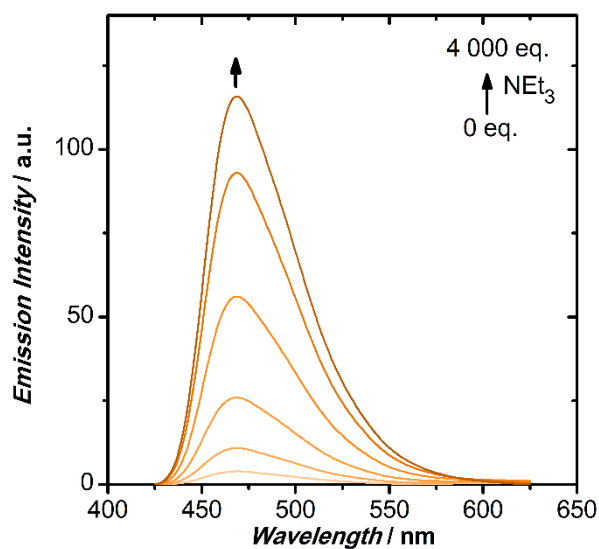


Figure S81. Fluorescence spectrum of 4 μM **H₂quin** in CH_2Cl_2 as $\text{NEt}_3/\text{CH}_2\text{Cl}_2$ is titrated, showing regeneration of the non-protonated species. Arrows indicate the direction of peak growth/decay; initial traces are coloured light orange and final traces are coloured dark orange. $\lambda_{\text{exc}} = 415$ nm.

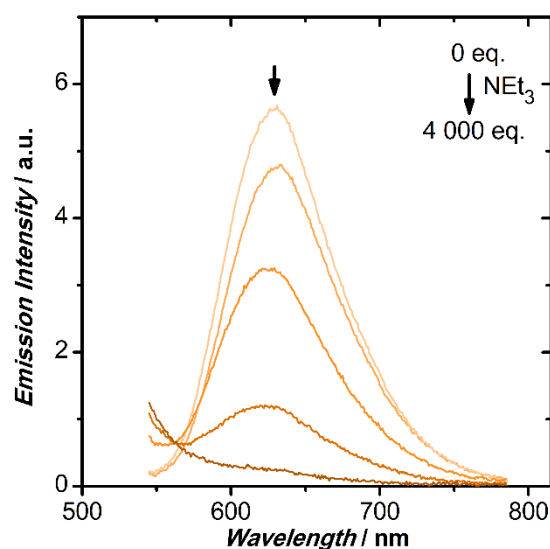


Figure S82. Fluorescence spectrum of 4 μM **H₂quin** in CH_2Cl_2 as $\text{NEt}_3/\text{CH}_2\text{Cl}_2$ is titrated, showing consumption of the protonated species. Arrows indicate the direction of peak growth/decay; initial traces are coloured light orange and final traces are coloured dark orange. $\lambda_{\text{exc}} = 535$ nm.

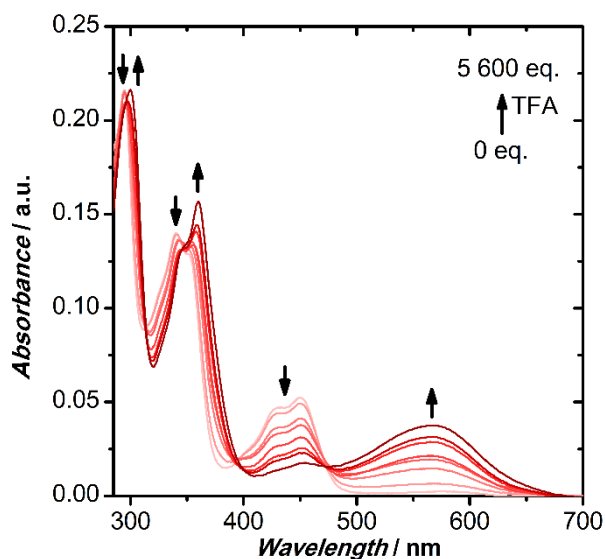


Figure S83. UV-visible absorption spectrum of 4 μM **Ph₂quin** in CH_2Cl_2 as TFA/ CH_2Cl_2 is titrated to generate the protonated species. Arrows indicate the direction of peak growth/decay; initial traces are coloured light red and final traces are coloured dark red.

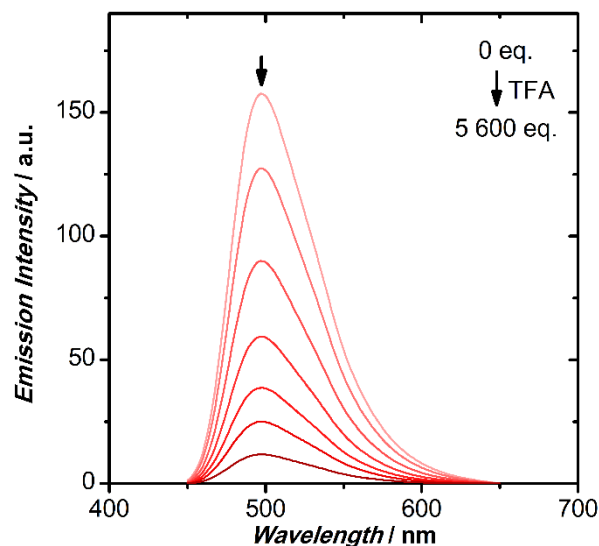


Figure S84. Fluorescence spectrum of 4 μM **Ph₂quin** in CH_2Cl_2 as TFA/ CH_2Cl_2 is titrated, showing decay of the non-protonated species. Arrows indicate the direction of peak growth/decay; initial traces are coloured light red and final traces are coloured dark red. $\lambda_{\text{exc}} = 440$ nm.

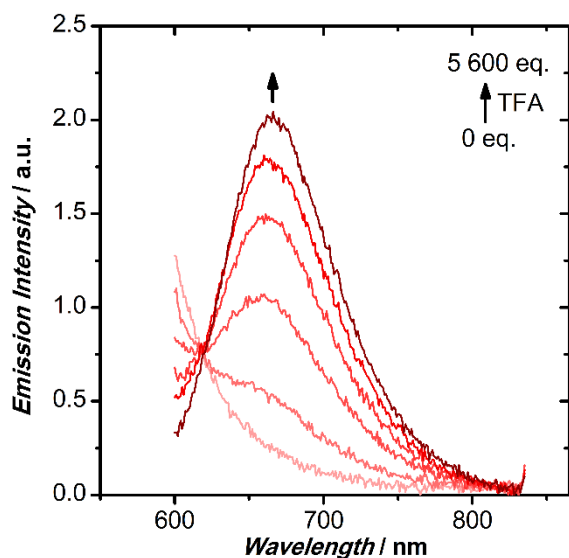


Figure S85. Fluorescence spectrum of 4 μM **Ph₂quin** in CH_2Cl_2 as TFA/ CH_2Cl_2 is titrated, showing generation of the protonated species. Arrows indicate the direction of peak growth/decay; initial traces are coloured light red and final traces are coloured dark red. $\lambda_{\text{exc}} = 565$ nm.

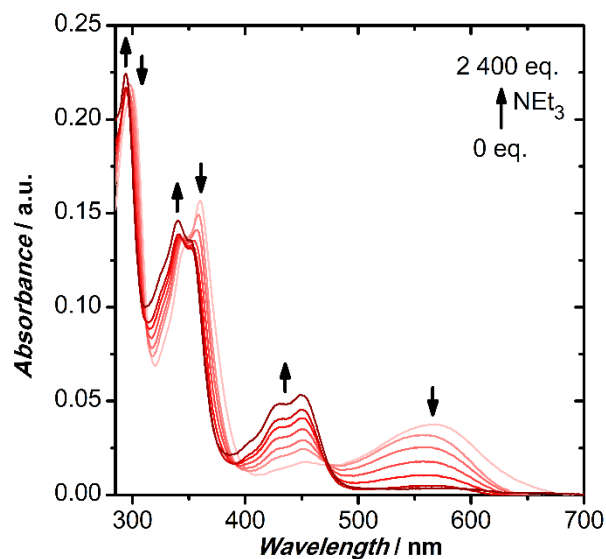


Figure S86. UV-visible absorption spectrum of 4 μM **Ph₂quin** in CH_2Cl_2 as NET_3 / CH_2Cl_2 is titrated to regenerate the non-protonated species. Arrows indicate the direction of peak growth/decay; initial traces are coloured light red and final traces are coloured dark red.

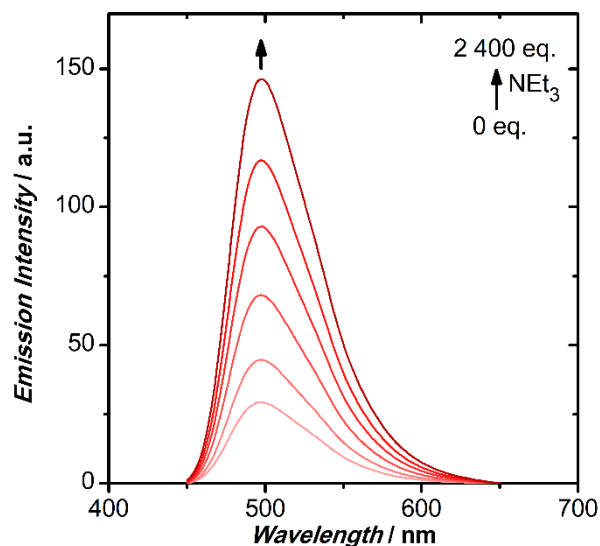


Figure S87. Fluorescence spectrum of 4 μM **Ph₂quin** in CH_2Cl_2 as $\text{NEt}_3/\text{CH}_2\text{Cl}_2$ is titrated, showing regeneration of the non-protonated species. Arrows indicate the direction of peak growth/decay; initial traces are coloured light red and final traces are coloured dark red. $\lambda_{\text{exc}} = 440$ nm.

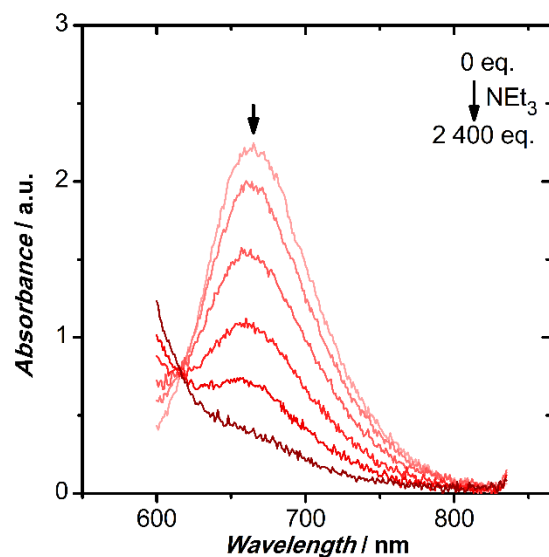


Figure S88. Fluorescence spectrum of 4 μM **Ph₂quin** in CH_2Cl_2 as $\text{NEt}_3/\text{CH}_2\text{Cl}_2$ is titrated, showing decay of the protonated species. Arrows indicate the direction of peak growth/decay; initial traces are coloured light red and final traces are coloured dark red. $\lambda_{\text{exc}} = 565$ nm.

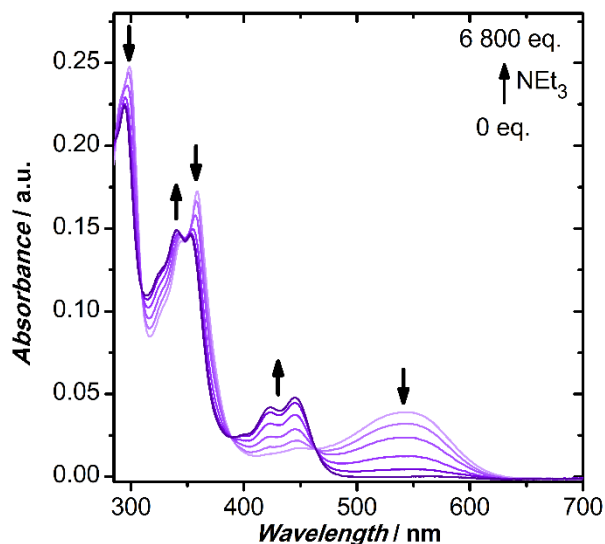


Figure S89. UV-visible absorption spectrum of 4 μM **NMe₂quin** in CH_2Cl_2 as $\text{NEt}_3/\text{CH}_2\text{Cl}_2$ is titrated to regenerate the singly protonated species. Arrows indicate the direction of peak growth/decay; initial traces are coloured light purple and final traces are coloured dark purple.

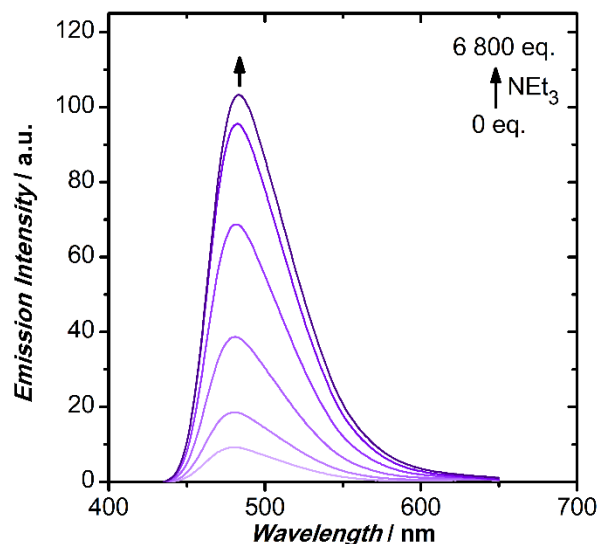


Figure S90. Fluorescence spectrum of 4 μM **NMe₂quin** in CH_2Cl_2 as $\text{NEt}_3/\text{CH}_2\text{Cl}_2$ is titrated, showing regeneration of the singly protonated species. Arrows indicate the direction of peak growth/decay; initial traces are coloured light purple and final traces are coloured dark purple. $\lambda_{\text{exc}} = 425$ nm.

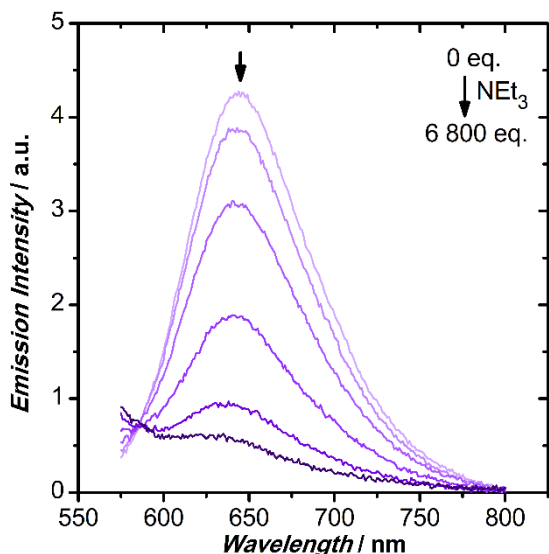


Figure S91. Fluorescence spectrum of 4 μM **NMe₂quin** in CH_2Cl_2 as $\text{NEt}_3/\text{CH}_2\text{Cl}_2$ is titrated, showing decay of the doubly protonated species. Arrows indicate the direction of peak growth/decay; initial traces are coloured light purple and final traces are coloured dark purple. $\lambda_{\text{exc}} = 545 \text{ nm}$.

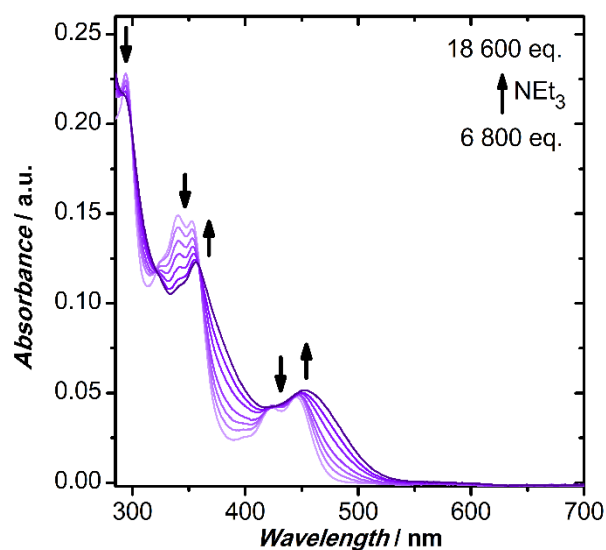


Figure S92. UV-visible absorption spectrum of 4 μM **NMe₂quin** in CH_2Cl_2 as $\text{NEt}_3/\text{CH}_2\text{Cl}_2$ is titrated to regenerate the non-protonated species. Arrows indicate the direction of peak growth/decay; initial traces are coloured light red and final traces are coloured dark red.

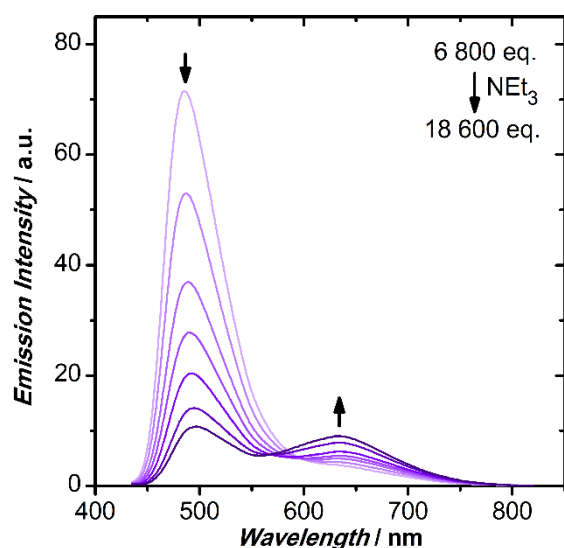


Figure S93. Fluorescence spectrum of 4 μM **NMe₂quin** in CH_2Cl_2 as $\text{NEt}_3/\text{CH}_2\text{Cl}_2$ is titrated, showing regeneration of the non-protonated species at the expense of the singly protonated species. Arrows indicate the direction of peak growth/decay; initial traces are coloured light purple and final traces are coloured dark purple. $\lambda_{\text{exc}} = 425 \text{ nm}$.

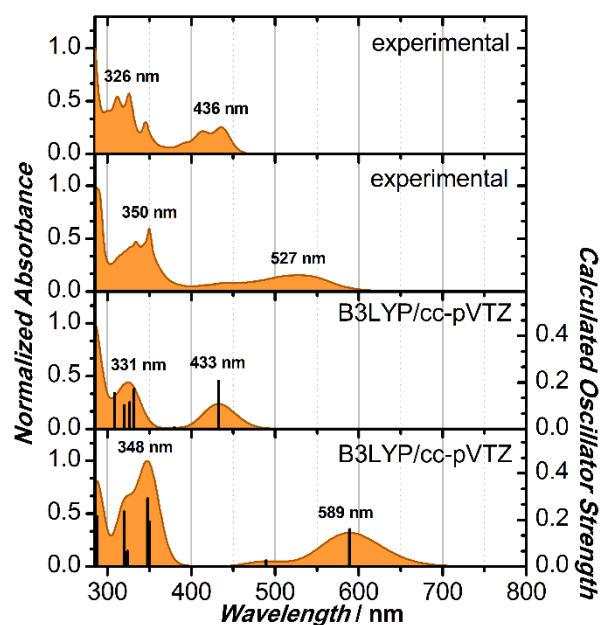


Figure S94. Comparison of the experimental absorption spectra of 4 μM **H₂quin** in CH_2Cl_2 with and without TFA (top), against the calculated analogues (bottom). The second lowest spectrum is neutral **H₂quin** in CH_2Cl_2 , followed by protonated species. Black lines indicate the positions of predicted transitions.

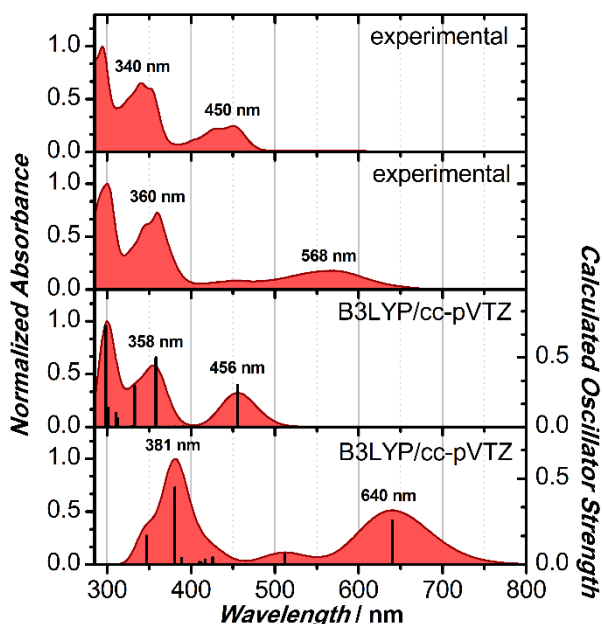


Figure S95. Comparison of the experimental absorption spectra of 4 μM **Ph₂quin** in CH_2Cl_2 with and without TFA (top), against the calculated analogues (bottom). The second lowest spectrum is neutral **Ph₂quin** in CH_2Cl_2 , followed by protonated species. Black lines indicate the positions of predicted transitions.

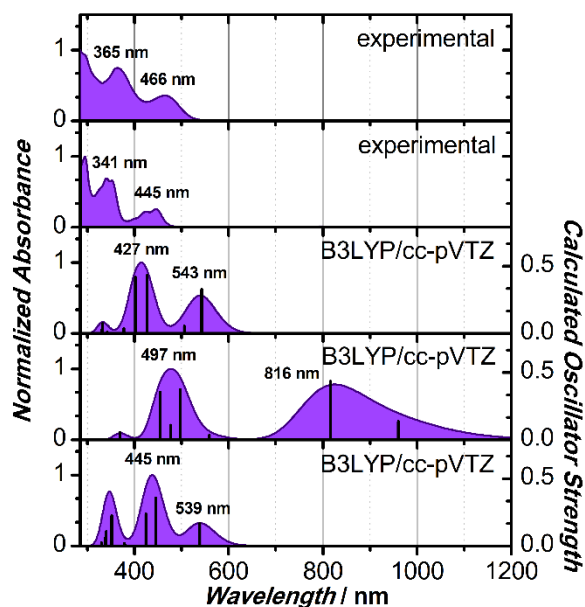


Figure S96. Comparison of the experimental absorption spectra of 4 μM **NMe₂quin** in CH_2Cl_2 with and without *minimal* TFA (top), against the calculated analogues (bottom). The third lowest spectrum is neutral in CH_2Cl_2 , followed by quinoxaline-protonated and then aniline-protonated. Black lines indicate the positions of predicted transitions.

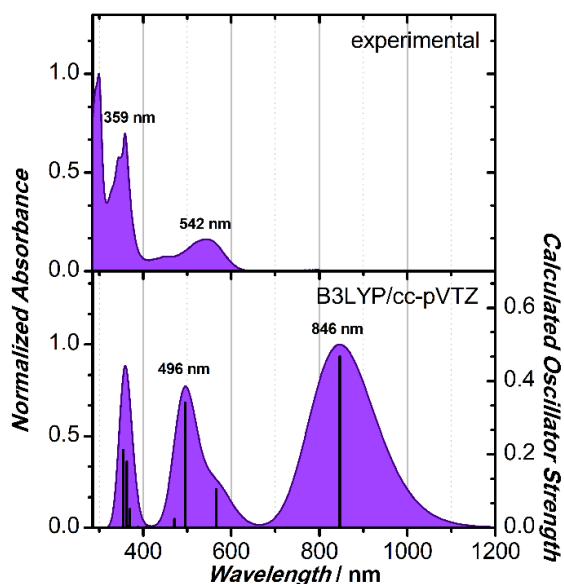


Figure S97. Comparison of the experimental absorption spectra of 4 μM **NMe₂quin** in CH_2Cl_2 with and without *excess* TFA (top), against the calculated doubly protonated analogue (bottom). Black lines indicate the positions of predicted transitions.

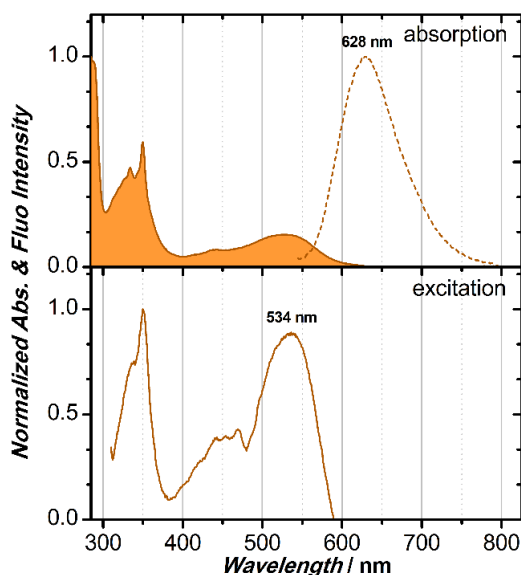


Figure S98. Combined absorption and fluorescence spectra of protonated 4 μM **H₂quin** in CH_2Cl_2 (top, $\lambda_{\text{exc}} = 535 \text{ nm}$), against the excitation spectrum (bottom, $\lambda_{\text{em}} = 600 \text{ nm}$).

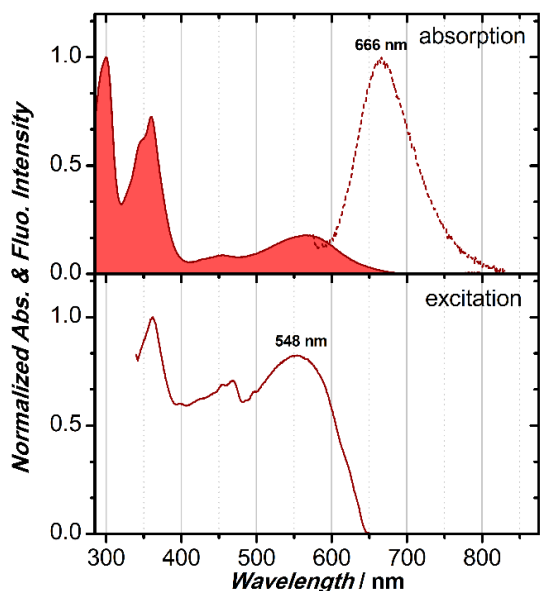


Figure S99. Combined absorption and fluorescence spectra of protonated 4 μM **Ph₂quin** in CH_2Cl_2 (top, $\lambda_{\text{exc}} = 565 \text{ nm}$), against the excitation spectrum (bottom, $\lambda_{\text{em}} = 660 \text{ nm}$).

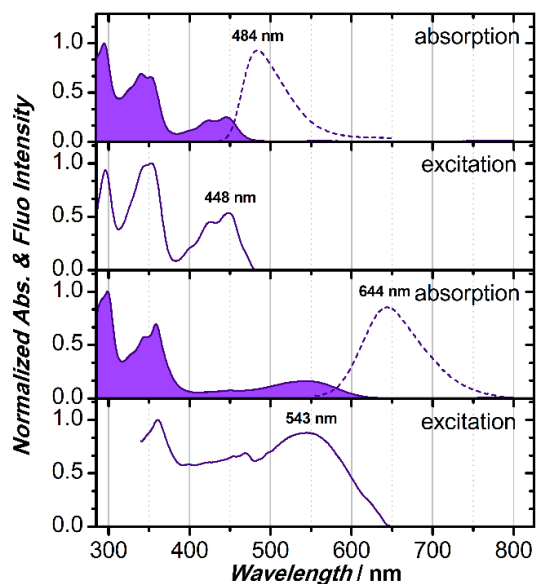


Figure S100. Combined absorption and fluorescence spectra of singly (top two spectra, $\lambda_{\text{exc}} = 425 \text{ nm}$) and doubly (bottom two spectra, $\lambda_{\text{exc}} = 565 \text{ nm}$) protonated 4 μM **NMe₂quin** in CH_2Cl_2 , against the excitation spectra ($\lambda_{\text{em}} = 545 \text{ nm}$ and 660 nm).

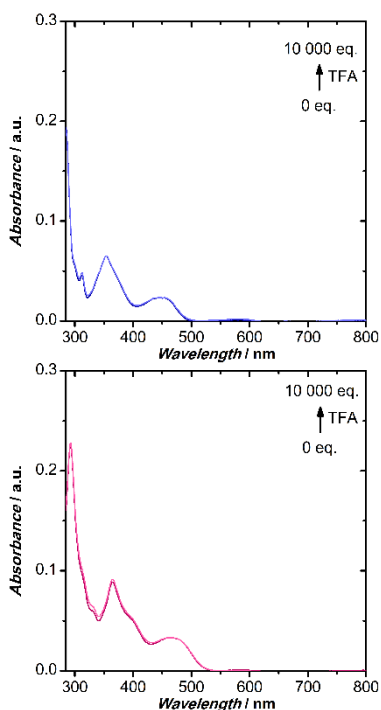


Figure S101. UV-visible absorption spectra of 4 μM **H₂pyr** (top) and **Ph₂pyr** (bottom) before and after addition of 10 000 eq of TFA. No new peaks emerge, and the spectra remain unchanged.

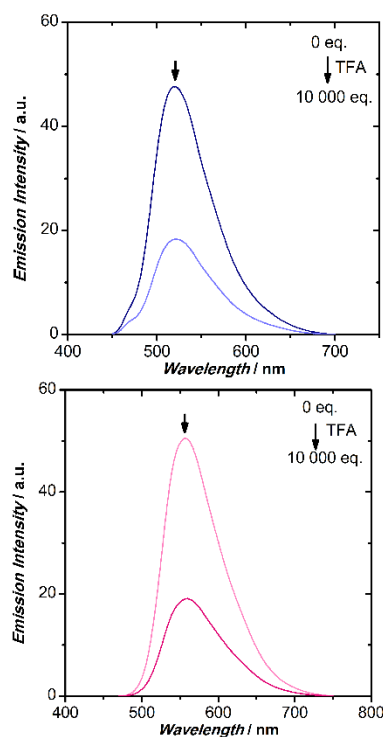


Figure S102. Fluorescence spectra of 4 μM **H₂pyr** (top, $\lambda_{\text{exc}} = 440 \text{ nm}$) and **Ph₂pyr** (bottom, $\lambda_{\text{exc}} = 460 \text{ nm}$) before and after addition of 10 000 eq of TFA. Quenching is observed after addition, but no new peaks emerge.

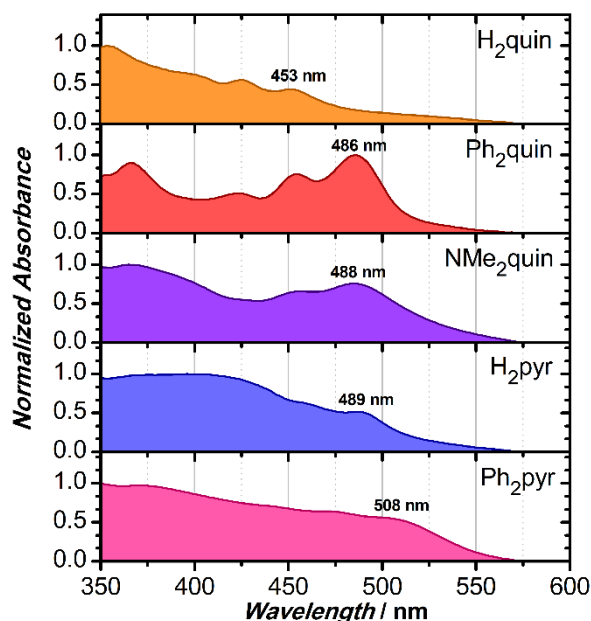


Figure S103. Transmission UV-visible absorption spectra of solid core-expanded pyrenes on microscope slides.

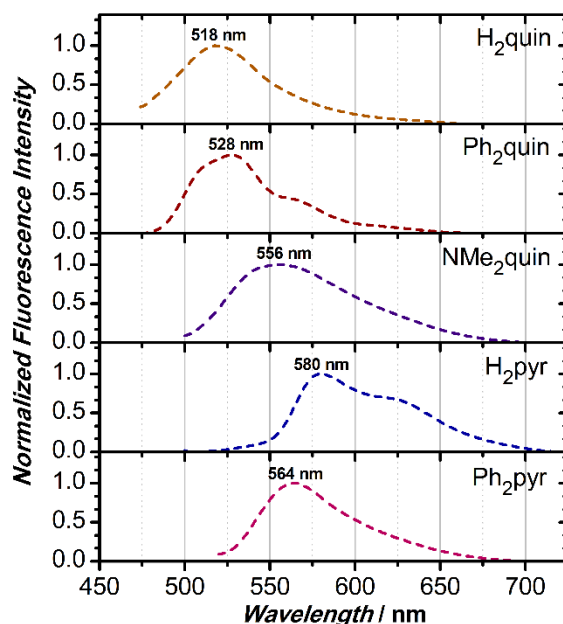


Figure S104. Fluorescence spectra of solid core-expanded pyrenes on microscope slides. $\lambda_{exc} = 453$ nm, 454 nm, 490 nm, 488 nm and 502 nm.

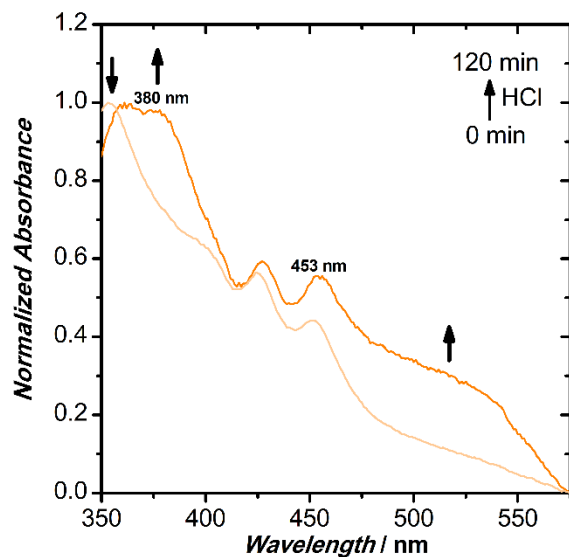


Figure S105. Transmission UV-visible absorption spectra of solid **H₂quin** after before (light orange) and after (dark orange) exposure to HCl vapours. The arrows indicate growth/decay of peaks.

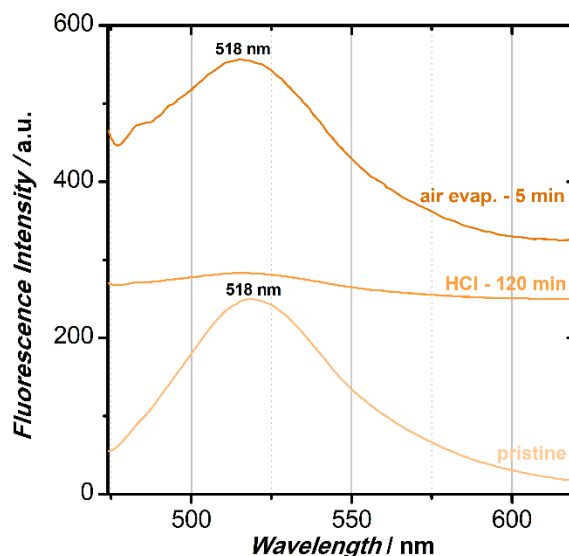


Figure S106. Fluorescence spectra of solid **H₂quin** before (bottom) and after (middle) exposure to HCl vapours. The spectral features are regained after allowing HCl to off-gas (top). $\lambda_{exc} = 453$ nm.

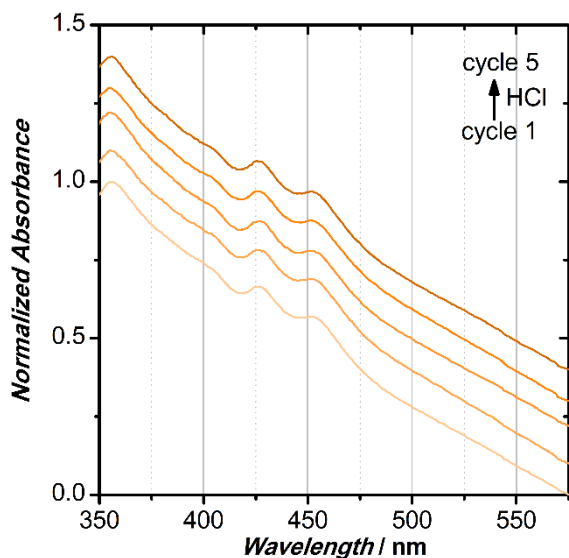


Figure S107. Transmission UV-visible absorption spectra of solid **H₂quin** after 5 cycles of HCl exposure/off-gassing. The light orange traces are the first cycles, and the dark orange traces are the final cycles.

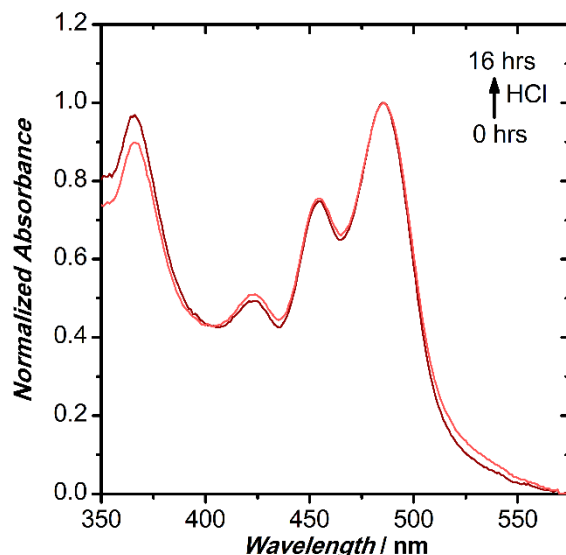


Figure S108. Transmission UV-visible absorption spectra of solid **Ph₂quin** after before (light red) and after (dark red) exposure to HCl vapours overnight. No change is apparent in the traces.

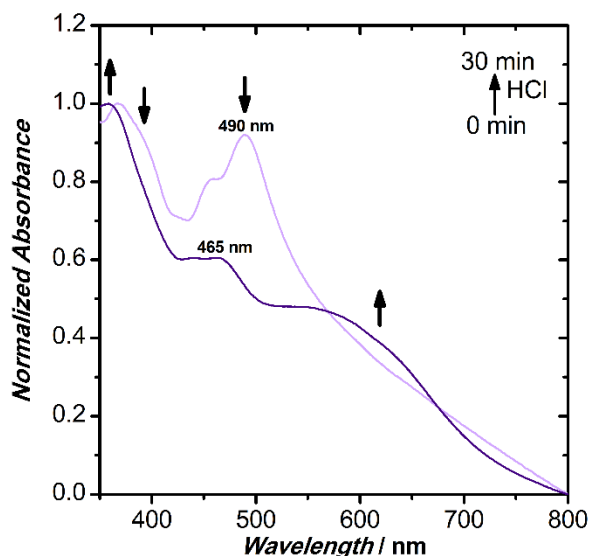


Figure S109. Transmission UV-visible absorption spectroscopy of solid **NMe₂quin** on a microscope slide, before (light purple) and after (dark purple) exposure to HCl vapours. The arrows indicate peak growth/decay.

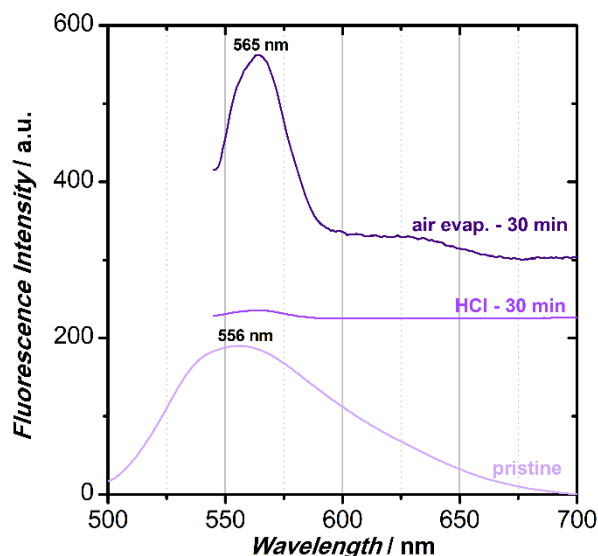


Figure S110. Fluorescence spectra of solid **NMe₂quin** before exposure to HCl (bottom) immediately following exposure (middle) and after off-gassing the HCl (top). $\lambda_{exc} = 490$ nm.

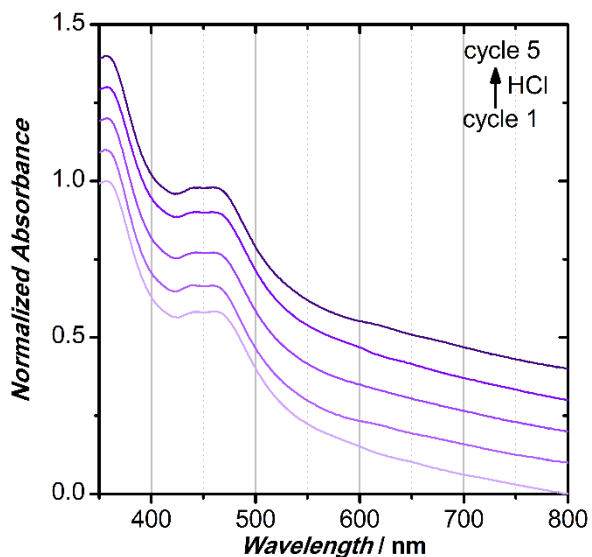


Figure S111. Transmission UV-visible absorption spectra of solid **NMe₂quin** after 5 cycles of HCl exposure/off-gassing. The light purple traces are the first cycles, and the dark purple traces are the final cycles.

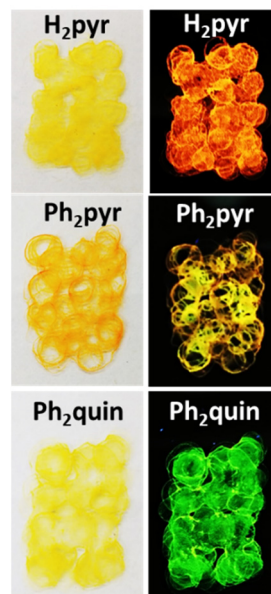


Figure S112. Photographs of solid core-expanded pyrenes deposited onto microscope slides under ambient (left) and 365 nm UV light (right).

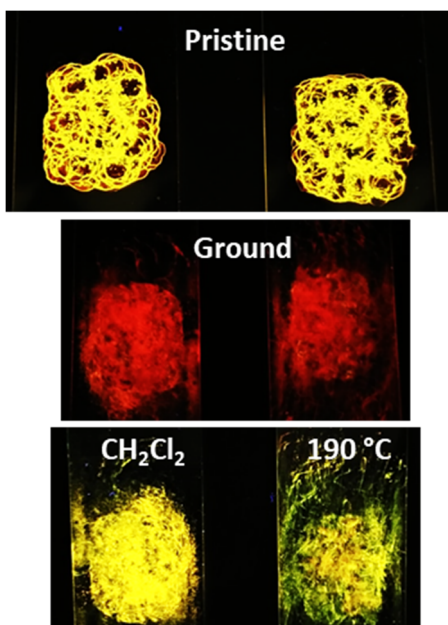


Figure S113. Photographs of solid **NMe₂quin** under UV light before grinding (top), after grinding (middle) and after regenerating by 1-hour exposure to **CH₂Cl₂** vapours (bottom-left) or by 1-hour heating at 190 °C (bottom-right).

- 1 Bruker-AXS, *SAINT*, Madison, Wisconsin, USA, 2017.
- 2 Bruker-AXS, *XPREP*, Madison, Wisconsin, USA, 2017.
- 3 O. V. Dolomanov, L. J. Bourhis, R. J. Gildea, J. A. K. Howard and H. Puschmann, *J. Appl. Crystallogr.*, 2009, **42**, 339–341.
- 4 G. M. Sheldrick, *Acta Crystallogr. Sect. Found. Adv.*, 2015, **71**, 3–8.
- 5 G. M. Sheldrick, *Acta Crystallogr. Sect. C Struct. Chem.*, 2015, **71**, 3–8.
- 6 B. H. Toby and R. B. Von Dreele, *J. Appl. Crystallogr.*, 2013, **46**, 544–549.
- 7 C. F. Macrae, I. J. Bruno, J. A. Chisholm, P. R. Edgington, P. McCabe, E. Pidcock, L. Rodriguez-Monge, R. Taylor, J. van de Streek and P. A. Wood, *J. Appl. Crystallogr.*, 2008, **41**, 466–470.
- 8 C. F. Macrae, P. R. Edgington, P. McCabe, E. Pidcock, G. P. Shields, R. Taylor, M. Towler and J. van de Streek, *J. Appl. Crystallogr.*, 2006, **39**, 453–457.
- 9 P. Grochulski, M. N. Fodje, J. Gorin, S. L. Labiuk and R. Berg, *J. Synchrotron Radiat.*, 2011, **18**, 681–684.
- 10 W. Kabsch, *J. Appl. Crystallogr.*, 1993, **26**, 795–800.
- 11 L. Krause, R. Herbst-Irmer, G. M. Sheldrick and D. Stalke, *J. Appl. Crystallogr.*, 2015, **48**, 3–10.
- 12 Sheldrick, G. M., *XDS2SAD*, Gottingen, Germany, 2008.
- 13 Sheldrick, G. M., *XPREP Version 2008*, 2008.
- 14 Spasyuk, D. M., *LinXTL*, Montreal, Canada, 2009.
- 15 A. L. Spek, *Acta Crystallogr. D Biol. Crystallogr.*, 2009, **65**, 148–155.
- 16 G. R. Fulmer, A. J. M. Miller, N. H. Sherden, H. E. Gottlieb, A. Nudelman, B. M. Stoltz, J. E. Bercaw and K. I. Goldberg, *Organometallics*, 2010, **29**, 2176–2179.
- 17 J. C. Walsh, K.-L. M. Williams, D. Lungerich and G. J. Bodwell, *Eur. J. Org. Chem.*, 2016, **2016**, 5933–5936.
- 18 G. Venkataramana, P. Dongare, L. N. Dawe, D. W. Thompson, Y. Zhao and G. J. Bodwell, *Org. Lett.*, 2011, **13**, 2240–2243.
- 19 M. Khadem, J. C. Walsh, G. J. Bodwell and Y. Zhao, *Org. Lett.*, 2016, **18**, 2403–2406.
- 20 S. N. Keller, N. L. Veltri and T. C. Sutherland, *Org. Lett.*, 2013, **15**, 4798–4801.
- 21 F. G. Oberender and J. A. Dixon, *J. Org. Chem.*, 1959, **24**, 1226–1229.
- 22 R. García, M. Melle-Franco and A. Mateo-Alonso, *Chem. Commun.*, 2015, **51**, 8037–8040.
- 23 H. W. Rothkopf, D. Wohrle, R. Mueller and G. Kossmehl, *Chem. Ber.*, 1975, **108**, 875–886.
- 24 A. D. Becke, *J. Chem. Phys.*, 1993, **98**, 5648–5652.
- 25 C. Lee, W. Yang and R. G. Parr, *Phys. Rev. B*, 1988, **37**, 785–789.
- 26 P. J. Stephens, F. J. Devlin, C. F. Chabalowski and M. J. Frisch, *J. Phys. Chem.*, 1994, **98**, 11623–1167.
- 27 T. H. Dunning, *J. Chem. Phys.*, 1989, **90**, 1007–1023.
- 28 Frisch, M. J.; Trucks, G. W.; Schlegel, H. B.; Scuseria, G. E.; Robb, M. A.; Cheeseman, J. R.; Scalmani, G.; Barone, V.; Petersson, G. A.; Nakatsuji, H.; Li, X.; Caricato, M.; Marenich, A. V.; Bloino, J.; Janesko, B. G.; Gomperts, R.; Mennucci, B.; Hratchian, H. P.; Ortiz, J. V.; Izmaylov, A. F.; Sonnenberg, J. L.; Williams-Young, D.; Ding, F.; Lipparini, F.; Egidi, F.; Goings, J.; Peng, B.; Petrone, A.; Henderson, T.; Ranasinghe, D.; Zakrzewski, V. G.; Gao, J.; Rega, N.; Zheng, G.; Liang, W.; Hada, M.; Ehara, M.; Toyota, K.; Fukuda, R.; Hasegawa, J.; Ishida, M.; Nakajima, T.; Honda, Y.; Kitao, O.; Nakai, H.; Vreven, T.; Throssell, K.; Montgomery, J. A., Jr.; Peralta, J. E.; Ogliaro, F.; Bearpark, M. J.; Heyd, J. J.; Brothers, E. N.; Kudin, K. N.; Staroverov, V. N.; Keith, T. A.; Kobayashi, R.; Normand, J.; Raghavachari, K.; Rendell, A. P.; and Burant, J. C.; Iyengar, S. S.; Tomasi, J.; Cossi, M.; Millam, J. M.; Klene, M.; Adamo, C.; Cammi, R.; Ochterski, J. W.; Martin, R.

- L.; Morokuma, K.; Farkas, O.; Foresman, J. B.; Fox, D. J., *Gaussian 16*, Gaussian Inc., Wallingford, CT, 2016.
- 29 B. Mennucci, E. Cancès and J. Tomasi, *J. Phys. Chem. B*, 1997, **101**, 10506–10517.
- 30 T. Yanai, D. P. Tew and N. C. Handy, *Chem. Phys. Lett.*, 2004, **393**, 51–57.
- 31 J.-D. Chai and M. Head-Gordon, *Phys. Chem. Chem. Phys.*, 2008, **10**, 6615.
- 32 R. Ditchfield, *Mol. Phys.*, 1974, **27**, 789–807.
- 33 K. Wolinski, J. F. Hinton and P. Pulay, *J. Am. Chem. Soc.*, 1990, **112**, 8251–8260.
- 34 R. Krishnan, J. S. Binkley, R. Seeger and J. A. Pople, *J. Chem. Phys.*, 1980, **72**, 650–654.
- 35 T. Clark, J. Chandrasekhar, G. W. Spitznagel and P. V. R. Schleyer, *J. Comput. Chem.*, 1983, **4**, 294–301.
- 36 S. Grimme, J. Antony, S. Ehrlich and H. Krieg, *J. Chem. Phys.*, 2010, **132**, 154104.
- 37 S. Grimme, S. Ehrlich and L. Goerigk, *J. Comput. Chem.*, 2011, **32**, 1456–1465.
- 38 A. D. Becke, *J. Chem. Phys.*, 1997, **107**, 8554–8560.
- 39 Y. Zhao and D. G. Truhlar, *Theor. Chem. Acc.*, 2008, **120**, 215–241.
- 40 D. F. Eaton, *Pure Appl. Chem.*, 1988, **60**, 1107–1114.
- 41 G. A. Reynolds and K. H. Drexhage, *Opt. Commun.*, 1975, **13**, 222–225.
- 42 R. F. Kubin and A. N. Fletcher, *J. Lumin.*, 1982, **27**, 455–462.
- 43 F. L. Arbeloa, P. R. Ojeda and I. L. Arbeloa, *J. Lumin.*, 1989, **44**, 105–112.